University of West Bohemia
Faculty of Applied Sciences

On the development of a virtual human body model based on multibody principle

Ing. Jan Špička

A doctoral thesis submitted in fulfilment of the requirements for the degree of doctor in Applied Mechanics

Supervisor: doc. Ing. Luděk Hynčík Ph.D.
Department of Mechanics

Plzeň 2020

FACULTY
OF APPLIED SCIENCES
UNIVERSITY
OF WEST BOHEMIA

Západočeská univerzita v Plzni
Fakulta aplikovaných věd

Vývoj virtuálního modelu člověka jako multibody systému

Ing. Jan Špička

Disertační práce k získání akademického titulu doktor v oboru
Aplikovaná mechanika

Školitel: doc. Ing. Luděk Hynčík Ph.D.
Katedra mechaniky

Plzeň 2020

Acknowledgement

The work was financially supported with internal research project of the University of West Bohemia SGS-2019-002: Biomechanical models of human body, biological tissues and biomechanical processes with application in industry and medicine.

Firstly, I would like to express my appreciation and thanks to my supervisor doc. Ing. Luděk Hynčík, Ph.D. and to my supervisor specialist doc. Ing. Michal Hajžman, Ph.D. for the continuous support of my study and research, for motivation and enthusiasm. This work was accomplished during my Ph.D. study at the Department of Mechanics of the Faculty of Applied Sciences of the University of West Bohemia in Pilsen. The kind support of the department's stuff is greatfully acknowledged. Further, my thanks belong to my colleagues from the New Technologies - Research Centre for their help.

I would like to express my gratitude to my family and my wife for their indispensable and infinite support. Last, but not least, I would like to thank to my guardian angel, for keeping me alive.

Jan Špička

Declaration of Authorship

I, Jan Špička, declare that the work in this dissertation thesis titled "On the development of a Virtual human body model based on multibody principle" is my own. I confirm that if any part has previously been published or presented, this has been clearly stated and attributed. I also confirm that I have quoted all sources used during the work. I honestly declare that I have followed the standard procedures and ethic of the scientific work.

Jan Špička

Date

Annotation

This work is focused on the virtual modelling of the human body, with the main focus on the full body models, utilized and developed for dynamics crash scenarios. This thesis firstly presents a brief overview of the current state of the art in the human models. However, the main aim of this work is to use multibody method for a spatial modelling of a system of constrained rigid bodies. The theory of Euler angles and Euler parameters are used here and their pros and cons are discussed. The full equation of motion is expanded with the algorithms for numerical stabilization, contact calculation and internal stiffness of the joints.

The full human body model is modelled via Euler parameters and consists of 17 rigid bodies connected via kinematics joints. Here, all bodies have shape of ellipsoid and all joints are modelled as spherical joints. The dimension, mass and inertia of each body is set based on literature and real data measurement. The model is built as a scalable model, where only total weight and height are pre-defined inputs and the particular model (dimensions, masses, inertia) is created by scaling of the reference model. In order to include range of motion of the joints, as well as their physiological stiffness, external torques are added on each body. These torques are function of the relative rotations between the adjoining bodies and are added as an external loading to the equation of motion. Relative rotation between the bodies is solved with the advantages of the Euler parameters (quatermions), that allow direct calculation of the current axis of rotation and relative angle of rotation around this axis. Contact algorithm is solved with the continuous force model, where several force models are included. The total equation of motion is numerically integrated in MATLAB, using standard ODE solvers. To ensure the numerical stability (which is generally not guaranteed in the constrained dynamical system), two methods for stabilization are utilized (Baumgarte and direct violation method).

The work presents the results of particular methods and algorithms on basic benchmark examples. Due to the lack of experimental data, some examples are verified only with the visual observation method. The final model of the human body was utilized in set of crash scenarios, where its behavior was tested. The model, especially its parameters (contact parameters, stiffness and numerical parameters) are not set up to approximate any particular scenario. They were setup in order to make the model working, realistic and numerically stable. Such status of model can be called *validation ready model*. If the application of this model in one particular case would be required, the full validation and parameters optimization will be essential, to correctly set the model up.

However, purpose of this work was to build a general algorithm for a solution of the multibody approach, to include additional algorithms for a human body modelling and to get overview how they work, how they can be coded, to understand them and to find their advantages and disadvantages. Despite some limitations of this model, the goal of this work was successfully achieved.

Keywords: human body model; multibody method; contact calculation; joint stiffness; Euler parameters

Anotace

Tato práce se zabývá virtuálními modely lidského těla, používané pro kolizní dynamické scénáře. V úvodu této práce je uveden krátký přehled aktuálních modelů lidského těla. Hlavním cílem této práce je využití multibody metody pro popis prostorového pohybu systému vázaných tuhých těles. Jsou zde využity koncepty Eulerových úhlů a Eulerových parametrů a diskutovány jejich výhody a nevýhody. Celková pohybová rovnice modelu je dále rozšířena o algoritmy pro numerickou stabilizaci, výpočet kontaktu a výpočet vnitřní tuhosti kloubů.

Pro kompletní popis lidského těla je využito Eulerových parametrů a takto vytvořený model se skládá ze 17 tuhých těles, vzájemně vázaných kinematickým kloubem. Všechna tělesa mají tvar elipsoidu a všechny klouby jsou modelovány jako sférické klouby. Rozměry, hmotnosti a setrvačnost každého tělesa jsou definovány z literatury a z reálných naměřených dat. Tento model je vytvořen jako škálovatelný, kde vstupy jsou pouze celková výška a hmotnost a konkrétní model (jeho hmotnost, rozměry a setrvačnost) je vytvořen vyškálováním referenčního modelu. Pro modelování fyziologického rozsahu pohybu jednotlivých klubů, a také pro modelování jejich vnitřní tuhosti, jsou do modelu přidány zátěžné momenty. Tyto momenty jsou funkcí relativního natočení mezi jednotlivými tělesy a posléze jsou přidány jako vnější zatížení do pohybové rovnice. Relativní natočení mezi tělesy je zde vyřešeno díky vlastnostem Eulerových parametrů (kvatermionů), ze kterých lze přímo získat aktuální osu rotace a úhel natočení okolo této osy. Kontaktní algoritmus je řešen pomocí modelu spojité kontaktní síly, s několika modely kontaktní síly. Pohybová rovnice celého mechanického systému je numericky integrována pomocí systému MATLAB a jeho standardními funkcemi ODE. Pro zajištění numerické stability, která pro úlohy vázané dynamiky není obecně zaručena, je využito dvou metod numerické stabilizace (Baumgartova stabilizace a metoda přímého porušení).

Tato práce prezentuje výsledky dílčích metod a algoritmů na jednoduchých elementárních úlohách. Vzhledem k nedostatku experimentálních dat jsou některé úlohy ověřovány pouze pomocí metody přímého vizuálního pozorování. Kompletní model lidského těla je použit v sérii několika kontaktních úloh, kde bylo testováno jeho chování. Tento model, speciálně jeho parametry (kontaktní parametry, tuhosti a numerické parametry), nejsou nastaveny tak, aby simulovaly konkrétní scénář. Byly nastaveny tak, aby výsledný model fungoval, aby dával korektndata a byl numericky stabilní. Tento status lze nazvat *model připravený pro validaci*. Pokud by bylo vyžadováno využití tohoto modelu v nějakém konkrétním příkladu, bylo by nutné provedení kompletní validace a optimalizace všech parametrů pro správné nastavení modelu. Účelem této práce je vytvoření obecného algoritmu pro řešení úloh vázaných tuhých těles s uvažováním dalších algoritmů pro potřeby modelování lidského těla, získání znalostí jak tyto algoritmy fungují, jak mohou být programově řešeny a jaké jsou jejich výhody a nevýhody. I přes určité limity výsledného modelu lze říci, že účelu této práce bylo dosaženo.

Klíčová slova: model lidského těla; vázaná tuhá tělesa; kontakt; tuhost kloubu; Eulerovy parametry

Anotación

Esta tesis se dedica a unos modelos virtuales del cuerpo humano, los cuales se utilizan para escenarios dinámicos de colisión. Esta tesis presenta en primer lugar una breve descripción de los modelos de cuerpo humano actuales. Sin embargo, el objetivo principal de esta tesis es el uso de métodos multibody para la modelación espacial del sistema de cuerpos rígidos ligados. Se usan los conceptos de los ángulos de Euler y de los Párametros de Euler y se discuten los beneficios y desventajas de ambos. La ecuación general del movimiento del modelo se amplía mediante algoritmos de estabilización numérica, cálculo de contacto y cálculo de rugosidad interna de articulaciones.

Para una descripción del cuerpo humano completa se usan los Parámetros de Euler. Un modelo así construído consiste de 17 cuerpos rígidos interconectados por una articulación cinemática. Todos los cuerpos son elipsoidales y todas las articualciones son modeladas como articulaciones esféricas. Dimensiones, pesos e inercia de cada cual cuerpo se definen de la literatura y de datos realmente medidos. Este modelo está diseñado para ser escalable, donde las entradas son solamente la altura total y el peso y el modelo específico (su peso, dimensiones e inercia) se crea escalando el modelo referencial. Para la modelación del rango fisiológico de las articulaciones individuales y también para la modelación de su rigidad internal se añaden pares de torsión externos a cada modelo. Estos pares de extensión son una función de rotación relativa entre los cuerpos idividuales y después son agregados como una carga externa a la ecuación de movimiento. La rotación relativa entre los cuerpos se resuelve gracias a las propiedades de los Parámetros de Euler (cuaternios), de los cuales es posible directamente obtener el eje de rotación actual y el ángulo de rotación alrededor de este eje. El algoritmo de contacto se resuelve mediante un modelo de fuerza de contacto continuo noc varios modelos de fuerza de contacto. Ecuación de movimiento del sistema mecánico completo está integrada numéricamente usando el sistema MATLAB y sus funciones estándares ODE. Para asegurar la estabilidad numérica, la cual generalmente no está garantizada para tareas de dinámica vinculada, se utilizan dos métodos de estabilización numérica (Estabilización de Baumgart y el método de infracción directa).

Esta tesis presenta los resultados de métodos parciales y algoritmos en tareas elementales simples. Debido a la falta de datos experimentales, algunas tareas solo se verifican mediante el método de observación visual directa. El modelo completo del cuerpo humano está usado en una serie de tareas de contacto, donde se ha probado el comportamiento del modelo. Este modelo, especialmente sus parámetros (parámetros de contacto, rigidez y parámetros numéricos) no están cofigurados para simular un escenario específico. Se han configurado para que el modelo resultante funcione bien y para que de datos razonables y será numéricamente estable. Este estado puede denominarse como modelo *listo para validación*. Si el uso de este modelo fué requerido en algún caso particular, sería necesario hacer una validación completa y optimización de todos los parámetros para el ajuste correcto del modelo.

El propósito de esta tesis es crear un algoritmo general para resolver problemas de cuerpos rígidos ligados, teniendo en cuenta otros algoritmos para las nececidades de modelación

del cuerpo humano, adquirir conocimientos sobre el funcionamiento de estos algoritmos, cómo se pueden resolver mediante programación y cuáles son sus ventajas y desventajas. A pesar de ciertos límites del modelo resultante, se puede decir que el propósito de la tesis se ha logrado.

Palabras clave: modelo del cuerpo humano, cuerpos rígidos ligados, contacto, Rigidez articular, parámetros de Euler

Contents

List of Figures

List of Tables

Chapter 1

Introduction

Modelling of the human body is a highly expanding discipline of the biomechanical research. With the advantages of the fast computer processing, the researchers have started to use computers for the biomechanical modelling more frequently. The goal is to investigate numerical models of the human in different approaches for different scenarios. One example of the highly expanding area of human modelling is an automotive safety field, where virtual model of the human body or parts of the body are often use to predict or eliminate fatal injuries or death. For such purpose, the detail deformable finite element modelling method is usually applied. The complex models of particular body tissues are widely developed within the automotive safety research. With the proper description of materials and geometry, these models can calculate deformations, velocities, accelerations, stresses or rupture of various human segments. On the other hand, there might be some cases, where such complex description are inefficient or inappropriate. If we are interested only in global behaviour (kinematic and dynamics) of the system (human body), the detailed description within the finite elements are inefficient and time and money consuming. Let us imagine a simple example of a man pedaling his bike. If we consider the man and bike as a one mechanical system and the goal is to describe kinematic of the bike with respect to the position of legs and crank respectively, calculation of the stresses and deformations of the body segments or internal organs are not required. For such purpose, the classical description of mechanism can be enough to capture to motion. More complex description can be consider with the articulated rigid body approach. If the researchers are interested in the muscle forces, musculoskeletal modelling method is an appropriate tool. Such model consists of constrained rigid bodies (articulated rigid body, multibody) and model of the muscles. However, if the detailed tissue injury and deformations are required, the finite element modelling is only one suitable tool. This demonstrative benchmark example should illustrate the suitability of the various modelling methods for different cases of interest. It is not always appropriate and effective to use the most advanced model in any case. It is always necessary to select proper and adequate model for the level of our interest.

Purpose of this work is to build an in-house software for simulation of a global behaviour

of the scalable human body under different loading scenarios. Author uses multibody (articulated rigid bodies) approach for the description of the human body. Such method allows user to calculate motion under various loading in a real time simulation (or close to real time). The multibody (MBS) method has an advantage of the possibility to implement other algorithms, such as contact scenario, muscle modelling, stiffness of the joint or activation of the model. The main aim of this paper was to derived all required equations, to test the algorithms in simple benchmark examples and finally to combine all of them in one complex model.

This paper summaries the current state of the art in the models of the human body. The mechanical models of the human called ATD (anthropometric test device) or dummy are presented in the second chapter. The dummies are divided based on the direction of impact, for which they are designed (frontal, side and rear impacts, respectively). The special category are the dummy of children ATD. This chapter also describes the differences between the virtual models of the dummies and virtual models of the human body. The list of the virtual (numerical) models is presented, where the models are divided based on the modelling methods, namely the multibody and the finite element modelling. The hybrid approach combining both the methods is also described.

Third chapter is focused on the theory of multibody system. Firstly, multibody method and suitability of its application is described. The theoretical background of description of the displacement, velocity and acceleration are introduced here. Author describes utilization of the Euler angles for parametrisation of the spatial motion. The derivation of the equation of motion for free and constrained body is described, as well as for system of constrained bodies. However, since the Euler angles are know for their singular positions, and thus the instability during numerical integration, the concept of four Euler parameters is further used. Displacement, velocity, acceleration, generalized forces and total equation of motion is derived using both these approaches. The difference between Euler angles and Euler parameters is explained and discussed their pros and cons. The total equation of motion of the full human body model is derived with the Lagrange equations of a second kind with multipliers, where the spatial motion is described with Euler parameters.

This chapter also includes methods of numerical stabilization and their application in simple constrained dynamics. Sensitivity analysis of these examples for variation of the stabilization methods and parameters of the stabilization is presented, to get a view, how the stabilization affects the results and to get a hint which method is suitable for a different scenario.

Since the model is built do be scalable, to enable user to create a various size of the human, only the weight and the height is initially defined. All other mechanical and geometric properties are calculated based on these values. The wide database of human anthropometric dimensions is used to calculate these values as well as analytical algorithm for calculating mass distribution of particular body segments.

The fifth chapter describes contact analysis in multibody method. The review of the contact detection algorithms is presented followed by review of contact force models.

Finally, the methodology used in this model is described.

Next chapter shows the initial results of the particular models (one free and constrained body, double pendulum with the internal stiffness) and also the full human body model. This work does not model any particular scenario, and do not try to simulate any exact case. It builds a multibody model of the human, containing 17 rigid bodies, connected with the kinematic joints, including internal stiffness, contact algorithm and several methods of numerical stabilization. Each of the attached methods consists of some parameters, that must be carefully set up, validated and verified for each new case. This paper build the so-called "validation ready" model, and shows its benefits and its limitation.

The last chapter summaries the work, the achieved results and suggests the future improvements and possibilities of the exploitation of this human body model.

Chapter 2

Human body models - State of the art

Human body is a very complex dynamical system comprising complicated segments, such as internal organs, head, extremities, spine etc., that are made of live bio-materials. These materials are generally heterogeneous, anisotropic, visco or hyperelastic and their mechanical properties depend on many factors such as temperature, loading history, concentration of some chemical substances such as hormones etc. Due to these reasons it is not very straightforward to design a model, representing human body and his behavior for wide set of applications. The aim of biomechanical research in the field of human body modelling is to build various models, for the specific purposes. It can be a model for automotive crash tests, blood flux inside body and organs, respectively or rigid body model for global description of the human body behavior. In case of automotive industry, the physical models of the human (dummy) are currently used in the experimental crash tests and vehicle development, testing and certification. Virtual human body models can represent a real human (geometry and materials, such as bones, soft tissue, flesh and internal organs), while the mechanical dummies are made from plastic, rubber, metal or foam. The dummies are made for multiple re-use without damage and needs to repair. Thus there is no biological damage and injury in terms of dummies. The injury risk of the human is deduced indirectly within instrumental response under different crash scenario. For the purpose of injury evaluation, or probability of injury, the criteria for the specific loading and the abbreviated injury scale (AIS) were developed [35, 62, 97]. Thus, the risk of injury is based only on some statistic database, which is the best we can have, but is is not perfect and it is not fully biofidelic. The experimental tests with dummy results in mechanical values, such as acceleration, velocity, forces, torque that are used to calculate/predict an injury risk.

2.1 Dummy

In the world of the crash tests, it is common practice to use mechanical dummies as surrogates for the human vehicle occupant. Mechanical dummies are biofidelic occupant surrogate devices, that are widely used in real crash test scenarios. A crash test dummy is a full-scale anthropometric test device (ATD) that simulates passenger of the vehicle. Dimensions, weight proportions and articulation are based on the average human body. The device is instrumented to record data about the dynamic behavior of the ATD, such as forces, moments, displacements, velocities or accelerations. The concept of using dummies in the crash tests is not perfect, since the dummies are only mechanical approximation of a real human. As Yang said [43]:"*If you design a car based on dummy response, you are going to design a car that is good for dummies, but not necessarily good for humans. We have data to say that crash dummies are helping the industry to design safer cars, but they are not human-like.*" Since humans cannot be used in real crash tests, the dummies are only workable alternative approved be governments. Hopefully, in the near future, the virtual models will be approved by governments to be officially used in the certification of the vehicles. Nowadays, the virtual models are approved only for certification of an active bonnet, where virtual model of a pedestrian can be used. Human volunteers can be only exceptionally served in experimental impact tests, but only in low speed tests, where there is no risk of injury. The dummies are generally designed especially for a package of crash scenarios, such as frontal, rear or side impact. The ATD (dummy) is generally only the physical model of an average man. It is biofidelic for a certain scenarios in particular parameters. The ATD is usually biofidelic in the dimensions, masses, physiological motion of the human, but they are stiffer then human body in the joints, in the particular segments, since they consist of metal and plastic segments, instead of flesh and bones. They do not include internal organs and they cannot predict any kind of real human injury. They can provide only mechanical response (force, acceleration, displacement...) for a certain loading and this values can be interpreted in the probability of injury, that are based on limited data from experimental tests. Crash test dummies are also designed to be "re-usable" which also decrease their biofidelity.

Consequently, the dummy is designed for one specific loading (crash scenario) and it can be used only in such conditions. So, the frontal passenger dummy cannot be used in other scenario than frontal crash test of a occupant. The great overview of the current status of the ATD is presented by Haug in [53], in producer Humanetics catalogue [58] or in a new book (2019) written by Scataglini and Gunter [96]. Generally, the dummies can be divide as follows:

- Frontal impact dummy
- Side impact dummy
- Rear impact dummy
- Child dummy
- Pedestrian dummy
- Military and Aerospace dummy

2.1.1 Frontal impact

Frontal impact dummies and frontal impact testing are the foundations of current world wide highway safety efforts. It has been published [5, 35], that many deaths and injuries were caused in frontal crashes. Before their introduction, it was assumed that victims of car crashes were victims of fate. These dummies have replaced this thinking with the use of current engineering methods to prevent death and injury on the road.

"The initial purpose of the frontal impact dummy and frontal impact testing was to test restraint system effectiveness in preventing head injury, thorax injury represented by rib compression and thorax acceleration, and leg injury as expressed by femur fracture and hip dislocation. Over the years the dummy has been developed to increase its capabilities to aid the vehicle designer, crash test engineer and federal regulator" [58].

This dummy has been very effective in reducing death and injury on the roads and led to a new generation of motorists and their children, who think *safety first* and automatically use their seat belts for crash protection. The overview of some existing dummies for the frontal impact test are presented bellow.

- **The Hybrid III dummy family**

  The Hybrid III dummy is a widely used ATD for frontal impact tests [58]. This dummy family contains standard Hybrid III 50th percentile male, 5th percentile female, 95th percentile male, 10 years old (yo) child, 6yo child and 3yo child, see Fig. 2.1. The previous version Hybrid II, average male is still using. The Hybrid III 50th percentile male crash test dummy is one of the most widely used crash test dummy in the world for the evaluation of automotive safety restraint systems in frontal crash testing. However, in last few years, it is replaced but more advanced Thor dummy. This Hybrid III dummy is regulated test device in Europe, Asia and in the United States, respectively. The 50th percentile Hybrid III represents a male with the weight equaling to 75.5 kg and height equaling to 175 cm [35, 58, 117, 41]. The 5th and 95th percentile dummy is an scaled equivalent of the average ATD. 95th percentile dummy has height of 188 cm and mass of 100 kg, while the "smaller

sister" female 5th percentile Hybrid III has height and weight of 152 cm and 50 kg respectively.

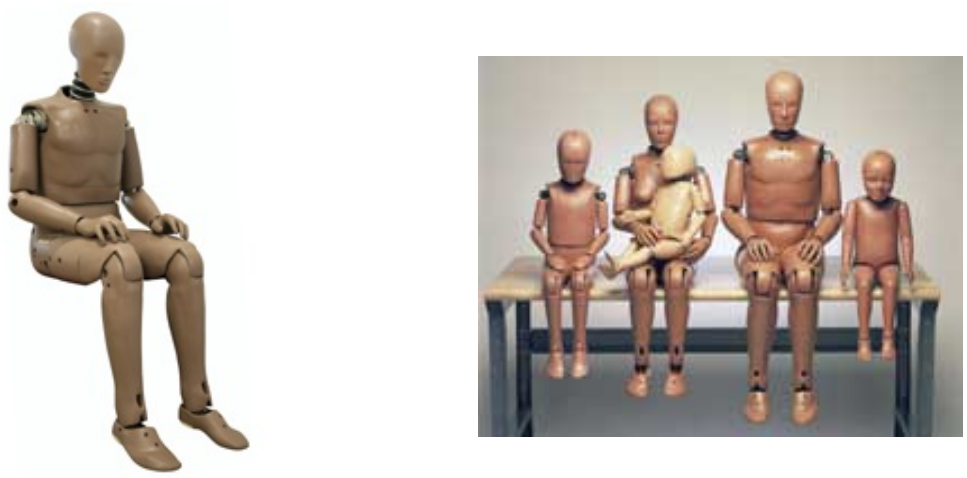

Figure 2.1: Hybrid III dummy 50th percentile [58] (left) and dummy family [2] (right)

- **THOR**

  This dummy was developed in the USA by NHTSA (National Highway Traffic Safety Administration [18]) and is used for the frontal test. THOR has more human-like features than Hybrid III, as a spine and pelvis that allow the dummy various seating positions, such as sitting upright or slouching [35, 58]. THOR has currently two anthropometric version: 50M (average male) and 5F (5th percentile female). THOR dummy is also widely used ATD, similarly as HIII. Moreover, it starts to play more important role in the car safety than Hybrid III. In addition, EuroNCAP is considering to use the THOR-50M dummy for the future frontal impact tests as a part of their continuous efforts to improve road safety. The THOR dummy is displayed at Fig. 2.2.

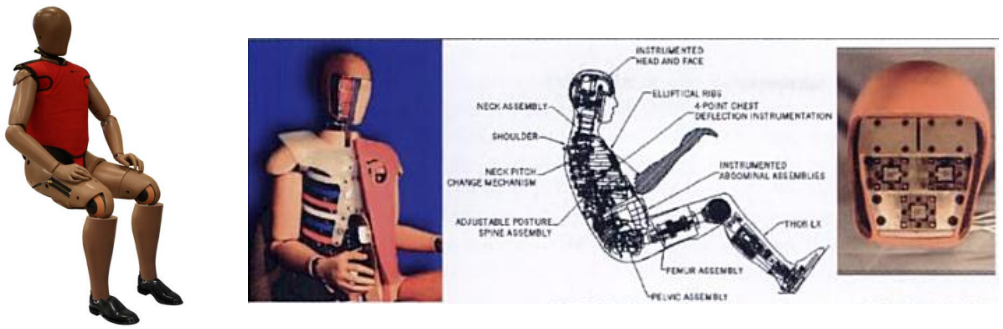

Figure 2.2: THOR dummy [58] (left) and components and load sensors [35] (right)

The Hybrid III and THOR dummies are the most common used ATD in a world of automotive safety development. Today, they are both triggered under company Humanetics [58], as a world producer and distributor of the real and virtual dummies. In the following, there is a list of several other frontal dummies, but they are rarely used. They are applied usually for some special cases, where the Hybrid or THOR cannot be used, or they work as a advanced tool of such ATD.

- **TNO-10**

  The TNO-10 dummy was developed as a loading device for testing vehicle belts in a simulated crash scenario [58]. This dummy represents a 50th percentile male. Since this dummy is used only for testing of the belts and for reasons of simplicity, the dummy has no arms and only one lower leg, see Fig. 2.3.

Figure 2.3: TNO-10 dummy [58]

- **Body Block**

  The dummy Body Block [58] is designed and manufactured to meet the requirements of the SAE (Society of Automotive Engineers) standard [20], steering Control System - Passengers Car - Laboratory Test Procedure - SAE J944A [21]. Despite the fact of canceling this standard at 1992, it is still continuously demanding by vehicle and equipment manufacturers. The Body Block dummy is shown in Fig. 2.4.

Figure 2.4: Body block dummy [58]

- **MAMA2B**

  Maternal Anthropometry Measurement Apparatus Version 2B (MAMA2B) [58] is a kit with pregnant abdomen and torso for a small pregnant dummy, see Fig. 2.5. This device can be fitted to the standard Hybrid III small female dummy. The MAMA-2B is still an ongoing research and development product.

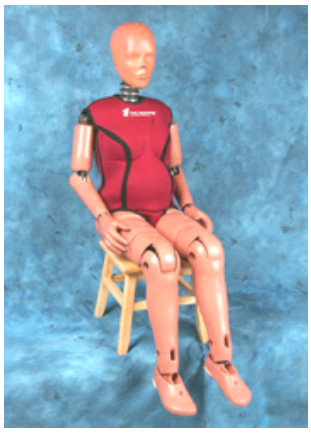

Figure 2.5: MAMA2B dummy [58]

- **OCATD 6**

  Occupant Classification Anthropomorphic Test Device 6 (OCATD 6) is a developing science designed device to address the need to adjust or suppress the deployment of an airbag depending on the size of the person sitting in the seat. New regulations in the US are expected to require the airbag to be suppressed if a child smaller than the average six year old is occupying the front passenger seat [58]. The OCATD 5 and OCATD 6 represents the 5 years and 6 years old small child, respectively, see Fig. 2.6.

Figure 2.6: OCATD 6 dummy [58]

2.1.2 Side impact

Nader in his work [82] demonstrated that many deaths and injuries were caused in side, low speed, 15-30 mph (25-50 km/h) crashes. Over a half of the fatalities were caused due to head injury, followed by thorax injury and debilitation due to femur breakage or hip dislocation. These could be caused by hitting the windshield, the headliner or the steering wheel during the side impact [58]. In order to capture such effects, the side impact dummies (SID) were developed and brief list of these dummies is given bellow. The SID (Side Impact Dummy) family of test dummies is designed to measure head, neck, rib, spine and internal organ loading in side collision. It also accesses spine and rib deceleration and compression of the chest cavity. The SID dummy is the US government testing standard, EuroSID is used in Europe to ensure compliance with safety standards.

- **EuroSID 2**

  EuroSID, see Fig. 2.7 was developed be the European Experimental Vehicles Committee (EEVC) and is currently used to access compliance with the European side-impact requirements [35]. EuroSID 2 is the next generation of EuroSID dummy that is incorporated with the number of advanced technologies, compared to the first generation. The EuroSID-2 was developed by the SID2000 program, a consortium of

European researchers, automotive manufacturers and dummy manufacturers. The EuroSID dummy does not have a lower arms. The total mass of this dummy is 72.0 kg.

Figure 2.7: EuroSID dummy [58]

- **BioSID**

  BioSID dummy is based on General Motor design. It is slightly more advanced compare to SID and EuroSID, but it is not defined as the official dummy to be used in certification tests. The dummy SID, EuroSID and BioSID are designed to represent 50th percentile male of the height 178 cm and mass equalling to 77 kg [35].

Figure 2.8: BioSID dummy [53]

- **WorldSID**

  WorldSID (5th female and 50th percentile male), see Fig. 2.9, stands for worldwide harmonized side impact crash dummy to be used for the assessment of vehicle occupant injury risk in lateral impact. It is designed to be used as a standard, regulatory test tool as well as a research tool for a multitude of impact conditions [58].

(a) WorldSID 5F[58]

Figure 2.9: WorldSID dummy 50M (left) and, 5F (right) [58]

- **SID-H3**

  The SID-H3 dummy, see Fig. 2.10, combines the body of the US DOT SID with the head and neck of the Hybrid III 50th percentile male test dummy [58].

Figure 2.10: SID-H3 dummy [58]

- **US DoT SID**

  US DoT SID is the first side-impact dummy was developed in 1970s by the National Highway Traffic Safety Administration (NHTSA [18]) of the US Department of Transportation (DoT). US DoT SID dummy, see Fig. 2.11, is still used in the US for the testing of side impact test of the new cars [35].

Figure 2.11: US DoT SID dummy [28]

- **SID-IIs**

  The SID-IIs female Small Side Impact Dummy is a new generation crash test dummy to specifically evaluate advanced automotive side impact protection systems, particularly side airbags, see Fig. 2.12.

Figure 2.12: SID-IIs 5th Female Side Impact dummy [58]

2.1.3 Rear impact

A rear impact dummy (RID) was developed mainly to measure the risk of minor neck injuries, known as a whiplash [25, 97], during low-speed rear crashes. This effect can be sometimes hard to quantify, but it is very debilitating for the undergoing persons. Such kind of injury can cause a serious problems to the patient, not only immediately after accident, but several months or years after. This injury is really hard to measure or quantify, since it can cause trouble of the head, neck and of the entire spine. Thus is really important to study and prevent this injury, because it can frequently happen also in low speed crash. This injury is caused mainly by relative motion of the head with respect to the neck and due to its higher mass and inertia, see Fig. 2.13.

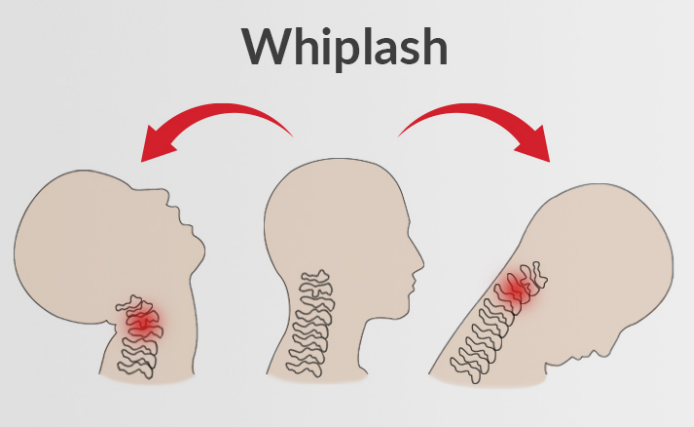

Figure 2.13: Whiplash injury mechanism [25]

- **BioRID II**

  BioRID was developed in the late 1990s with the group of the Chalmers University of Technology in Gothenburg (Sweden), restraint manufacturer Autoliv and car makers Saab and Volvo. It is designed in order to represent a 50th percentile size man, 5 feet 10 inches tall (178 cm) and weight of 170 pounds (77 kg), see Fig. 2.14. BioRID was designed especially to capture the relative motion of the head and torso. In the crash scenarios, where the vehicle is struck in the rear, the BioRID dummy can help to learn how the seatback or head restraint system influence the likelihood of the whiplash injury [35, 58].

Figure 2.14: BioRID dummy [58]

2.1.4 Child dummy

These dummies are important in the development of protective equipment for children in the vehicles. Investigation in the children restrain system is efficient way how to minimize the number of fatalities or injuries of a young population. During the past, there was a common practice for the parents to hold their children only with their arms. Under deceleration even during the low speed impact, the child's effective weight can be multiplied 10 to 20 times, making them impossible to hold. Thus, there were the need to develop and test the dummies for smaller, younger occupants to provide them and effective crash protection. The child is not only a down scaled version of an adult person, it has different mass and inertia distribution and body dimension of the body segments. So, the development of a special children dummy is more then required for the better protection of our young population.

- Hybrid III dummy

  The wide family of the Hybrid III dummy also contain the child dummies. There exist the 3 years old (3yo), 6 years old (6yo) and 10 years old (10yo) child dummies, see Fig. 2.15. These small human body dummies were also successfully tested and validated within wide set of experiments and simulations [35, 58].

(a) Hybrid III 3yo (b) Hybrid III 6yo (c) Hybrid III 10yo

Figure 2.15: Hybrid III child dummies [58]

- **SID-IIs**

  The Small Side Impact Dummy (SID-IIs or SID-2-s) is a new generation crash test dummy for evaluation advanced automotive side impact protection. Anthropometry is based on the Hybrid III 5th Female Dummy, similarly to the weight of 12-13 years old child [58], see Fig. 2.16.

Figure 2.16: SID-IIs dummy [58]

- **CAMI**

  The CAMI are a small family with the newborn dummy (CAMI 6 months old). This dummy is based upon a leather skeleton, which has approximately the external shape of the 6 month old occupant, see Fig. 2.17. The six moths old dummy has the weight of 7.7 kg and the sitting height is approximately 45 cm [58].

Figure 2.17: CAMI dummy [58]

- **P-series Child dummy**

  The P-series dummies are the simplified ATD used for infant occupant protection. The dummy consists of a plastic skeleton covered with flesh and skin simulating polymer, see Fig. 2.18.

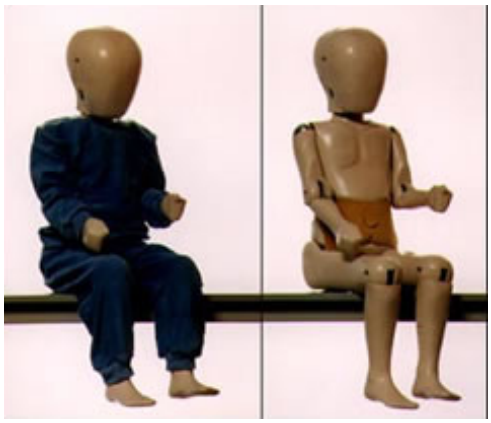

Figure 2.18: P-series child dummy [58]

- **Q-series Child dummy**

  The Q-dummies were developed as a series of child dummies that covers almost the complete child population up to 10 years, see Fig. 2.19. The Q-series dummies are still testing tools for the European regulation UN-ECE Regulation 44 and are also adopted by many other standards [58]. The Q-series dummy differs considerably from the P-dummies. It is not only advanced in terms of its biomechanical and anthropometric characteristics, it is also developed to be used in both front and side impact testing, making it the first "multi-directional" dummy.

Figure 2.19: Q-series child dummy [58]

- **CRABI**

  The Child Restrain Air Bag Interaction (CRABI) dummy family concerns 6 months old dummy (mo), 12 months and 18 months old dummy, see Figs. 2.20. It was designed by the First Technology Safety System (FTSS) to evaluate child restrain system, including an airbag [35, 58].

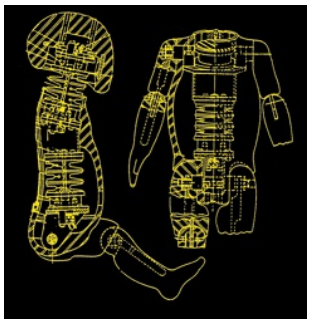

(a) 6mo child dummy

(b) 12mo child dummy

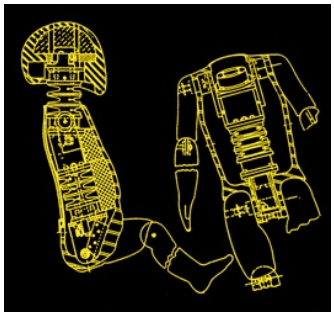

(c) 18mo child dummy

Figure 2.20: CRABI child dummies [58]

2.1.5 Pedestrian dummy

Pedestrian dummies, see Fig. 2.21 are really important in the development of modern vehicles. Tests with these dummies help to dictate the frontal shape of the vehicle so that the effects of car-pedestrian impacts are mitigated to prevent injury and death.

"Pedestrian dummies are used to aid the vehicle designer in developing the forward surfaces of the car both in shape and impact response to lessen the negative effect of a pedestrian impact. Wound injuries were caused by rigid hood ornaments. Leg breakage was caused by bumper impact. High grilles caused thoracic damage. Head injury was caused by impact with the bonnet and windshield. Knock-down and run over accidents were caused by interaction with the front of the vehicle" [58].

For the pedestrian testing, the Hybrid III dummy was modified in all three version (5F, 50M and 95M). These pedestrian dummies were modified in torso and a knee area, especially for testing of the impact of the car-bonnet and bumper to the body. This dummy can be also used in the non-automotive application (wheel chair, recreation vehicles, sport gear and medical devices).

Figure 2.21: Hybrid III M50 pedestrian kit [58]

Besides the total pedestrian model, there are also a set of section models, used for the development of the vehicles, safer for the pedestrian. The most commonly used ones are head-from impactor and leg-form impactor. Since the head and leg (knee) are the most injured region of the pedestrian [5], the highest effort is spend with these two impactors, see Figs. 2.22.

Figure 2.22: Head-form (left) and Leg-form impactor (right) [58]

2.1.6 Military and aerospace dummy

Aerospace and military dummies cover a wide range of applications such as civilian aircraft testing, fixed wing and rotary; military parachutes; aircraft with crew ejection seat systems or ballistic and blast impact counter-measures. The dummies for the military and aerospace applications are generally based on the standard automotive dummies, but they are improved and modified for their specific usage. The full body dummies are based on Hybrid III and EuroSID.

- **FAA HIII 50M**

  The Federal Aviation Administration (FAA) Test Dummy is a modification of the Hybrid III 50th percentile male automotive crash test dummy, see Fig. 2.23. The FAA dummy modifications are made in the lower torso and in the legs to equip the dummy to be used in testing per Federal Aviation Administration regulations for emergency landing dynamic conditions, [15]. The FAA dummy is modified to give it an erect seated posture, replacing the "driver slouch" of the automotive dummy, [58].

Figure 2.23: FAA Hybrid III M50 dummy [58]

- **MIL SID**

  The military side impact dummy (MIL SID) is a dummy with the core components from 50M EuroSID 2 and head and neck section from 50M Hybrid III dummy incorporated with the new type of neck load cell and military lower legs, see Fig. 2.24. Such dummy is currently used for evaluation of a mine blasts and under body blasts. The MIL SID dummy has capability to measure lateral and vertical force loading the body.

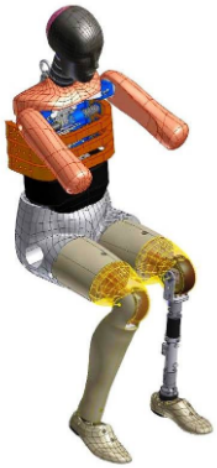

Figure 2.24: Military 50M side impact dummy [58]

- **Body region dummy**

  The military and aviation applications sometimes requires only some body part models, similarly to the automotive, for the particular configurations. The parachute dummy, is only a torso corresponds to a 95M dummy, see Fig. 2.25a. The parachute

dummy is the most rugged dummy of all. It is designed to withstands a repeated free fall with the minimum damage.

The Military Lower extremity legs dummy is a special version of the 50M dummy leg designed for the analysis of the under vehicle mine impact and blast, see Fig. 2.25b. It is a straight leg design with energy-absorbing elements, optimized for measurement of vertical forces and accelerations. This special leg is used in the MIL SID dummy.

Facial and Ocular CountermeasUre (FOCUS) headform impactor is a dummy developed for the eye and facial injury analysis to test and evaluate various protective devices and other equipment under impact events, see Fig. 2.25c.

(a) Parachute torso dummy [58]

(b) Military Lower Extremity (50th Male) Legs [58]

(c) Facial and Ocular CountermeasUre headform impactor [58]

2.2 Virtual human body model

Virtual models of the human body, human body parts as well as virtual model of the dummies are virtual approximations of their physical origin (real human or dummy). Such models play really important role in the development of the vehicles. However, they are not fully accepted within the regulations for the certification [41], they are abundantly used in the process of development and innovation. They enable the researches to perform and simulate thousands of scenarios, that cannot be physically tested. Or, they can by tested, but with the really high cost. The virtual models of the human can be designed for the multiple applications, or single purpose, but there is no one model, that can be used for unlimited scenarios. Each model has its suitable range of usage, has its limitations and has its own pros and cons. Generally, the models can by dived based on the behavior or mathematical principle used (rigid - MBS, deformable - FEM or partially deformable - Hybrid).

2.2.1 Virtual model of the dummy

Besides the mechanical dummies (occupant surrogates) and virtual models of a real human body, there also exist numerical models of the dummies. They are designed in order to model the dummies, with all their segments and materials (metal, plastic, rubber or foam). The simulation responses performed with this dummy model should correspond with the responses of the experimental dummy, not with the real human. However, the mechanical dummies are designed to be the best, suitable approximation of the human body, but still only approximation. Their virtual models are basically model of the model. Several studies comparing dummy, real human body, virtual models of the dummy or virtual models of the human body were published [29, 30, 39, 74, 80, 87].

Generally, for each physical dummy, there exists its virtual model, designed in the specific computational software [28, 35, 43, 58, 117]. The most common dummy has several versions of the virtual models (finite element model, multibody model or only CAD geometry) and can have equivalent models for several software (LS-Dyna [42], Pam-Crash [14], Ansys [10], Radioss [8] or Abaqus [7]). These virtual models of the dummy can have several versions, based on their purposes. Only a brief example of one dummy model is presented on the Hybrid III dummy. Similar database of the virtual models is available also for the THOR dummy. These virtual dummy models were developed based on material, components and full body tests performed with the real dummy.

- **Hybrid III dummy FEM model**

  The dummy family Hybrid III was modelled based on finite element method (FEM) in order to develop virtual model of the mechanical dummy. The models of the entire Hybrid III dummy family were designed and these finite element models are shown in Fig. 2.26. As was previously discussed, the finite element model is a very

complex mechanical system, based on discretization of the continuous system into a discrete subsystems. As an example of the complexity of such FEM model, 50th percentile dummy model has more than several thousands elements [28, 78].

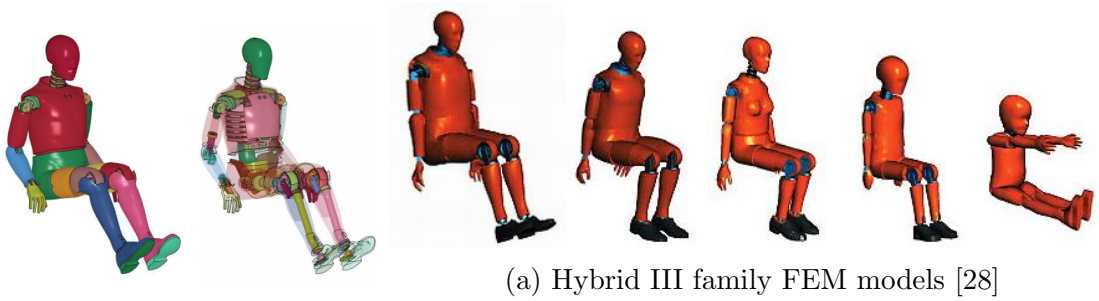

(a) Hybrid III family FEM models [28]

Figure 2.26: Detailed HIII FEM model [78] (left) and HIII family [28] (right)

- **Hybrid III dummy MBS model**

  Some of the dummy models are made either as a complex finite element model and as a simple multibody model. Multibody modelling is based on the linked tree structure of the rigid bodies. Such models can also contain a few deformable parts. They execute faster than complex FEM model, but they are not able to yield detailed deformation and thus the injury. As an example of the MBS model of the dummy, Hybrid III MBS model are shown in the Fig. 2.27.

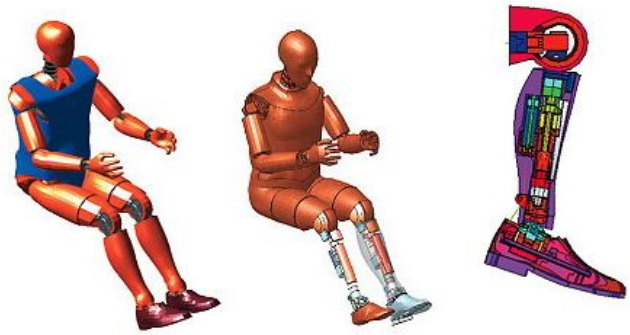

Figure 2.27: Hybrid III MBS dummy model [28]

- **Side impact dummy FEM model**

  Finite element models of the side impact dummies, namely the EuroSID and US DoT SID are presented in the Fig. 2.28.

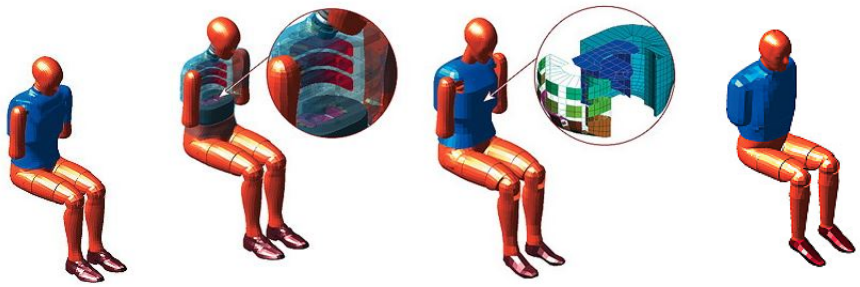

Figure 2.28: EuroSID FEM (left) and US DoT SID FEM (right) dummy model [28]

2.2.2 Virtual human body model

Virtual human body models play an important role for designing, development and optimization of the vehicles and safety system, interacting with the occupant or passenger. Application of the virtual human body models in the numerical testing can help to design, test and optimize passive and active safety technologies, such as restraint systems, road barriers, airbag systems, emergency breaking, collision avoidance system, active bonnet etc. Generally, there exist two main approaches for the human body modelling. The first group is detailed deformable finite element models and second one is articulated rigid body models (multibody). Recently, the combine (hybrid) approach starts to be an important tool in the automotive research. From each of the group, one can find large database of the models, developed for the specific applications or developed with the particular research group or under different software. Nowadays, more and more researches are building their own numerical/virtual models of the human body or its segments. Generally speaking, the main problem of the human models are appropriate material models and validation of the models. The human body geometry is quite good known and do not significantly vary with the subject. Respectively, there is a correlation between total height and total mass and anatomical segments dimensions. Moreover, with the highly developed technologies such as computer tomography (CT) and magnetic resonance image (MRI) and post-processing tools (Mimics [17], Slicer [6] or Amira [9]), the generation of the body geometry can be quite straightforward task, but still time consuming. However, the material definition is very complicated and it suffers with several issues. The main one is a lack of the experimental data. Some tests are just not possible to be done, some tests were done with the ill-known conditions, and thus the results are disputable, and some tests were performed with the different specimen/subject, in the different laboratory (conditions), with the different outputs etc. and thus it is hard to used them and trigger together. Moreover, the materials of the live-human subject are very complicated materials and depend on many specifications (age of the specimen, loading history, history of storage, sensitivity of measuring devices, experiences of the testers, chemical substance inside the sample (hormones...) and so on. The group from USA [23, 24] recently came with the idea of worldwide database of materials and validation tests. However, because

of complicated interpretation of the results and because of property rights, this idea is not going to happened in the near future. Thus, there exist thousands of virtual human body models, each of them with some specific advantages and disadvantages and its particular field of applications. This document brings a brief overview of the most advanced and known model as well as some specific and interesting models that can have relationship with the University of West Bohemia.

This overview of the biomechanical models for occupant safety is structured based on the mathematical method used in the model (deformable FEM, rigid MBS and hybrid approach).

- **MBS**

  Simple model based on the system of the articulated rigid bodies, that can be constrained in the kinematics chain. Such approach is called Articulated Rigid Body (ARB) or MultiBody System (MBS). In terms of the classical mechanics, these models concern only basic segments of human body linked with the joints, corresponding to the real human body joints. These segments are approximated with the rigid bodies, where only the location of centre of gravity, mass, geometry and tensor of inertia are required. They execute in very fast central processor unit computer time (CPU), but cannot reflect detailed deformation of the bodies, and thus, for example injuries of the human. This approach is useful, when the deformations of the segments are not required and the global behavior of the model is to be analyzed. The deformation of the bodies can be partially implemented via the contact stiffness and damping ratio. Despite the fact, that these models are really simple, they still play important role in the process of vehicle development.

- **FEM**

  Complex model are based on discretization of the continuum, within finite elements (Finite Element Method-FEM). In terms of mechanics, these models are based on detailed geometry of the whole human body, segments of the human body and possibly all the internal organs. For every tissue and organ, respectively, the exact material properties are required and these are not easy to be determined and validated. On the other hand, with the detailed finite element model, the stress, strain, deformation can be calculated. These quantities are more readily linked to the injury of the human body.

- **Hybrid**

  This approach combines FEM and MBS approach, to build a model simple enough to enable fast calculation but also includes deformable elements, to calculate local deformations and predict injury risk of the occupant.

Multibody model

- **MADYMO**

  MAthematics DYnamics MOdel is engineering software tool, used for the design, analyzing and optimization of the occupant and pedestrian safety [22]. It is a virtual software based on the multibody principle. Human model under MADYMO software provides a tool set capable of realistic human response prediction for a broad range of loading conditions, where no crash test dummy exists. The MADYMO human model portfolio comprises both passive and active models. MADYMO human models can be used for front, side, rear and vertical impact as well as intermediate impact directions and more complicated scenarios like roll-over. MADYMO software includes active adult human model, passive adult human model, child human model and pedestrians human model, see Fig. 2.29. The MADYMO model is validated human body model used in a real application, it is a scalable model, comprises passive and active muscles and it reports better biofidelity than standard crash test dummies.

(a) MADYMO active model

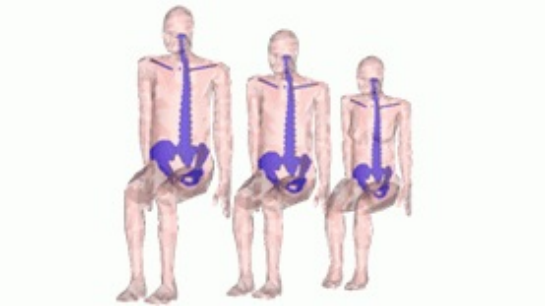

(b) MADYMO passive model

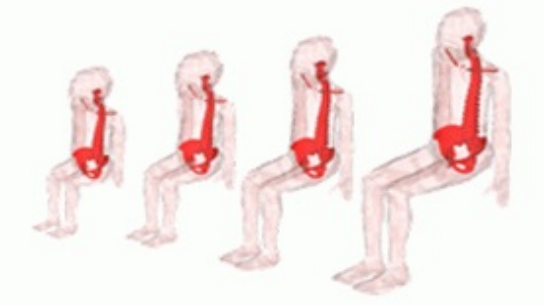

(c) MADYMO child model

(d) MADYMO pedestrian model

Figure 2.29: MADYMO articulated rigid body models [4]

- Human Articulated Rigid Body (HARB) - Robby

  This model was developed by the cooperation of the University of West Bohemia and ESI Group (Engineering Simulation for Industry) [50]. The model consists of rigid

bodies (head, fully articulated spine, thorax, abdomen, upper and lower extremities), connected with kinematics joints with non-linear biomechanical responses. The Robby family contains 50th percentile male (Robby), 5th percentile female (Robina) and also 6 years old child (Bobby), see Fig 2.30. The aim of this model was to divide the human body model given by meshed geometry into the several rigid bodies representing the real human geometry. Furthermore advanced shoulder joint, including passive muscle model, was added to the system. The Robby model was validated against sled test [60], where head and thorax acceleration were observed and compared with the experiment. For more details, see [35, 60, 61].

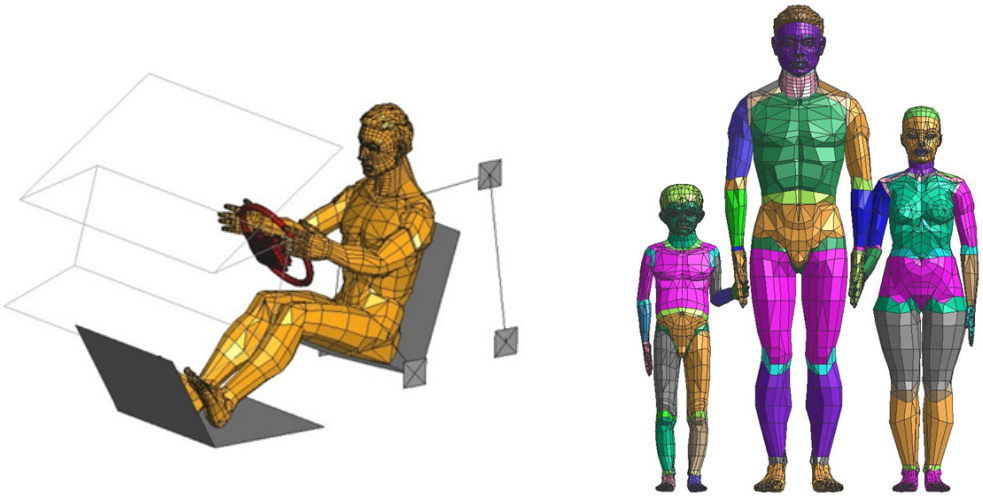

Figure 2.30: Robby model in sled test configuration (left) and Robby family: Robby, Robina and Bobby [60] (right

- **Anybody**

  The musculoskeletal simulation software AnyBody (AMS, AnyBody Technology A/S, Aalborg, Denmark, V. 7. 2. 0.) [72] is used for modelling of the active human body models, see Fig. 2.31. The rigid segments of the human body are connected via joints and active muscles. This software enable user to run forward and inverse dynamics. The AMS software is a very helpful tool in prevention and rehabilitation of the injury, or calculation of the body loading under defined motion. Together with the advantage of the 3D motion software, the reaction forces of the internal joints can be calculated. The Anybody software is currently used also in the biomechanics of athletes, to increase their training performance or to avoid injury or recover after the injury. This model is partially open platform, where the users can added the newly developed and validated model into a special repository, that can be used (after approval) by other userd.

Figure 2.31: Human body model in the AnyBody Modelling system [72]

- **Parametric multibody model in *alaska***

  This model of a human body was built based in real data from z IfM Chemnitz [31]. It consists of 12 rigid bodies connected via 12 mechanical joint. The model respects basic human anatomy and it was developed for the purpose of car simulations, see Fig. 2.32. It is suitable for vehicle driver or passenger simulations. Such parametric model is driven with the initial height and weight as an input and the mass, geometric and inertial characteristic of the bodies are calculated with respect to this inputs. The model was created by Polach [90] in alaska modelling software [75].

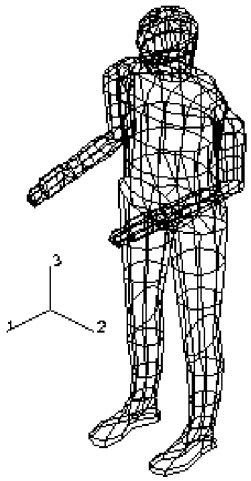

Figure 2.32: Multibody model of male-human body in software *alaska* 2.3 [90]

One of the important advantages of the MBS model is the easy way to set up a different position for a different test configurations (positionability) and scalebility. The segments

can be easy translated or rotated around the particular joint. Despite the fact, that these models can generally catch only global behaviour of the human body, they report significant benefits for hybrid human models or active models for safety [62] or the calculations, where the global dynamics of the body is the main goal. They are very usefull for instance in the parametric studies, sensitivity analysis or numerical optimizations. The results from this kind of calculation can be also used as an input (loading) for the FEM modelling.

Finite Element Model

- **GHBMC**

  The GHBMC is an international consortium of car-makers and suppliers working with research institutes and government agencies on the advanced human body model for crash simulations. The goal of the consortium is to concentrate human body modelling research into a single global effort. Members of the GHBMC currently include for example General Motors Corp., FCA US LLC, Honda R&D Co., Hyundai Motor Co., Nissan Motor Corp. Ltd., PSA Peugeot-Citroën, Renault s.a.s., Joyson Safety Systems. Ford Motor Co., NHTSA (National Highway Transportation Safety Administration)or Autoliv Inc. contributing to the technical development. The GHBMC has developed a family of virtual humans including male and female seated occupants of various sizes and pedestrians including a six year old child.

  The GHBMC model is intended for use in vehicle crash simulations and is placed in a driver position, see Fig. 2.33. The model was tested and validated over than 20 impact scenarios [46, 62] and the validations is still increasing for more performed tests. The latest version of the model is very complex with detailed tissue geometry and it has about 2-3 millions finite elements [12, 16, 37, 36].

  The GHBMC model is really the most advanced and detailed model of a human body. It consists of detailed geometry of the human body, down to the single ligaments, neurons, muscles or cartilage segments, see Fig. 2.35a. The total GHBMC family include 13 individual models plus age scaled and obese model, see Fig. 2.34. The GHBMC is currently dealing with age scaling models up to 65yo, with the morphing of the model, obese population, active muscle model implementation etc. For all these variations, the highly detailed database of material and components tests are required as well as set of validation tests. The GHBMC model stands for numbers of publications worldwide connected mainly with automotive safety, the list of paper can be seen in [12, 16].

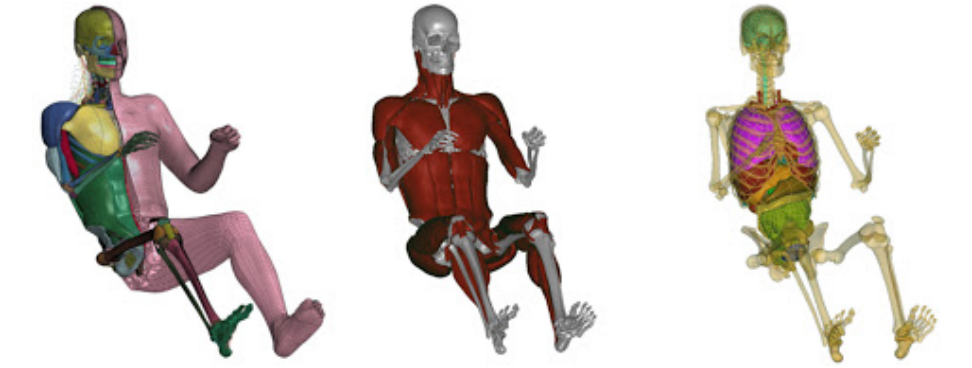

Figure 2.33: GHBMC 50th percentile model in the driver position [12]

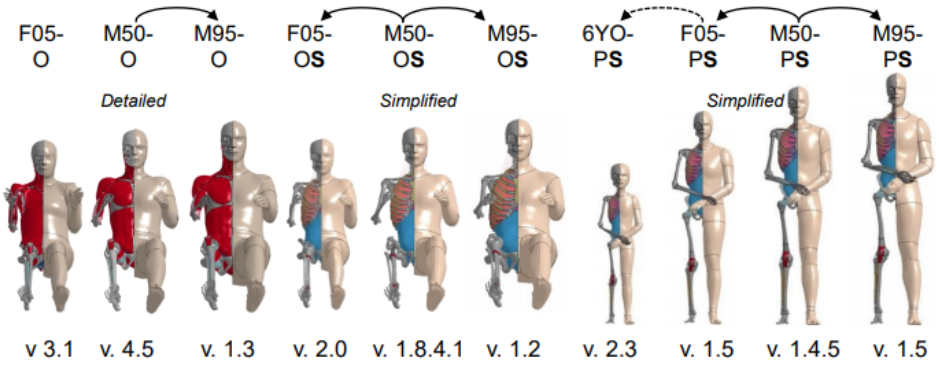

Figure 2.34: Family of the GHBMC [36]

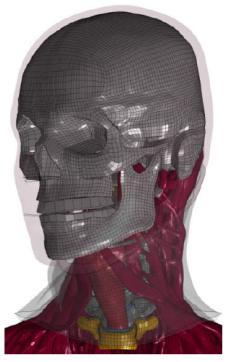

(a) Detail of the head and neck model [16]

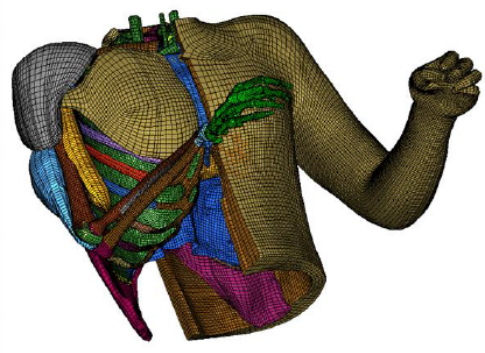

(b) Detail of the thorax [12]

Figure 2.35: GHMBC model in detail

- **THUMS**

  The Total HUman for Safety (THUMS) was assembled and tested by a joint development of Toyota Motor Corporation and Toyota Central R&D Labs [3, 35, 62, 119]. The THUMS model represents human body in detail, including the outer shape, bones, muscles, ligaments, tendons and internal organs. Therefore, THUMS can be successfully assembled in automotive crash simulations to create a vehicles, safer to occupants and pedestrians.

  THUMS is a full family comprises numbers of models, such as 50th and 95th percentile male, 5th percentile female, 3, 6 and 10 years old child models or pedestrian model, see Fig. 2.36. Current version of THUMS ver. 4.0, 50th male, has about 1.8 millions elements and consists of numerous 3D and 2D parts, representing different tissues of a human body, see Fig. 2.37.

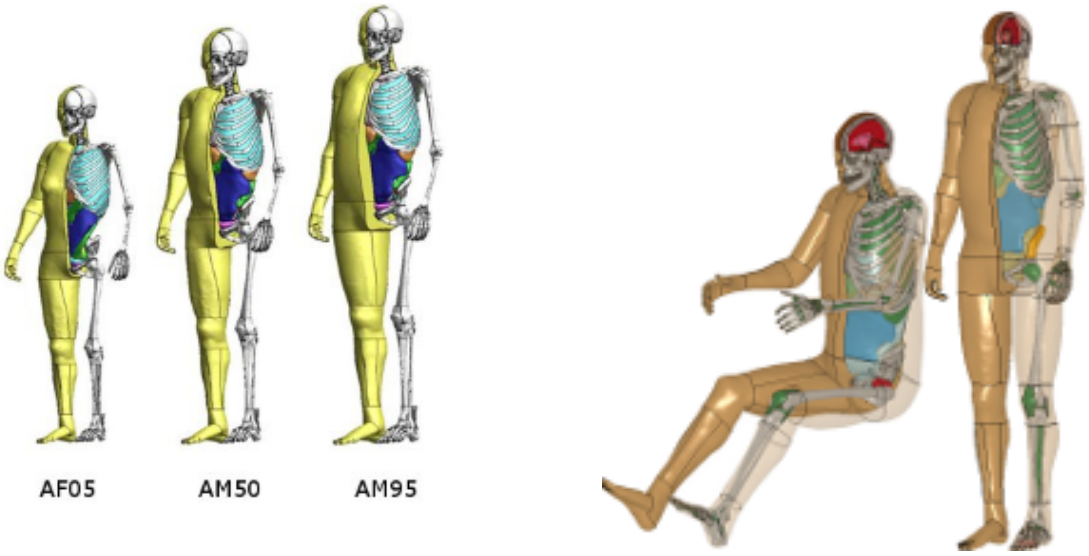

Figure 2.36: THUMS model [11, 13]

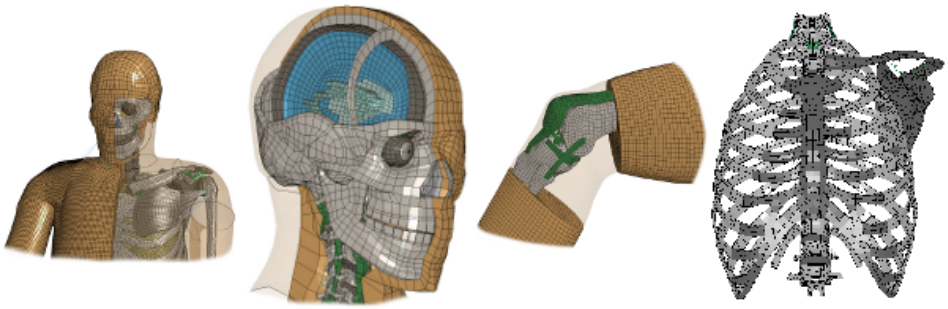

Figure 2.37: Detail of the THUMS model [13]

- **Simulated Injury Monitor-SIMon**

  This model was developed by experts at NHTSA [18] and it can directly simulate injury of the body. The SIMon software package is being developed for the advanced interpretation of injury mechanisms based on kinematic and kinetic data measured via anthropomorphic test dummy and applying to the human mathematical models embedded in SIMon. The SIMon software is primarily focused on development of new generation of head and brain models [104]. The current state of the model are shown in the Fig. 2.38.

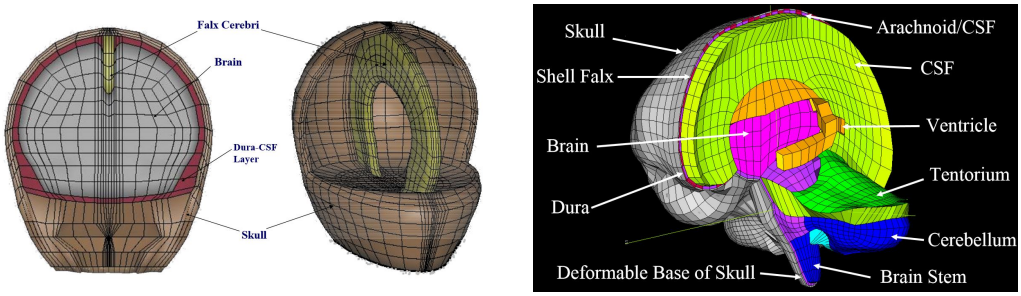

Figure 2.38: SIMon FEM model of head and brain [95]

- **LAB Human Model**

  The LAB (Laboratoire d'Accidenologie et de Biomécanique of PSA: Peugot, Citroën, Renault) in collaboration with several companies, developed a 50th percentile male human body model based on finite element method with about 10 000 elements, see Fig. 2.39. The model was validated within database of about 30 tests [35].

Figure 2.39: LAB human model in driver position [35]

- **RADIOS-HUMOS**

  The Human Models for Safety (HUMOS) was developed under European HUMOS project [94] by the cooperation of TNO, ESI Software and Mecalog. RADIOSS is a

part of Alair HyperWorks numerical software package [8]. The head and skull were developed with the collaboration of the University of Strasbourg. The RADIOSS-HUMOS model is displayed at Fig. 2.40, for more information, see [8, 35, 94].

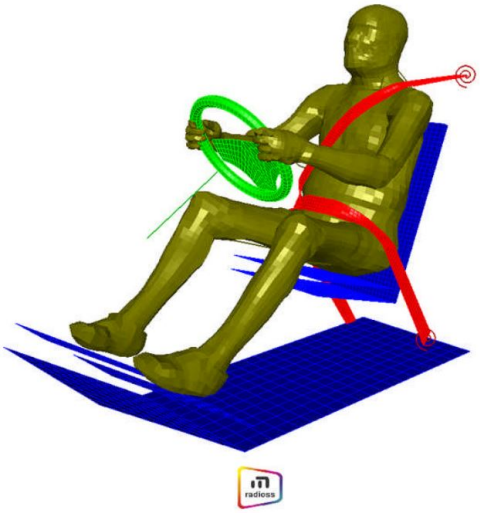

Figure 2.40: RADIOSS-HUMOS human model in driver position [65]

- **WSU Human FE model**

  The Wayne State University (WSU) model was a basement for many workers and institutions for their own biomechanical research (General Motors, ESI, Nissan, Toyota, etc.) [35]. Over the last few years the research at WSU is mainly focused on detail modelling of the head and brain respectively, see Fig 2.41. For example WSU's brain model itself consists more then 300 000 elements. These models are more advanced and they have been validated within the experiments, performed at the centre itself. As an example of the complexity, the bone of the skull has three main layers (thin inner and outer layer and one thick inside layer). Each of this layer is included in WSU model and each of them has its own material properties. The model of the human head and model of whole human body is displayed at the Fig. 2.41. The WSU is now mainly focus on the traumatic brain injury (TBI) and improvement of the head and brain model towards the TBI model prediction and decreasing the number of TBI in the population. WSU stands for the top research in the brain modelling and brain injury calculation.

(a) WSU human body model [1]

(b) WSU head model [43]

Figure 2.41: Wayne State University FEM model

- **Honda Human FE model**

  Baseline Honda Human model represents anthropometry of the 50th percentile male, which might be scaled to any size of adult and also 6 years old child model. The model was created mainly for a pedestrian analysis crash scenario [41].

- **JAMA Human FE Model**

  The Japan Automotive Manufacturers Association, Inc (JAMA) model is based on the coupling of the upper body from THUMS (Ver.1.4), the lower body from Honda model, see Fig. 2.42. The model was modified to improve biofidelity and numerical stability [41, 86]. The JAMA human body model is available for two solvers, PAM-CRASH and LS-DYNA, respectively.

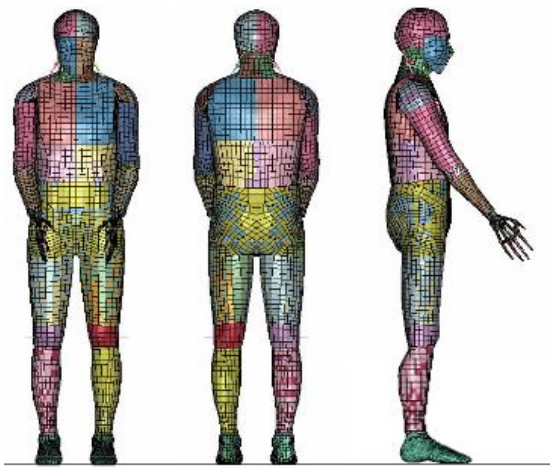

Figure 2.42: JAMA pedestrian FE model [102]

- **OSCCAR**

  OSCCAR - future occupant safety for crashes in car is a new European project, that point to the future occupant modelling and safety. OSCCAR uses a comprehensive integrated approach for the development of future advanced occupant protection systems. It will provide a unique human body model (HBM)-based development and assessment framework, covering main challenges of future road safety due to the introduction of highly automated vehicles as well as changes in demographics: relevant accident scenarios (mixed traffic), future vehicle interior designs, new occupant sitting positions, aging and obese population etc. This demands for targeted changes and adaptions of scenarios, procedures and tools for occupant safety development, assessment and homologation, not addressed by current regulations or consumer crash tests [19]. Project OSCCAR does not built a new human body model, it creates a database of the models, tests, crash scenarios, passive, active and future safety systems. OSCCAR will develop and demonstrate advanced occupant protection principles, fully integrated assessment methods for complex test crash scenarios and contribute to the harmonization of human body models.

Hybrid Model

The combination of the multibody structure together with the deformable finite elements can build a new set of models. Let us called this hybrid approach. Human body models based on multibody and finite elements method have some advantages and disadvantages. Since the simple MBS model has great benefit in the calculation time (minutes), it has low contribution in the stress and deformation knowledge, and thus low contribution in the injuries risk. On the other hand, complex FEM provides precise information about detailed deformations, stress and injuries. However, this benefit is balanced with the required knowledge of material properties of all the segments and with the long duration of calculation time (hours or days). For these reasons, the mixed approach starts to play an important role in the biomechanics focused on the safety. The aim of the mixed (hybrid) approach is the combination of MBS model and FEM (detailed) model of some segments of the human body (head, abdomen, etc.). Thanks to detailed FE model of the entities, such models are able to describe injuries with the benefit of reasonable calculation time.

- **Virthuman**

  The example of the hybrid human body model is a Virthuman model [62, 63, 64, 67, 76, 113, 114] developed under cooperation of company MECAS ESI s.r.o [50] and University of West Bohemia in Pilsen. The main advantages of this model are short of calculation time, scalability of the modelm positionability and injury prediction algorithm. The developed scaling algorithm can automatically generate virtual human body model of a given weight, height, age, gender and anthropometric percentile, see Fig. 2.43. The displayed models are only example of possible humans.

The only limitations for the scaling is the range of the database, containing around 10 000 persons between 6 and 65 years old [32].

The Virthuman model consists of the rigid elements representing external shape of the human body connected via non-linear springs and dampers to the rigid MBS segments. Such segments form an open tree structure based on the multibody principle. The particular rigid segments are connected via kinematic joints that represent real human joints (shoulder, elbow, knee, etc.) or breakable joints for the description of the bone fracture. This model was especially validated also for the pedestrian modelling [114, 115].

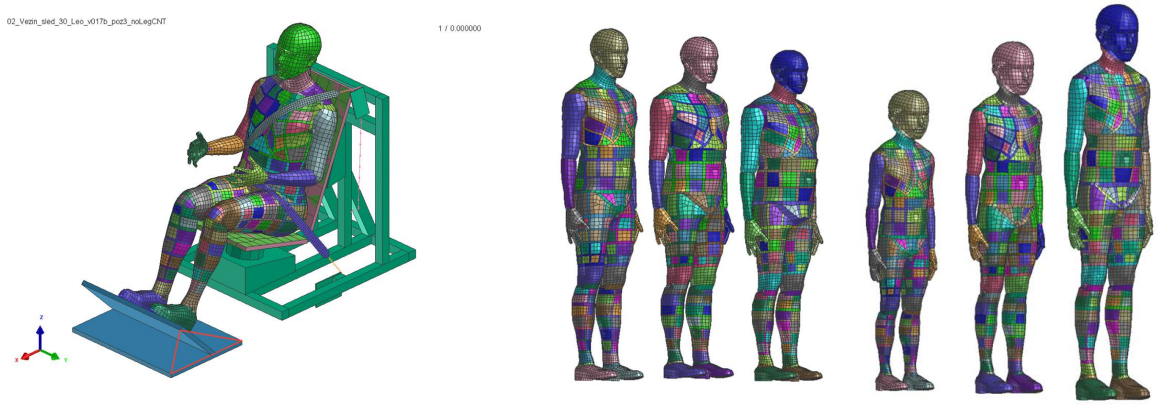

Figure 2.43: Virthuman model; Sled test (left), scaled models (right) [62]

The research of the digital/virtual models of the human body, as well as dummy development is massive part of the research and development and it is not possible to create a full database or list of all the existing models. Moreover, the highly developed models, such as GHBMC or THUMS have number of versions, updated by the users, for their own purposes or software. The great effort of summary of the current state in virtual human body model was done by Scataglini in her book [96], Duffy in [39], Haug in [53] or in [29].

Chapter 3

MBS model - Theory

Previous chapter presents the review of current state of the mechanical human body models (dummy), virtual models of the dummy and virtual models of human body. Purpose of this work is to create the model of the human, for fast impact scenarios and thus, the the multibody approach was chosen. This work is a-priory focused on global human body behavior during different loading scenarios. There are several reasons for a such decision and they are discussed bellow.

- Firstly, multibody analysis is not as complex as FEM, and thus it is less time and money consuming to build such a model (software). The reader can observe in the previous chapter 2, that multibody or articulated rigid body techniques is less used compare to FEM in the fields of biomechanical research and industry. Numbers of companies, especially car-makers companies, have invested a lot in the development of numerical FE models for a detailed analysis of a human body during crash tests. These models usually consist of several thousands, or milions of elements, hundreds of material descriptions and numbers of contact definitions. Thus it would be very expensive to get all of these descriptions of the human body and would be impossible to build a model, that could be really successfully validated and can be used in a real simulations. Generally, the main advantage of the multibody modelling is that we can receive reasonable results of human body motion in the relatively short computation time. The segments of multibody model are rigid bodies, so only the geometry, inertia properties, mass and location of centre of gravity are required. The individual segments can be constrained with the joints. For the description of the joints, only their location, range of motion and possible internal stiffness are required. The contact of the bodies with the external shape requires definition of contact parameters.

- A great benefit of the multibody modelling lays on the variability of the application within one previously developed model. Since the positions of each child body in the kinematic chain (tree structure) are defined relative to the position the parent body [4], they can be easyly modified. Dimensions of the bodies and relative position

of the kinematic joints can be easily changed to simulate wide spectra of initial positions and size of the model. Thanks to these features, the MBS model is quite easy to position and scale compare to FEM model. In the finite element modelling, every change of size and initial position results in the rebuilding (re-meshing), pre-simulation or morphing of the model, which is not easy task. Scaling algorithm is clearly described by Hynčík [62]. This scaling process defines the size of particular bodies in the system with respect to some pre-defined values, such as height or weight of the human.

- In the multibody approach, the rigid bodies are linked with the joint in the open or close kinematics tree structure. The joints can have an internal stiffness or damping. However, multibody principle is suitable tool also for adding spring, damper or active elements into the system [107, 108]. In this particular case of biomechanical modelling, these elements can approximate human muscles and the generated force can represent contracting force of the muscle or reaction force inside the joints, similarly with the AnyBody Modelling System [72].

- Besides the force elements, the joints between constrained bodies can be supplemented with the proportional-integral-derivative (PID) controller [92]. This supplemented elements can control the joint variables (rotation motion, force, torque etc.) and meet the required motion or just stabilize the human body model in the desired position [72].

- Another advantage of the multibody models is relatively simple way how to implement contact. The world of crash tests is based on the contacts and calculation of the contact scenarios. There is a contact of a vehicle with some infrastructure or with another vehicle occurring in the crash scenario. Due to the deceleration of the car, the innner entities (driver, passengers, cargo etc.) are moving inside the vehicle and can get into a contact one to each other or with the structure. Evaluation of contact force generally have two steps, detection of the contact and contact point respectively, and evaluation of the contact force. Spicka in his work [110] summaries the possible way how to detect contact and presents the new algorithm for contact detection. Several contact force models and contact detection algorithms were published in [26, 48, 70, 73, 81, 89, 100, 110, 116].

3.1 Spatial dynamics

The aim of this chapter is to describe dynamical analysis of the spatial body motion and to describe main principles of the multibody method. In case of planar (2D) analysis the actual position of a rigid body can be described using three coordinates. Two coordinates describe translation of a reference point and one coordinate defines relative rotation of the body around this reference point. The orientation angle is defined in such a way, that the angular velocity of the body is a time derivative of the orientation angle. Furthermore,

the order of the finite rotation is commutative, since the body always rotates around the same axis. One of the main difference between planar and spatial analysis is due to the complexity of the description of orientation of the body in the 3D space. In the spatial analysis, an unconstrained (free) motion of a rigid body is described using six coordinates. In the general case, these coordinates are independent (free motion). Three coordinates describe the translation of the reference point, that is fixed on the body and the remaining three coordinates define the orientation of the body in the space. In this case, the order of finite rotations is not commutative and thus, the sequence of body rotation is important aspect of the analysis. The angular velocities are not the time derivatives of the set of orientation angles. These angular velocities can be expressed in terms of selected orientation coordinates and their time derivatives. Several ways how to describe orientation and how to parametrise the spatial rotation were derived. The most common are well know three Euler angles, Cardan angles or set of four parameters of quatermions. The very common set of quatermions are Euler parameters [33, 83, 84, 85, 99, 110]. Euler angles and Cardan angles are described with the same principle (three mutual rotations), but the difference is in the sequence of these rotations. While the Euler angles use sequence Z-X-Z, the Cardan angles sequenced the rotation X-Y-Z (the letter describes the relative axis of rotation) [83].

In multibody principle the current position of a rigid body is described using a set of coordinates that define the global position vector of the body. Such vector comprises the translation of reference point on the body as well as the orientation of the body (rotation around the reference point). The absolute velocity and acceleration vector of an arbitrary point on the body can be described with respect to this coordinates. The spatial motion is quite complex process compare to the planar motion. Derivation of equation of motion is presented and the simplification for a special case, when the reference point is selected as the body centre of mass is discussed. This special case is called a centroidal system and it leads to the formulation of the Newton-Euler equations. There is no inertia coupling between translation and rotation of the body in the centroidal system. Analysis of a constrained dynamic is also presented. This work used the description mainly based on Nicravesh and Shabana. The derivation of the equations, description of all variables, principles and features can be find in [84, 85, 83, 99]. In the following section, some matrices or vector are expressed in both, local and global coordinate system. Hereafter, the symbol $\overline{vector}$ stands for expression in the local coordinate (body fixed) system, while the matrix/vector without the *overline* always means global (inertia, frame fixed) coordinate system.

3.2 Theory

Description of the body motion in the 3D space is a complex process and several different approaches how to describe it were defined. Generally, the free motion as well as constrained motion can be decomposed to a translation motion of the reference point

and rotation of the body around this point. Translation of the body is defined with the translation of any point on the body, no matter which approach was chosen. However, the parametrisation of the spatial rotation is the key point of the modelling. This work summaries the two method (three independent Euler angles - EA and four Euler parameters - EP) and discusses their pros and cons. Since the spatial rotation has 3 degrees of freedom, it is visible that four Euler parameters are not totally independent, while the Euler angles are.

3.2.1 Euler angles

Displacement and orientation

Translation/displacement of the rigid body i can be defined with the translation of one point on this body. Kinematics of the rigid body can by fully described within translation of the reference point O, see Fig. 3.1 and with relative rotation of the body around this reference point as

$$\mathbf{r}^i = \mathbf{R}^i + \mathbf{A}^i(\psi_i, \vartheta_i, \varphi_i)\overline{\mathbf{u}}^i, \tag{3.1}$$

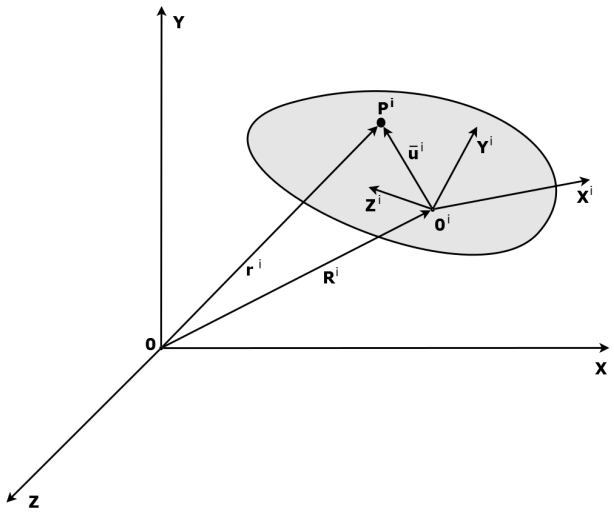

Figure 3.1: Rigid body coordinate system

where $\mathbf{r}^i$ are coordinates of any particular point with respect to the global (inertia) coordinate system XYZ, $\mathbf{R}^i$ is the global position vector of the origin of the reference (body-fixed) coordinate system $X^iY^iZ^i$, $\mathbf{A}^i(\psi_i, \vartheta_i, \varphi_i)$ is transformation (cosines) matrix from the body/local coordinate system to the global coordinate system, $\overline{\mathbf{u}}^i$ is position vector of the particular point on the body i with respect to the local (body-fixed) coordinate system $X^iY^iZ^i$. Transformation matrix $\mathbf{A}^i$ is a 3x3 matrix and the three-dimensional vectors above are defined as

$$\mathbf{r}^i = [r^i_x, r^i_y, r^i_z]^T \tag{3.2}$$

$$\mathbf{R}^i = [R_x^i, R_y^i, R_z^i]^T \tag{3.3}$$

$$\overline{\mathbf{u}}^i = [\overline{u}_x^i, \overline{u}_y^i, \overline{u}_z^i]^T. \tag{3.4}$$

Rotation

Cosine matrix $\mathbf{A}^i$ is matrix defining orientation of body-fixed coordinate system $X^iY^iZ^i$ with respect to the global coordinate system XYZ. From the definition [34, 83, 99], transformation matrix of any motion can be decomposed to the set of transformation matrices of the basic motions (translation and rotation). This matrix has some special properties, for example orthogonality etc. For more information see [33, 34, 83, 99]. The most frequently used parameters for description of the orientation in 3D space are the three independent Euler angles. As an example of different approaches in parametrisation of the orientation in space, three Bryant, Cardan or Rodriguez angles and four Euler and Rodriguez parameters are mentioned. Generally, these four-parameters are know as a quatermion.

Euler angles represent three successive rotations about three axis. By performing these three rotations in the proper sequence, the body (body-fixed coordinate system) can reach any orientation in the space. There is no limitation for the sequences of these three rotations and for the selection of the axis of rotation. Each of the sequence has some advantages and disadvantages. The main troubles of the parametrisation are connected with the singular positions, where the integration process can fail. Each of the rotational sequence has some singular positions. The sequence of rotations known as ZXZ, which is the widely used in real applications is called Euler angles. The first motion is rotation of the body fixed coordinate system $X^iY^iZ^i$, with angle ψ about the local Z axis. Transformation matrix of such motion called *precession* is define as

$$\mathbf{A}_{pre}(\psi) = \begin{bmatrix} \cos(\psi) & -\sin(\psi) & 0 \\ \sin(\psi) & \cos(\psi) & 0 \\ 0 & 0 & 1 \end{bmatrix}. \tag{3.5}$$

The coordinate system $X^iY^iZ^i$ is then rotated with the the angle ϑ about current axis X^i. Change of the orientation is known as a *nutation* and the transformation matrix is described as

$$\mathbf{A}_{nut}(\vartheta) = \begin{bmatrix} 1 & 0 & 0 \\ 0 & \cos(\vartheta) & -\sin(\vartheta) \\ 0 & \sin(\vartheta) & \cos(\vartheta) \end{bmatrix}. \tag{3.6}$$

Finally, the coordinate system $X^iY^iZ^i$ rotates with an angle φ around current axis Z^i and the resulting matrix of the *spin* is given by

$$\mathbf{A}_{spin}(\varphi) = \begin{bmatrix} \cos(\varphi) & -\sin(\varphi) & 0 \\ \sin(\varphi) & \cos(\varphi) & 0 \\ 0 & 0 & 1 \end{bmatrix}. \tag{3.7}$$

When the transformation matrices of the three motions, Eq. 3.5, 3.6 and 3.7 are substituted into a general formula for body motion analysis Eq. 3.1, the final equation is obtained as

$$\mathbf{r}^i = \mathbf{R}^i + \mathbf{A}^i_{pre}(\psi)\mathbf{A}^i_{nut}(\vartheta)\mathbf{A}^i_{spin}(\varphi)\overline{\mathbf{u}}^i. \tag{3.8}$$

Transformation matrix $\mathbf{A}^i$ in terms of the Euler angles $(\psi_i, \vartheta_i, \varphi_i)$ is defined as a multiplication of the three matrices as

$$\mathbf{A}^i = \begin{bmatrix} \cos\varphi_\mathrm{i}\cos\psi_\mathrm{i} - \cos\vartheta_\mathrm{i}\sin\varphi_\mathrm{i}\sin\psi_\mathrm{i} & -\cos\psi_\mathrm{i}\sin\varphi_\mathrm{i} - \cos\varphi_\mathrm{i}\cos\vartheta_\mathrm{i}\sin\psi_\mathrm{i} & \sin\psi_\mathrm{i}\sin\vartheta_\mathrm{i} \\ \cos\varphi_\mathrm{i}\sin\psi_\mathrm{i} + \cos\psi_\mathrm{i}\cos\vartheta_\mathrm{i}\sin\varphi_\mathrm{i} & \cos\varphi_\mathrm{i}\cos\psi_\mathrm{i}\cos\vartheta_\mathrm{i} - \sin\varphi_\mathrm{i}\sin\psi_\mathrm{i} & -\cos\psi_\mathrm{i}\sin\vartheta_\mathrm{i} \\ \sin\varphi_\mathrm{i}\sin\vartheta_\mathrm{i} & \cos\varphi_\mathrm{i}\sin\vartheta_\mathrm{i} & \cos\vartheta_\mathrm{i} \end{bmatrix}. \tag{3.9}$$

Velocity

Absolute velocity of any arbitrary point on the rigid body can be derived by differentiating of Eq. 3.1 with respect to the time

$$\dot{\mathbf{r}}^i = \dot{\mathbf{R}}^i + \dot{\mathbf{A}}^i\overline{\mathbf{u}}^i. \tag{3.10}$$

Let us define a skew symmetric matrix $\tilde{\boldsymbol{\omega}}^i$ as

$$\tilde{\boldsymbol{\omega}}^i = \dot{\mathbf{A}}^i\mathbf{A}^{iT} = \begin{bmatrix} 0 & -\omega^i_3 & \omega^i_2 \\ \omega^i_3 & 0 & -\omega^i_1 \\ -\omega^i_2 & \omega^i_1 & 0 \end{bmatrix}, \tag{3.11}$$

in which ω^i_1, ω^i_2 and ω^i_3 are components of angular velocity vector $\boldsymbol{\omega}^i$ defined as

$$\boldsymbol{\omega}^i = [\omega^i_1, \omega^i_2, \omega^i_3]^T. \tag{3.12}$$

After several mathematical operations [83, 99], the absolute velocity vector of any point can be expressed as

$$\dot{\mathbf{r}}^i = \dot{\mathbf{R}}^i + \tilde{\omega}^i\mathbf{A}^i\overline{\mathbf{u}}^i, \tag{3.13}$$

or

$$\dot{\mathbf{r}}^i = \dot{\mathbf{R}}^i + \boldsymbol{\omega}^i \times \mathbf{u}^i. \tag{3.14}$$

Angular velocity can be expressed in term of Euler angles and their time derivatives as

$$\boldsymbol{\omega}^i = \mathbf{G}^i\dot{\boldsymbol{\theta}}^i, \tag{3.15}$$

where

$$\mathbf{G}^i = \begin{bmatrix} 0 & \cos\psi_i & \sin\vartheta_i\sin\psi_i \\ 0 & \sin\psi_i & -\sin\vartheta_i\cos\psi_i \\ 1 & 0 & \cos\vartheta_i \end{bmatrix} \tag{3.16}$$

and $\dot{\boldsymbol{\theta}}^i$ is a vector of derivatives of Euler angles defined as

$$\dot{\boldsymbol{\theta}}^i = [\dot{\psi}_i, \dot{\vartheta}_i, \dot{\varphi}_i]^T. \tag{3.17}$$

The columns of matrix $\mathbf{G}^i$ represent unit vectors along the axis about which the Euler angles rotate. These are expressed in the global coordinate system. It turns out useful to define this matrix also in the local coordinate system, using transformation matrix $\mathbf{A}$ as

$$\mathbf{L}^i = \overline{\mathbf{G}}^i = \mathbf{A}^{iT}\mathbf{G}^i = \begin{bmatrix} \sin\vartheta_i \sin\varphi_i & \cos\varphi_i & 0 \\ \sin\vartheta_i \cos\varphi_i & \cos\varphi_i & 0 \\ \cos\vartheta_i & 0 & 1 \end{bmatrix} \tag{3.18}$$

and thus the vector of angular velocity can be defined in terms of local coordinate system as

$$\overline{\omega}^i = \overline{\mathbf{G}}^i \dot{\boldsymbol{\theta}}^i = \mathbf{L}^i \dot{\boldsymbol{\theta}}^i. \tag{3.19}$$

Lagrange equation - Energy balance

Multibody approach lays on the principle of virtual work and consequently derivation of equation of motion using this variation principle. As a modification of this approach, the Lagrange equations were derived [33, 34, 83, 89, 99], in order to develop advanced method for derivation of equation of motion. Generally, two main principles for Lagrange equations was established: Lagrange equations of the first kind, or equations in Cartesian coordinates with undetermined Lagrange multipliers, and Lagrange equations of the second kind with multipliers, or equations in generalized coordinates. Lagrange equations of the first kind are derived in terms of independent coordinates, while the generalized coordinates correspond to the set of both, independent and dependent coordinates. The number of generalized coordinates are equal or higher than degree of freedom (DOF) of the system. Let us consider the mechanical system with n degree of freedom. When the Lagrange equations of the first kind in classic Cartesian coordinates are used, exactly n independent coordinates are required to described this system. However, if the Lagrange equations of the second kind in generalized coordinates are applied, usually $m > n$ coordinates are used. Consequently, n independent coordinates, and r=m-n constraint equations for r dependent coordinates is performed. Kinematics constraint equations generally depict in a form

$$C_j(s_k, t) = 0, \qquad \text{j=1, 2, ...,r} \tag{3.20}$$

where

$$s_k, \qquad \text{k=1, 2, ...,m,} \qquad \text{m > n,} \tag{3.21}$$

represents generalized coordinates used in the description of the mechanical system.

Lagrange equations of the second kind can have a following form

$$\frac{d}{dt}\frac{\partial L}{\partial \dot{\boldsymbol{q}}} - \frac{\partial L}{\partial \boldsymbol{q}} = \boldsymbol{Q} + \sum_{j=1}^{r} \lambda_j \frac{\partial C_j}{\partial \boldsymbol{q}} \tag{3.22}$$

where $L = E_k - E_p$ is scalar quantity called Lagrangian, $\mathbf{Q}$ represents the generalized forces, λ_j are Lagrange multipliers, C_j are the constraint equations and $\mathbf{q}$ is the vector of generalized coordinates that comprises independent and dependent coordinates. The main task of Lagrange equation is to derive an equation of a kinetic and potential energy balance. Kinetic energy of the spatial mechanical system of n bodies for the *non-centroidal* case, i.e. when centre of gravity does not coincide with the origin of the local body-fixed coordinate system, i.e. with the reference point, can be expressed as

$$E_k = \sum_{i=1}^{n} \left[\frac{1}{2} (\dot{\mathbf{R}}^i)^2 m^i + \frac{1}{2} \boldsymbol{\omega}^i \mathbf{I}_A^i \boldsymbol{\omega}^i + \dot{\mathbf{R}}^i (\boldsymbol{\omega}^i \times \mathbf{d}^i) m^i \right] \tag{3.23}$$

where $\dot{\mathbf{R}}^i$ is the translation velocity vector of the origin of the body local coordinate system, m_i is mass of the *i-th* body, $\boldsymbol{\omega}^i$ is vector of rotational velocity of the local coordinate system, $\mathbf{I}_A^i$ is inertia matrix of *i-th* body with respect to the reference point A and $\mathbf{d}^i$ is the coordinate vector of centre of gravity with respect to the local coordinate system. Potential energy is a function of generalized forces, such as gravity or external and internal forces. The current expression depends on a particular system and thus is not presented here.

Equation of motion

Unconstrained dynamics

Principle of Lagrange equation is a very general tool for deriving equation of motion of a body, or system of bodies moving in the space. However, it is not always very straightforward task to follow and to finish all steps of the algorithm. For example the derivatives of energies with respect to all generalized coordinates might cause difficulties, especially in case of non-centroidal analysis or time dependent constraints. Shabana [99] or Nicravesh [83] present the total equation of motion of *i-th* body, written in matrix form as

$$\underbrace{\begin{bmatrix} \mathbf{m}_{RR}^i & \mathbf{m}_{R\theta}^i \\ \mathbf{m}_{R\theta}^i & \mathbf{m}_{\theta\theta}^i \end{bmatrix}}_{\mathbf{M}^i} \underbrace{\begin{bmatrix} \ddot{\mathbf{R}}^i \\ \ddot{\boldsymbol{\theta}}^i \end{bmatrix}}_{\ddot{\mathbf{q}}^i} = \underbrace{\begin{bmatrix} (\mathbf{Q}_e^i)_R \\ (\mathbf{Q}_e^i)_\theta \end{bmatrix}}_{\mathbf{Q}_e^i} + \underbrace{\begin{bmatrix} (\mathbf{Q}_\nu^i)_R \\ (\mathbf{Q}_\nu^i)_\theta \end{bmatrix}}_{\mathbf{Q}_\nu^i}, \qquad \text{i=1, 2, ...,n} \tag{3.24}$$

where $\mathbf{M}^i$ is the mass matrix of *i-th* body, $\mathbf{q}^i$ is the vector of three translation and three rotational coordinates of the body and $\mathbf{Q}_e^i$ and $\mathbf{Q}_\nu^i$ are the vectors of generalized force associated with generalized translations and orientations, respectively (ride-hand-side of EOM). Equation 3.24 is matrix equation that governs unconstrained motion of a rigid body. This equation can be simplified, if the centroidal system is considered, thus if the origin of local coordinate system is rigidly attached to the body centre of gravity. In this

case, some terms in Eq. 3.24 vanished and equation of motion comes to the form

$$\underbrace{\begin{bmatrix}\mathbf{m}^i_{RR} & \mathbf{0}\\ \mathbf{0} & \mathbf{m}^i_{\theta\theta}\end{bmatrix}}_{\mathbf{M}^i}\underbrace{\begin{bmatrix}\ddot{\mathbf{R}}^i\\ \ddot{\boldsymbol{\theta}}^i\end{bmatrix}}_{\ddot{\mathbf{q}}^i} = \underbrace{\underbrace{\begin{bmatrix}(\mathbf{Q}^i_e)_R\\ (\mathbf{Q}^i_e)_\theta\end{bmatrix}}_{\mathbf{Q}^i_e} + \underbrace{\begin{bmatrix}\mathbf{0}\\ (\mathbf{Q}^i_\nu)_\theta\end{bmatrix}}_{\mathbf{Q}^i_\nu}}_{\mathbf{Q}^i}, \qquad \text{i=1, 2, ...,n} \tag{3.25}$$

and consequently standard matrix form

$$\mathbf{M}^i\ddot{\mathbf{q}}^i = \mathbf{Q}^i \tag{3.26}$$

The matrices and vectors in Eq. 3.24 and 3.25 are defined as

$$\mathbf{m}^i_{RR} = m^i\mathbf{I} \tag{3.27}$$

where is m^i is total mass of the $i-th$ body and $\mathbf{I}$ is 3x3 identity matrix.

$$\mathbf{m}^i_{\theta\theta} = \overline{\mathbf{G}}^{i^T}\overline{\mathbf{J}}^i\overline{\mathbf{G}}^i \quad = \quad \mathbf{G}^{i^T}\mathbf{A}^i\overline{\mathbf{J}}^i\mathbf{A}^{i^T}\mathbf{G}^i \tag{3.28}$$

in which $\overline{\mathbf{J}}^i$ is the 3x3 symmetric inertia matrix (tensor) of the rigid body expressed in local coordinate system and can be defined as

$$\overline{\mathbf{J}}^i = \begin{bmatrix} i_{xx} & i_{xy} & i_{xz}\\ & i_{yy} & i_{yz}\\ \text{sym.} & & i_{zz}\end{bmatrix} \tag{3.29}$$

Matrices $\mathbf{A}^i$, $\mathbf{G}^i$ and $\overline{\mathbf{G}}^i$ are defined above in Eq. 3.9, 3.16 and 3.18 respectively. Vector of translation accelerations $\ddot{\mathbf{R}}^i$ and rotational accelerations (or second derivatives of Euler angles) $\ddot{\boldsymbol{\theta}}^i$ were previously defined. Vector $(\mathbf{Q}^i_e)_R$ of the generalized forces associated with generalized translation is defined as

$$(\mathbf{Q}^i_e)_R = \mathbf{F}^i_1 + \mathbf{F}^i_2 + ... + \mathbf{F}^i_h = \sum_{j=1}^{h}\mathbf{F}^i_j \tag{3.30}$$

where $\mathbf{F}^i_1, \mathbf{F}^i_2, ...\mathbf{F}^i_h$ are set of external forces acting on the body. Vector $(\mathbf{Q}^i_e)_\theta$ of the generalized forces associated with generalized orientation is defined with expression

$$(\mathbf{Q}^i_e)_\theta = \mathbf{G}^{i^T}\left[\sum_{j=1}^{h}\mathbf{M}^i_j + \sum_{k=1}^{l}(\mathbf{u}^i_k \times \mathbf{F}^i_k)\right] \tag{3.31}$$

where $\mathbf{M}^i_j$ are the torques acting on the body and and $\mathbf{u}^i_k$ are the points in which the external forces $\mathbf{F}^i_k$ act. When there is no external torque loading the body, the Eq. 3.31 can be simplified to the form

$$(\mathbf{Q}^i_e)_\theta = -\left(\mathbf{A}^i\tilde{\overline{\mathbf{u}}}^i_p\overline{\mathbf{G}}\right)^T\mathbf{F}^i \tag{3.32}$$

Matrix $\tilde{\overline{\mathbf{u}}}_p^i$ is a skew symmetric matrix associated with local position vector of the force, generally defined as

$$\tilde{\mathbf{a}} = \begin{bmatrix} 0 & -a_3 & a_2 \\ a_3 & 0 & -a_1 \\ -a_2 & a_1 & 0 \end{bmatrix} \tag{3.33}$$

Vector $(\mathbf{Q}_\nu^i)_\theta$ is the inertia forces vector that absorbs terms quadratic in the velocities and is defined as

$$(\mathbf{Q}_\nu^i)_\theta = -\mathbf{G}^{iT}\left[\overline{\boldsymbol{\omega}}^i \times \left(\overline{\mathbf{J}}^i\overline{\boldsymbol{\omega}}^i\right) + \overline{\mathbf{J}}^i\dot{\overline{\mathbf{G}}}^i\dot{\boldsymbol{\theta}}^i\right] \tag{3.34}$$

where a $\dot{\overline{\mathbf{G}}}^i$ is time derivative of Eq. 3.18, thus

$$\dot{\overline{\mathbf{G}}}^i = \begin{bmatrix} \cos\vartheta_i \sin\varphi_i\dot{\vartheta}_i + \sin\vartheta_i\cos\varphi_i\dot{\varphi}_i & -\sin\varphi_i\dot{\varphi}_i & 0 \\ \cos\vartheta_i\cos\varphi_i\dot{\vartheta}_i - \sin\vartheta_i\sin\varphi_i\dot{\varphi}_i & -\cos\varphi_i\dot{\varphi}_i & 0 \\ -\sin\vartheta_i\dot{\vartheta}_i & 0 & 0 \end{bmatrix} \tag{3.35}$$

Constrained dynamics

When a system of n bodies linked in kinematic chain or tree structure is considered, principle of Lagrange multipliers is used to adjoin the kinematic constraint equations to the equation of motion. Shabana [99] presents derivation of the matrix equation of motion of system containing n bodies using Euler angles for the parametrisation of the rotation motion as

$$\begin{bmatrix} \mathbf{M}^1 & \mathbf{0} & \cdots & \mathbf{0} & \mathbf{C}_{\mathbf{q}^1}^T \\ \mathbf{0} & \mathbf{M}^2 & \cdots & \mathbf{0} & \mathbf{C}_{\mathbf{q}^2}^T \\ \vdots & \vdots & \ddots & \vdots & \vdots \\ \mathbf{0} & 0 & \cdots & \mathbf{M}^n & \mathbf{C}_{\mathbf{q}^n}^T \\ \mathbf{C}_{\mathbf{q}^1} & \mathbf{C}_{\mathbf{q}^2} & \cdots & \mathbf{C}_{\mathbf{q}^n} & \mathbf{0} \end{bmatrix} \begin{bmatrix} \ddot{\mathbf{q}}^1 \\ \ddot{\mathbf{q}}^2 \\ \vdots \\ \ddot{\mathbf{q}}^n \\ \boldsymbol{\lambda} \end{bmatrix} = \begin{bmatrix} \mathbf{Q}_e^1 + \mathbf{Q}_\nu^1 \\ \mathbf{Q}_e^2 + \mathbf{Q}_\nu^2 \\ \vdots \\ \mathbf{Q}_e^n + \mathbf{Q}_\nu^n \\ \mathbf{Q}_d \end{bmatrix} \tag{3.36}$$

where $\mathbf{C}_{\mathbf{q}^i}$ is the constraint Jacobian matrix [33, 83, 99, 110, 111] and $\mathbf{Q}_d$ is defined as

$$\mathbf{Q}_d = \begin{bmatrix} -\sum_{\alpha=1}^{n}\sum_{j=1}^{n} C_1^{j\alpha}\dot{q}^j\dot{q}^\alpha \\ -\sum_{\alpha=1}^{n}\sum_{j=1}^{n} C_2^{j\alpha}\dot{q}^j\dot{q}^\alpha \\ \vdots \\ -\sum_{\alpha=1}^{n}\sum_{j=1}^{n} C_{3r}^{j\alpha}\dot{q}^j\dot{q}^\alpha \end{bmatrix} \tag{3.37}$$

where $C_i^{j\alpha}$ is a second derivative of i-th constraint equation with respect to particular generalized coordinates, thus

$$C_i^{j\alpha} = \frac{\partial^2 C_i}{\partial q^j \partial q^\alpha} \tag{3.38}$$

Equation 3.36 can be written in a complex form as

$$\begin{bmatrix} \mathbf{M} & \mathbf{C}_q^T \\ \mathbf{C}_q & \mathbf{0} \end{bmatrix} \begin{bmatrix} \ddot{\boldsymbol{q}} \\ -\boldsymbol{\lambda} \end{bmatrix} = \begin{bmatrix} \mathbf{Q}_e + \mathbf{Q}_\nu \\ \mathbf{Q}_d \end{bmatrix} \tag{3.39}$$

where $\mathbf{M}$ is the total mass matrix, $\mathbf{C}_q$ is the Jacobian matrix, $\boldsymbol{\lambda}$ is the vector of r Lagrange multipliers, $\mathbf{Q}_e$ and $\mathbf{Q}_v$ are the total vectors of applied and inertia forces, respectively, and $\mathbf{Q}_d$ is total vector that absorbs terms quadratic in the velocities. This equation leads to index one differential-algebraic equations (DAE). They can be solved for vector of unknown accelerations and Lagrange multipliers. Generalized accelerations can be directly integrated in order to obtain generalized velocities and coordinates, respectively.

Joint definition

Dynamical system in the multibody analysis usually contains a set of kinematic joints, that define the connectivity between bodies in the system. Each joint eliminates some degrees of freedom from the system to meet required motion. The overview of common joints and number of their DOF is presented in the Tab. 3.1. Note that maximum DOF is six. Sum of free and eliminated number of degree of freedom must be equal to six. Parameter r

Type of joint	Number of DOF	DOF	Eliminated DOF
Spherical	3	r, r, r	t, t, t
Cylindrical	2	r, t	t, t, r, r
Prismatic	1	t	t, t, r, r, r
Universal	2	r, r	t, t, t, r
Rigid	0		t, t, t, r, r, r
Revolute	1	r	t, t, t, r, r

Table 3.1: Joints specification

in the Tab. 3.1 denotes rotational degree of freedom and t stands for translation degree of freedom. Kinematics relationship called constraint equation can be written in the following vector form

$$\mathbf{C}(\mathbf{q}, t) = \mathbf{0} \tag{3.40}$$

This equation varies for a different type of the kinematics joints. Since this work deals mainly with spherical joint, only this one is analysed here. The overview of the particular equations for the kinematic joints can be manually derived, or found in [83, 99]

Spherical joint: When the bodies i and j are constrained with a spherical joint, relative translations between these two bodies are eliminated, and only 3 degrees of freedom of relative rotations are allowed. Kinematics constraint of the spherical joint required two points, P^i and P^j on bodies i and j, respectively, that coincide through the motion, see Fig. 3.2.

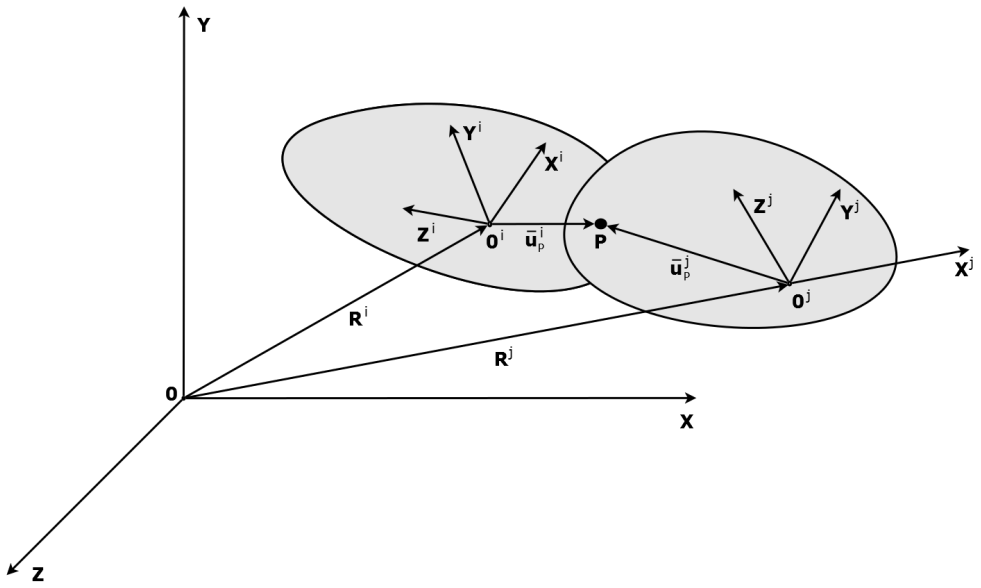

Figure 3.2: Spherical joint

The constraint equation between body i and j can be written as

$$\mathbf{C}(\mathbf{q}^i, \mathbf{q}^j) = \mathbf{R}^i + \mathbf{A}^i \overline{\mathbf{u}}_P^i - \mathbf{R}^j - \mathbf{A}^j \overline{\mathbf{u}}_P^j = \mathbf{0} \tag{3.41}$$

where $\mathbf{R}^i$ and $\mathbf{R}^j$ are the global position vectors of origin of the body coordinate systems, $\mathbf{A}^i$ and $\mathbf{A}^j$ represent the transformation matrices between local and global coordinate systems, $\overline{\mathbf{u}}_P^i$ and $\overline{\mathbf{u}}_P^j$ are the position vectors of point $\boldsymbol{P}$ with respect to the local coordinate system $X^iY^iZ^i$ of i-th body and the local coordinate system $X^jY^jZ^j$ of j-th body, respectively. The Jacobian matrix for a spherical joint between *i-th* and *j-th* body can be expressed as

$$\mathbf{C}_\mathbf{q} = \left[\mathbf{C}_{\mathbf{q}^i},\ \mathbf{C}_{\mathbf{q}^j}\right] = \left[\mathbf{I}, \mathbf{A}^i \tilde{\overline{\mathbf{u}}}_P^{iT} \overline{\mathbf{G}}^i, -\mathbf{I}, -\mathbf{A}^j \tilde{\overline{\mathbf{u}}}_P^{jT} \overline{\mathbf{G}}^j\right] \tag{3.42}$$

where $\tilde{\overline{\mathbf{u}}}_P^i$ and $\tilde{\overline{\mathbf{u}}}_P^j$ are the skew symmetric matrices associated with local position vectors $\overline{\mathbf{u}}_P^i$ and $\overline{\mathbf{u}}_P^j$, respectively. Now, all terms in Eq. 3.36 are defined, and the acceleration, velocities and displacements can be calculated.

NOTE: Singular position: When the nutation angle ϑ equalls to zero, the precession and spin coincides and the integration process failed, since in cannot distinguish between these two motion.

3.2.2 Euler parameters

The principle of equation of motion derived within Euler angles suffers with singular positions and thus ill numerical stability. Therefore, the concept of 4 Euler parameters is often used to solved this issue. These parameters are not totally independent, since they describe spatial rotations of the 3 DOF within 4 variables. The Euler parameters seem to have no physical meaning, since it is set of four parameters for 3 DOF motion. However, this idea lays on the basic Euler theorem [83]:

The general displacement of a body with one point fixed is a rotation about some axis.

This theorem defines the orientation of the body-fixed coordinate system at any time t, as a rotation of this body about one imaginary axis. Based on this theorem, the Euler parameters were defined, in the way that three variables define axis of rotation (vector) and the last parameter is rotation about this particular axis.

Since these parameters are not independent, the constraint equation between Euler parameters p_i must be defined as

$$\sum_{k=0}^{3}(p_k)^2 = 1, \tag{3.43}$$

or in vector formulation

$$\boldsymbol{p}^T\boldsymbol{p} - 1 = 0. \tag{3.44}$$

Euler parameters in terms of Euler angles

Euler parameters might be tough to interpret in a physical meaning (especially the initial values, definition some identities or coupling with Euler angles), so it is useful to define the Euler parameters as a function of well known Euler angles as

$$p_0 = \cos\left[\frac{1}{2}(\psi+\phi)\right]\cos\frac{\theta}{2} \tag{3.45}$$

$$p_1 = \cos\left[\frac{1}{2}(\psi-\phi)\right]\sin\frac{\theta}{2} \tag{3.46}$$

$$p_2 = \sin\left[\frac{1}{2}(\psi-\phi)\right]\sin\frac{\theta}{2} \tag{3.47}$$

$$p_3 = \sin\left[\frac{1}{2}(\psi+\phi)\right]\cos\frac{\theta}{2} \tag{3.48}$$

and similarly the derivatives of the Euler angles as a function of Euler velocities

$$\dot{p_0} = -\sin\frac{\theta}{2}\,\frac{\dot{\theta}}{2}\,\cos\left[\frac{\psi+\phi}{2}\right] - \cos\frac{\theta}{2}\sin\left[\frac{\psi+\phi}{2}\right]\frac{\dot{\psi}+\dot{\phi}}{2} \tag{3.49}$$

$$\dot{p_1} = \cos\frac{\theta}{2}\,\frac{\dot{\theta}}{2}\,\cos\left[\frac{\psi-\phi}{2}\right] - \sin\frac{\theta}{2}\sin\left[\frac{\psi-\phi}{2}\right]\frac{\dot{\psi}-\dot{\phi}}{2} \tag{3.50}$$

$$\dot{p_2} = \cos\frac{\theta}{2}\,\frac{\dot{\theta}}{2}\,\cos\left[\frac{\psi-\phi}{2}\right] + \sin\frac{\theta}{2}\cos\left[\frac{\psi-\phi}{2}\right]\frac{\dot{\psi}-\dot{\phi}}{2} \tag{3.51}$$

$$\dot{p_3} = -\sin\frac{\theta}{2}\,\frac{\dot{\theta}}{2}\,\sin\left[\frac{\psi+\phi}{2}\right] + \cos\frac{\theta}{2}\sin\left[\frac{\psi+\phi}{2}\right]\frac{\dot{\psi}+\dot{\phi}}{2} \tag{3.52}$$

Displacement

Displacement of the body does not depend on the method for parametrisation of a spatial rotation. As was previously described, the approaches vary only in the spatial rotation description. Thus, translation component of the equation of motion remains unchanged. The coordinates X, Y and Z describe motion of the rigid body (its local coordinate system) in a global Cartesian coordinate system.

Orientation

Orientation of the rigid body in the space is expressed via translation of one point and rotation of the body around this particular point. The actual position of the point $\boldsymbol{P}$ on body i, expressed via Euler parameters are formally the same as in the case of Euler angles, Eq. 3.1 as

$$\boldsymbol{r}^i = \boldsymbol{R}^i + \mathbf{A}^i(\boldsymbol{p}_k^i)\overline{\mathbf{u}^\mathbf{i}} \tag{3.53}$$

but the transformation matrix $\mathbf{A}$ is a function of Euler parameters, not Euler angles, and can be expressed as:

$$\boldsymbol{A} = \begin{bmatrix} p_0^2 + p_1^2 - \frac{1}{2} & p_1p_2 - p_0p_3 & p_1p_3 + p_0p_2 \\ p_1p_2 + p_0p_3 & p_0^2 + p_2^2 - \frac{1}{2} & p_2p_3 - p_0p_1 \\ p_1p_3 - p_0p_2 & p_2p_3 + p_0p_1 & p_0^2 + p_3^2 - \frac{1}{2} \end{bmatrix} \tag{3.54}$$

Note that the term expressed in local coordinate system of the body is mark with *overline* symbol, while the definition in the global coordinate system has no additional mark.

Velocity

The relation between angular velocity $\boldsymbol{\omega}$ and time derivatives of the Euler parameters can be defined in a similar way as in the Euler angles approach [83]. This relation can be defined both in the global Eq. 3.55 and local coordinates system Eq. 3.56 respectively. The identities between time derivatives of Euler parameters $\dot{\boldsymbol{P}}$ and angular velocity vector $\boldsymbol{\omega} = [\omega_x, \omega_y, \omega_z]^T$ can be written as

$$\boldsymbol{\omega} = 2\boldsymbol{G}\dot{\boldsymbol{p}} \tag{3.55}$$

or in the local coordinate system as

$$\overline{\boldsymbol{\omega}} = 2\boldsymbol{L}\dot{\boldsymbol{p}} \tag{3.56}$$

where $\boldsymbol{G}$ and $\boldsymbol{L}$ are transformation matrices between global and local coordinate system. These are defined as

$$\boldsymbol{G} = \begin{bmatrix} -p_1 & p_0 & -p_3 & p_2 \\ -p_2 & p_3 & p_0 & -p_1 \\ -p_3 & -p_2 & p_1 & p_0 \end{bmatrix} \tag{3.57}$$

and

$$\boldsymbol{L} = \begin{bmatrix} -p_1 & p_0 & p_3 & -p_2 \\ -p_2 & -p_3 & p_0 & p_1 \\ -p_3 & p_2 & -p_1 & p_0 \end{bmatrix} \tag{3.58}$$

The matrices $\boldsymbol{G}$ and $\boldsymbol{L}$ has some features, such as orthogonality of the rows and there exist some useful identities between these matrices [83]:

$$\boldsymbol{G}\boldsymbol{G}^T = \boldsymbol{I} \tag{3.59}$$

and

$$\boldsymbol{L}\boldsymbol{L}^T = \boldsymbol{I}, \tag{3.60}$$

or

$$\boldsymbol{A} = \boldsymbol{G}\boldsymbol{L}^T \tag{3.61}$$

Similarly for the time derivatives of these matrices

$$\boldsymbol{G}\dot{\boldsymbol{p}} = -\dot{\boldsymbol{G}}\boldsymbol{p} \tag{3.62}$$

and

$$\boldsymbol{L}\dot{\boldsymbol{p}} = -\dot{\boldsymbol{L}}\boldsymbol{p} \tag{3.63}$$

Equation of motion: Unconstrained dynamics

A general equation of motion for rigid body is formulated here on the basic of the dynamics principle MBS and defined for example in the [83] or [99]. The translation equation of motion does not change with the Euler parameters approach and is given as

$$\boldsymbol{M}\ddot{\boldsymbol{R}} = \boldsymbol{Q}_R, \tag{3.64}$$

where $\boldsymbol{M}$ is a mass matrix related to translation coordinates, $\boldsymbol{R}$ are vector of translation accelerations and $\boldsymbol{Q}_R$ is general force vector associated with translation.

Nikravesh in his work [83] presented rotational equation of motion in terms of Euler parameters in three formulations . Each of the formulation has some special feature and the total equations of motion of free and constrained body are presented here. Later on, the first formulation is used for the further analysis and for building of the model.

Firstly, similarly with the concept of Lagrange equation of the second kind, the constraint equation between Euler parameters, and its second derivatives, need to be added into the system. The second derivatives of the equation 3.44 can be expressed as

$$\boldsymbol{p}^T\ddot{\boldsymbol{p}} + \dot{\boldsymbol{p}}^T\dot{\boldsymbol{p}} = 0 \tag{3.65}$$

Generalized forces:

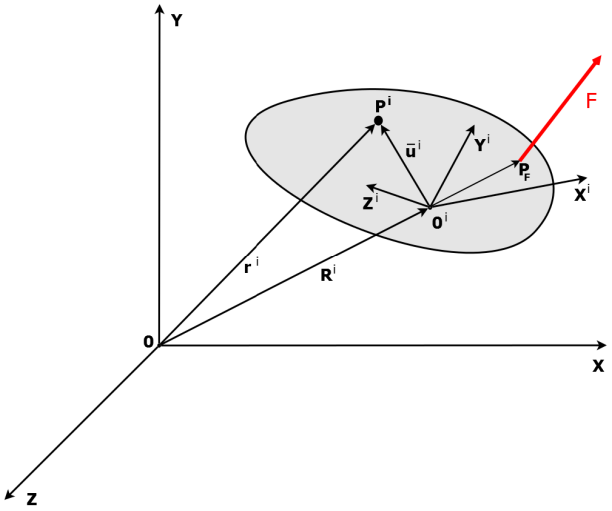

Figure 3.3: Rigid body in the 3D space, coordinates and acting force

Let us assume the generalized force $\boldsymbol{f}$ acting on a body in the point $\boldsymbol{P}_F$, as shown in Fig. 3.3. The component of the force and moment vector $\boldsymbol{f}$ and $\boldsymbol{n}^\star$, respectively, can be defined based on virtual work and converted into Euler parameters. Finally, the seven components of the force-moment vector is obtained as

$$\begin{bmatrix} \boldsymbol{f} \\ \boldsymbol{n}^{\star} \end{bmatrix} = \begin{bmatrix} \boldsymbol{f} \\ 2\boldsymbol{G}^T \tilde{\boldsymbol{u}}_F{}^T \boldsymbol{f} \end{bmatrix} \tag{3.66}$$

where $\tilde{\boldsymbol{u}}_F$ is a skew symmetric matrix of position vector of the point $\boldsymbol{P}_F$, where the force acts.

Since the position, mutual rotations, loads and inertia of the free body (unconstrained) are known, the total equation of motion can be written. If we consider parametrisation of the spatial rotation within Euler parameters, the three formulations of the global motion can be defined. For detailed description of these three formulations, see [83, 84, 85].

Formulation 1

Formulation 1 introduces parameter σ into the system as a Lagrange multiplier and overall equation of motion of unconstrained (free) body in a matrix form is

$$\begin{bmatrix} \boldsymbol{M} & \boldsymbol{0} & \boldsymbol{0} \\ \boldsymbol{0} & \boldsymbol{J} & 2\boldsymbol{p} \\ \boldsymbol{0}^T & 2\boldsymbol{p}^T & 0 \end{bmatrix} \begin{bmatrix} \ddot{\boldsymbol{R}} \\ \ddot{\boldsymbol{p}} \\ \sigma \end{bmatrix} + \begin{bmatrix} \boldsymbol{0} \\ 2\boldsymbol{H}\dot{\boldsymbol{p}} \\ \dot{\boldsymbol{p}}^T\dot{\boldsymbol{p}} \end{bmatrix} = \begin{bmatrix} \boldsymbol{f} \\ \boldsymbol{n}^{\star} \\ 0 \end{bmatrix} \tag{3.67}$$

where

$$\boldsymbol{J} = 4\boldsymbol{L}^T\overline{\boldsymbol{J}}\boldsymbol{L}, \tag{3.68}$$

$$\boldsymbol{H} = 4\dot{\boldsymbol{L}}^T\overline{\boldsymbol{J}}\boldsymbol{L}, \tag{3.69}$$

$$\boldsymbol{n}^{\star} = 2\boldsymbol{G}^T\boldsymbol{n} = 2\boldsymbol{G}^T\tilde{\boldsymbol{u}}_F^T\boldsymbol{f} = 2\boldsymbol{L}^T\overline{\boldsymbol{n}}. \tag{3.70}$$

The final matrix equation of motion can be written

$$\begin{bmatrix} \boldsymbol{M} & \boldsymbol{0} & \boldsymbol{0} \\ \boldsymbol{0} & 4\boldsymbol{L}^T\overline{\boldsymbol{J}}\boldsymbol{L} & 2\boldsymbol{p} \\ \boldsymbol{0}^T & 2\boldsymbol{p}^T & 0 \end{bmatrix} \begin{bmatrix} \ddot{\boldsymbol{R}} \\ \ddot{\boldsymbol{p}} \\ \sigma \end{bmatrix} = \begin{bmatrix} \boldsymbol{f} \\ \boldsymbol{n}^{\star} + 8\dot{\boldsymbol{L}}^T\overline{\boldsymbol{J}}\boldsymbol{L}\dot{\boldsymbol{p}} \\ -2\dot{\boldsymbol{p}}^T\dot{\boldsymbol{p}} \end{bmatrix}, \tag{3.71}$$

or in standard compact form

$$\boldsymbol{M}_{total}\ddot{\boldsymbol{q}} = \boldsymbol{Q}_{total}. \tag{3.72}$$

Formulation 2

The second formulation is basically only a transformation of all the equations from Euler angles method into the Euler parameters. This method is rarely used compare to the first formulation, since it suffers with similar issues as Euler angles (singular positions). The second formulation does not introduce any additional parameter, such as σ, but on the other hand, it does not increase number of variables and equations. The equation of motion in the seven variables has a form

$$\begin{bmatrix} \boldsymbol{M} \\ 2\overline{\boldsymbol{J}}\boldsymbol{L} \\ \boldsymbol{p}^T \end{bmatrix} \begin{bmatrix} \ddot{\boldsymbol{R}} \\ \ddot{\boldsymbol{p}} \end{bmatrix} + \begin{bmatrix} \boldsymbol{0} \\ \boldsymbol{L}\boldsymbol{H} \\ \dot{\boldsymbol{p}}^T \end{bmatrix} \begin{bmatrix} \dot{\boldsymbol{R}} \\ \dot{\boldsymbol{p}} \end{bmatrix} = \begin{bmatrix} \boldsymbol{f} \\ \overline{\boldsymbol{n}} \\ 0 \end{bmatrix}. \tag{3.73}$$

Formulation 3

Third formulation does not work directly with the Euler parameters. It is expressed in terms rotational velocities $\boldsymbol{\omega}$, which can be explicitly defined within Euler parameters. Moreover, in the definition of the rotations and in the constraints definition, the Euler parameters still appear. The overall equation of motion for the unconstrained body goes to a form

$$\begin{bmatrix} \boldsymbol{M} \\ \overline{\boldsymbol{J}} \end{bmatrix} \begin{bmatrix} \ddot{\boldsymbol{R}} \\ \dot{\overline{\boldsymbol{\omega}}} \end{bmatrix} + \begin{bmatrix} \boldsymbol{0} \\ \tilde{\overline{\boldsymbol{\omega}}}\overline{\boldsymbol{J}}\overline{\boldsymbol{\omega}} \end{bmatrix} = \begin{bmatrix} \boldsymbol{f} \\ \overline{\boldsymbol{n}} \end{bmatrix}. \tag{3.74}$$

If all three formulations are compared together, Eq. 3.72 contains 8 variables (three for translation motion, four Euler parameters and variable σ with the function of Lagrange multiplier); Formulation 2, Eq. 3.73, defines the spatial motion with 7 variables; while formulation 3, Eq. 3.74, contains only 6 variables.

Each of the formulation has some pros and cons and these can be discussed. Based on the experience on the multibody modelling and aim of this work, the formulation 1 will be used here and after. Thus, the kinematics constraints, constrained equation of motion as well as equation for system of constrained bodies are presented in this formulation 1.

Generally, the formulation within Euler parameters has advantages of singularity-free, it is more computationally efficient compared to Euler angles and the matrix formulation is explicitly prepared for the computer programming and is more straightforward to implement in a program for kinematic and dynamic analysis.

Equation of motion: Constrained dynamics

Multibody system can be considered as a set of rigid bodies connected via kinematic joints. The list of available joints is described above, together with the degree of freedom, constrained with this particular joint. The subject of interest in this work is model of human body (17 rigid connected via spherical joints) and thus, the constraint equation will be derived for the case of spherical joint.

In the case of Euler parameters, the constraint equation remains formally the same as in case of Euler angles, Eq. 3.41, but the matrix $\boldsymbol{A}$ has changed. Moreover, the derivatives of this equation changed significantly, since there is more variables.

Generally, the second derivatives of the constraint equation is added to the free body equation of motion Eq. 3.71 and these together formulate the constrained dynamics of the body. After some mathematics operations, substitutions and rearrangements, the equation of motion of the constrained body using the first formulation can be defined as,

$$\begin{bmatrix} \boldsymbol{M} & \boldsymbol{0} & \boldsymbol{0} & \boldsymbol{C}_{\boldsymbol{q}R} \\ \boldsymbol{0} & 4\boldsymbol{L}^T\overline{\boldsymbol{J}}\boldsymbol{L} & 2\boldsymbol{p} & \boldsymbol{C}_{\boldsymbol{q}P} \\ \boldsymbol{0}^T & 2\boldsymbol{p}^T & 0 & \boldsymbol{0} \\ \boldsymbol{C}_{\boldsymbol{q}R} & \boldsymbol{C}_{\boldsymbol{q}P} & \boldsymbol{0} & \boldsymbol{0} \end{bmatrix} \begin{bmatrix} \ddot{\boldsymbol{R}} \\ \ddot{\boldsymbol{p}} \\ \sigma \\ -\boldsymbol{\lambda} \end{bmatrix} = \begin{bmatrix} \boldsymbol{f} \\ \boldsymbol{n}^\star + 8\dot{\boldsymbol{L}}^T\overline{\boldsymbol{J}}\boldsymbol{L}\dot{\boldsymbol{p}} \\ -2\dot{\boldsymbol{p}}^T\dot{\boldsymbol{p}} \\ \boldsymbol{h}_i - \boldsymbol{h}_j \end{bmatrix} \tag{3.75}$$

where $\boldsymbol{h}_i$ is defined as

$$\boldsymbol{h}_i = -2\dot{\boldsymbol{G}}_i\dot{\boldsymbol{L}}_i^T\overline{\boldsymbol{u}}_P^i \tag{3.76}$$

and $\boldsymbol{C}_{\boldsymbol{q}R}$ and $\boldsymbol{C}_{\boldsymbol{q}P}$ are Jacobi matrices associated with the traslation and orientation coordinates respectively defined as

$$\boldsymbol{C}_{\boldsymbol{q}R} = \boldsymbol{I}, \tag{3.77}$$

$$\boldsymbol{C}_{\boldsymbol{q}P} = 2\boldsymbol{G}\tilde{\overline{\boldsymbol{u}}}_P. \tag{3.78}$$

If the system of system of n bodies constrained in the kinematic chain is considered, the total equation of motion for this mechanical system can be written based on the equation Eq. 3.75. The constraint equation between bodies must be defined and included to this equation via RHS and Jacobi matrix $\boldsymbol{C}_{\boldsymbol{q}}$. The parameter σ is an artifical variable and was defined in that way, to ensure the mass matrix to be square and regular (existence of exact inverse matrix). This parameter can be interpreted as a Lagrange multipliers associated with the constraint equation between Euler parameters Eq. 3.44. However, this variable remains in the vector of generalized coordinates $\boldsymbol{q}$ and does not come to a Lagrange multipliers vector (constraint between bodies) and is integrated in the same way as $\boldsymbol{R}$ and $\boldsymbol{P}$.

When the system of n bodies, linked with the r spherical joints is considered, the total equation of motion has a following form, where the dimension of the sub-matrices are also written:

$$\begin{bmatrix} \underset{[8n\times 8n]}{\boldsymbol{M}} & \underset{[8n\times 3r]}{\boldsymbol{C}_{\boldsymbol{q}}^T} \\ \underset{[3r\times 8n]}{\boldsymbol{C}_{\boldsymbol{q}}} & \underset{[3r\times 3r]}{\boldsymbol{0}} \end{bmatrix} \begin{bmatrix} \underset{[8n\times 1]}{\ddot{\boldsymbol{q}}} \\ \underset{[3r\times 1]}{-\boldsymbol{\lambda}} \end{bmatrix} = \begin{bmatrix} \underset{[8n\times 1]}{\boldsymbol{F}} \\ \underset{[3r\times 1]}{\boldsymbol{\gamma}} \end{bmatrix} \tag{3.79}$$

3.2.3 Numerical analysis

The equation of motion Eq. 3.79 represents system of $8n + 3r$ mixed of differential and algebraic equations (DAE). In order to numerically solve such system, the method of elimination of the Lagrange multipliers is used here to transform this equation into the set of differential equations, that can be numerically solved using standard tool, such as MATLAB [77]. Equation 3.79 can be distributed into two vector equations as

$$\boldsymbol{M}\ddot{\boldsymbol{q}} - \boldsymbol{C_q}^T\boldsymbol{\lambda} = \boldsymbol{F}, \tag{3.80}$$

and

$$\boldsymbol{C_q}\ddot{\boldsymbol{q}} = \boldsymbol{\gamma}. \tag{3.81}$$

After rearranging of the Eq. 3.80, the acceleration can be expressed as

$$\ddot{\mathbf{q}} = \mathbf{M}^{-1}\left(\boldsymbol{F} + \boldsymbol{C_q}^T\boldsymbol{\lambda}\right), \tag{3.82}$$

and substituted into Eq. 3.81 as

$$\boldsymbol{C_q}\boldsymbol{M}^{-1}\left(\boldsymbol{F} + \boldsymbol{C_q}^T\boldsymbol{\lambda}\right) = \boldsymbol{\gamma}. \tag{3.83}$$

After some basic mathematical operations, vector of Lagrange multipliers is expressed in the following form

$$\boldsymbol{\lambda} = \left(\boldsymbol{C_q}\boldsymbol{M}^{-1}\boldsymbol{C_q}^T\right)^{-1}\left(\boldsymbol{\gamma} - \boldsymbol{C_q}\boldsymbol{M}^{-1}\boldsymbol{F}\right). \tag{3.84}$$

When Eq. 3.84 is substituted into the Eq. 3.82, vector of Lagrange multipliers is eliminated and the vector of unknown generalized accelerations can be expressed as

$$\ddot{\boldsymbol{q}} = \boldsymbol{M}^{-1}\left[\boldsymbol{F} + \boldsymbol{C_q}^T\left(\boldsymbol{C_q}\boldsymbol{M}^{-1}\boldsymbol{C_q}^T\right)^{-1}\left(\boldsymbol{\gamma} - \boldsymbol{C_q}\boldsymbol{M}^{-1}\boldsymbol{F}\right)\right] \tag{3.85}$$

The Equation 3.85 can be numerically solved in MATLAB computational environment using implemented solvers ODE for numerical integration. However, such equation can has some undesirable properties. It leads to be numerically unstable for certain cases, and so called drift-off effect consisted of the violation of constraints occurs during the solution. The violation problem comes from the fact, that the numerical solution using second derivatives of constraint equation is not the same as the solution using original equation.

3.3 Numerical stability of multibody system

When the set of constraints are imposed into a dynamical system, it is important that the solution must satisfied the constraint equations at all levels. To prevent numerical irregularities during the solution, stability of equation of motion must be preserved. This

chapter discuss numerical stability of the governing equation of motion when integrated to yield the time history of a system. Firstly, the Baumgarte stabilization technique used to stabilize and reduce the error due to conventional representation of the constraint equations is presented. Secondly, correction method by Yu and Chen is introduced [120]. Finally, other approaches such as penalty method or a method by Amirouche and Ider, that modify the constraint equations are briefly introduced.

3.3.1 Baumgarte stabilization

One of the most commonly used stabilization method is a constraint violation stabilization or a constraint regularization with the Baumgarte stabilization method [27, 45, 51]. The constraint equation Eq. 3.40 is modified to following equations

$$\ddot{\boldsymbol{C}} + 2\alpha\dot{\boldsymbol{C}} + \beta^2\boldsymbol{C} = \boldsymbol{0}, \tag{3.86}$$

which is solved during numerical solution of DAE Eq. 3.79. The coefficients α and β are chosen as positive constants. Vector $\boldsymbol{\gamma}$ in the Eq. 3.79 can be replaced by a new vector

$$\overline{\boldsymbol{\gamma}}(\boldsymbol{q}, \dot{\boldsymbol{q}}, t) = \boldsymbol{\gamma}(\boldsymbol{q}, \dot{\boldsymbol{q}}, t) - 2\alpha\dot{\boldsymbol{C}} - \beta^2\boldsymbol{C}, \tag{3.87}$$

and substitute into the expression of the generalized accelerations Eq. 3.85 as

$$\ddot{\boldsymbol{q}} = \boldsymbol{M}^{-1}\left[\boldsymbol{F} + \boldsymbol{C_q}^T\left(\boldsymbol{C_q}\boldsymbol{M}^{-1}\boldsymbol{C_q}^T\right)^{-1}\left(\boldsymbol{\gamma} - 2\alpha\dot{\boldsymbol{C}} - \beta^2\boldsymbol{C} - \boldsymbol{C_q}\boldsymbol{M}^{-1}\boldsymbol{F}\right)\right]. \tag{3.88}$$

Equations 3.88 is a total EOM of constrained dynamical system including also additional stabilization elements. The Baumgarte constraint violation method is one of the oldest stabilization method and it was adopted from feedback control theory to construct a modified differential equations, which implicitly accounted for violation in the constraint equations. Additional terms can be comprehend as a proportional-derivative (PD) controller [92]. However this method has some disadvantages.

- Different types of violation are not considered in the constraint equation since the same correction parameters are used. Thus some violations might be eliminated, while others cannot.
- Baumgarte technique is an indirect stabilization method. It adds feedback control terms in the dynamics equation to control the constraint violations instead of correcting the values of state variables to satisfy the constraint equations.
- There is no general rule how to select the coefficients α and β, it is based on the experience or could be set with respect to the sensitivity analysis of the particular system onto these parameters. If the values are too large, the dynamic equation will be influenced significantly and the obtained results are not acceptable to describe behavior of the system. On the other hand, if the values are too small, the violations

cannot be controlled effectively. The selection of α and β between 0 and 10 are suggested in [51]. The relationship between the constants $\beta = \alpha\sqrt{2}$ or $\beta = \sqrt{2\alpha}$ is proposed in[51, 120]. Zhenkuan [122] developed a method for automatic selection of parameters α and β. The proposed selections are that

$$\alpha = \frac{1}{h}, \qquad \beta = \frac{\sqrt{2}}{h}, \tag{3.89}$$

where is h the step-length of integration. However, when applying the variable step-length integrator, this method of automatic selection becomes impractical.

Despite these disadvantages, the Baumgarte stabilization technique is still one of the most often used method for stabilization of constraint dynamic equations. It is relatively easy to apply and it was proved to work for wide range of mechanical systems.

3.3.2 Direct violation correction method

Purpose of this method lays in correction of the values of generalized coordinates and generalized velocities after each time step in order to satisfy the constraint equations [120]. There are no additional terms added to the equation of motion.

Generalized coordinates correction

Let us assume that at *i-th* time step $t = t_i$, the generalized coordinates of the system are $\widehat{\boldsymbol{q}}_i$. If this calculated coordinates do not satisfy the constraint equation, thus

$$\boldsymbol{C}(\widehat{\boldsymbol{q}}_i, t) \neq \boldsymbol{0} \tag{3.90}$$

with the given error tolerance, a correction term $\delta\boldsymbol{q}_i$ is added to satisfy the constraint equation. The corrected generalized coordinates $\boldsymbol{q}_i$ are expressed as

$$\boldsymbol{q}_i = \widehat{\boldsymbol{q}}_i + \delta\boldsymbol{q}_i, \tag{3.91}$$

in such way that

$$\boldsymbol{C}_i = \boldsymbol{C}(\boldsymbol{q}_i, t_i) = \boldsymbol{C}(\widehat{\boldsymbol{q}}_i, t_i) + \delta\boldsymbol{C}_i = \boldsymbol{0}. \tag{3.92}$$

The generalized coordinates correction term is defined as

$$\delta\boldsymbol{q}_i = -(\boldsymbol{C}_{\boldsymbol{q}})_i^T \left[(\boldsymbol{C}_{\boldsymbol{q}})_i (\boldsymbol{C}_{\boldsymbol{q}})_i^T\right]^{-1} \boldsymbol{C}(\widehat{\boldsymbol{q}}_i, t_i), \tag{3.93}$$

where the term $(\boldsymbol{C}_{\boldsymbol{q}})_i = \boldsymbol{C}_{\boldsymbol{q}}(\widehat{\boldsymbol{q}}_i, t_i)$ is Jacobian of the constraints expressed in original (uncorrected) generalized coordinates and $(\boldsymbol{C}_{\boldsymbol{q}})_i$ is Jacobian matrix in terms of modified coordinates. Finally the corrected generalized coordinates, which satisfy the constraint equation

$$\boldsymbol{C}(\boldsymbol{q}_i, t) = \boldsymbol{0}, \tag{3.94}$$

takes the form

$$\boldsymbol{q}_i = \widehat{\boldsymbol{q}}_i - (\boldsymbol{C}_{\boldsymbol{q}})_i^T \left[(\boldsymbol{C}_{\boldsymbol{q}})_i (\boldsymbol{C}_{\boldsymbol{q}})_i^T\right]^{-1} \boldsymbol{C}(\widehat{\boldsymbol{q}}_i, t_i) \tag{3.95}$$

Generalized velocities correction

When the violation in velocity constraint equations is beyond a specific error tolerance, i.e.,

$$\dot{\boldsymbol{C}}_i = \dot{\boldsymbol{C}}(\boldsymbol{q}_i, \widehat{\dot{\boldsymbol{q}}}_i, t) \neq \boldsymbol{0}, \tag{3.96}$$

where $\widehat{\dot{\boldsymbol{q}}}_i$ are calculated (uncorrected) generalized velocities. The correction term $\delta\dot{\boldsymbol{q}}_i$ is added to generalized velocities to satisfy the constraint equation. In a similar way as defined in previous paragraph, the generalized velocities are corrected as

$$\dot{\boldsymbol{q}}_i = \widehat{\dot{\boldsymbol{q}}}_i + \delta\dot{\boldsymbol{q}}_i \tag{3.97}$$

The generalized velocities correction term is defined as

$$\delta\dot{\boldsymbol{q}}_i = -(\boldsymbol{C}_{\boldsymbol{q}})_i^T \left[(\boldsymbol{C}_{\boldsymbol{q}})_i (\boldsymbol{C}_{\boldsymbol{q}})_i^T\right]^{-1} \dot{\boldsymbol{C}}(\boldsymbol{q}_i, \widehat{\dot{\boldsymbol{q}}}_i, t_i), \tag{3.98}$$

Consequently the corrected generalized velocities, which satisfy the constraint equation

$$\dot{\boldsymbol{C}}(\boldsymbol{q}_i, \widehat{\dot{\boldsymbol{q}}}_i, t) = \boldsymbol{0}, \tag{3.99}$$

takes the form

$$\dot{\boldsymbol{q}}_i = \widehat{\dot{\boldsymbol{q}}}_i - (\boldsymbol{C}_{\boldsymbol{q}})_i^T \left[(\boldsymbol{C}_{\boldsymbol{q}})_i (\boldsymbol{C}_{\boldsymbol{q}})_i^T\right]^{-1} \dot{\boldsymbol{C}}(\boldsymbol{q}_i, \widehat{\dot{\boldsymbol{q}}}_i, t_i). \tag{3.100}$$

Thus the violation in coordinates and velocities constraint equation can be eliminated after each integration time step. The proposed method can be applied under holonomic constraints only. However, the selection of the given error tolerances has no general rules. Yu in his work [120] suggests the values between 10^{-5} and 10^{-8}.

3.3.3 Penalty formulation method

Another stabilization technique is based on a penalty formulation. The concept of this method is the constraints enforcing using the special penalty term that is added to the Lagrangian of the system. The additional term can be define as

$$\frac{1}{2}\boldsymbol{C}^T\boldsymbol{B}\boldsymbol{C}, \tag{3.101}$$

where $\boldsymbol{B}$ is diagonal matrix with the particular penalty factors b_i on the main diagonal. One of the representation of penalty technique is the augmented Lagrangian formulation [38]. The regularization of the vanishing constraint by Amirouche and Ider is described in [27]. This is a special technique for stabilization equation of motion of the multibody system with singular positions and redundant constraints. It is based on eliminations of particular rows of constraint equation.

Several other stabilization methods for numerical integration of equation of motion were developed, see [27, 51, 122]. The selection of the proper methods always depends on the particular model, and cannot be anyhow generalized. Moreover, the combination of more techniques is also possible.

3.4 Sensitivity Analysis

In the previous chapter, the equation of motion for the constrained dynamic Eq. 3.79 was derived and several methods for numerical stabilization were described. Since there is no general rule, which method is more suitable for particular dynamical system, and what values of the parameters should be used, examples of spatial pendulum and double pendulum respectively (one or two body constrained with the spherical joint) are analyzed. Variation of the parameters for the Baumgarte and direct violation method applied on the spatial pendulum and double pendulum are performed, to identify more suitable method and to test the effect of the parameter variations. This sensitivity analysis can help in further modelling to choose the stabilization method and to better understand how the parameters affect the particular model. Since the further model of the human body contains only spherical joints, just spherical joints are analyzed.

3.4.1 Spatial pendulum

The example here is the ellipsoid body, linked with the frame at point P (spherical joint) at the top of the main axis, loaded with the gravity, see Fig. 3.4 and in this case, zero initial velocities. The case of non-zero initial velocities was analyzed as well. However, it was found out, that the dynamical system with one body is not stable for any value of non-zero initial velocities. The body initially lays in the horizontal position (main axis of the body is parallel with the global axis X). The geometry and mass of the body are summarized in the Table 3.2. The simulation time is 5 s.

m	1	[kg]	Mass of the body
a	0.6	[m]	Length of the main principle axis
b	0.4	[m]	Length of the second principle axis
c	0.2	[m]	Length of the third principle axis
d$\mathbf{R}$	$\mathbf{0}$	[m/s]	Initial velocities vector

Table 3.2: Mechanical properties of the body

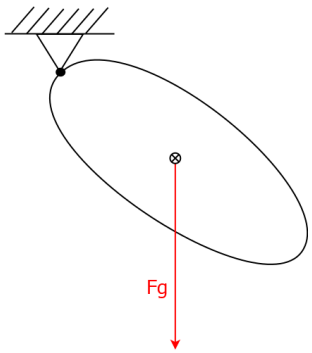

Figure 3.4: Spatial pendulum

Firstly, Baumgarte stabilization method with the variation of $\alpha \in \{0, 1, 5, 10, 50, 100, 1000\}$ and consequently $\beta = \alpha\sqrt{2}$ and zero initial velocities is done. The monitored parameters are maximum violation of the constraint equation and calculation CPU time on the computer Dell Inspiron 15 7000. The CPU time is not an important aspect of the calculation in its absolute value. It is provided here only to compare the particular calculation one to each other (so the relative difference between CPU is rather important aspect).

d$\mathbf{R}$	α	β	Direct violation	Stable	Max. violation [m]	CPU [s]
0	0	0	NO	YES	0.03	0.157
0	1	1.41	NO	YES	$6.0E{-4}$	0.149
0	5	7.07	NO	YES	$1.2E{-4}$	0.164
0	10	14.14	NO	YES	$6.0E{-5}$	0.155
0	50	70.71	NO	YES	$7.0E{-5}$	0.297
0	100	141.42	NO	YES	$8.0E{-6}$	0.450
0	1000	1414.21	NO	YES	$5.0E{-6}$	2.2

NOTE: symbol d$\mathbf{R}$ is an expression for dx, dy and dz. Here, all three velocities are equal to zero.

Table 3.3: Sensitivity analysis of α and β for pendulum

Secondly, $\alpha = 0$ and thus Baumgarte method is not active and only direct violation method is used. The direct violation method is specified with the error tolerance ϵ and $d\epsilon$ for the constraint equations (coordinate Eq. 3.90 and velocity constraint equations Eq. 3.96). The variation here is specified within these error tolerance. For the simplicity, both the tolerances equal and the results are in Tab. 3.4.

d**R**	α	β	Direct violation	$\epsilon = d\epsilon$	Stable	Max. violation [m]	CPU [s]
0	0	0	YES	$1.0E{-}3$	YES	0.07	0.179
0	0	0	YES	$1.0E{-}2$	YES	0.015	0.164
0	0	0	YES	$1.0E{-}1$	NO	0.08	0.154
0	0	0	YES	$5.0E{-}1$	NO	0.03	0.141
0	0	0	YES	1.0	NO	0.03	0.134

Table 3.4: Sensitivity analysis of ϵ and $d\epsilon$ for pendulum

The third case of sensitivity analysis consists of combination of both methods. From the previous analysis, the best case of direct violation was chosen (i.e. $\epsilon = d\epsilon = 1.0e-2$) and together with the variation of α and β.

d**R**	α	β	Direct violation	$\epsilon = d\epsilon$	Stable	Max. violation [m]	CPU [s]
0	1	1.41	YES	$1.0E{-}2$	YES	$1.5E{-}3$	0.169
0	5	7.07	YES	$1.0E{-}2$	YES	$5.0E{-}3$	0.191
0	10	14.14	YES	$1.0E{-}2$	YES	$1.2E{-}4$	0.231
0	50	70.71	YES	$1.0E{-}2$	YES	$1.5E{-}5$	0.436
0	100	141.42	YES	$1.0E{-}2$	YES	$7.0E{-}6$	0.804
0	1000	1414.21	YES	$1.0E{-}2$	YES	$3.0E{-}4$	8.789

Table 3.5: Sensitivity analysis of both methods for pendulum

In the following Figures 3.5, the violation of the constraint (relative motion of the joint) are plotted within the coordinates X, Y, and Z. These should from the definition remain zero, but due to the violation of the constraint, they are not. If the $\epsilon = 0$, the direct violation method is not active.

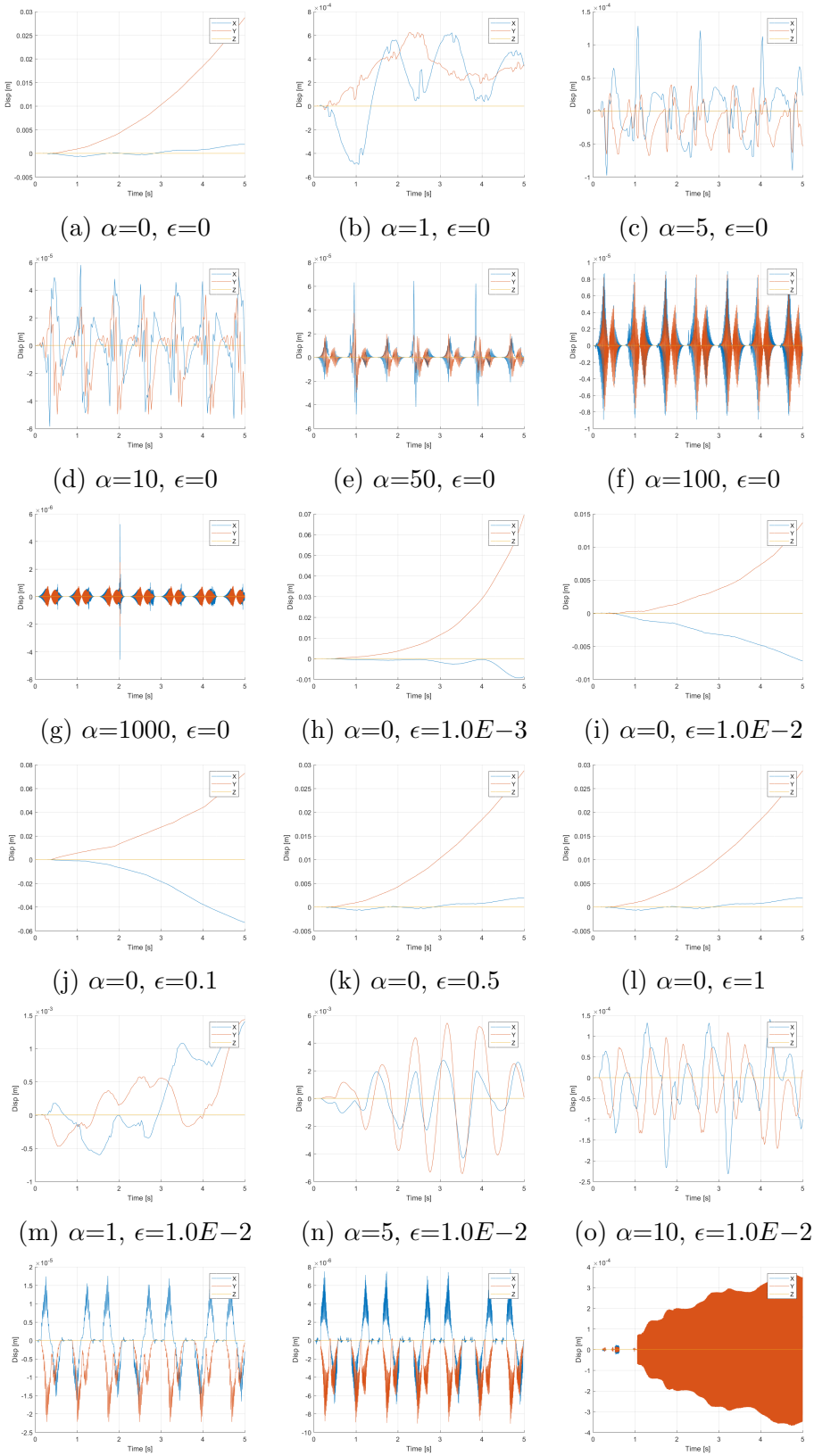

(a) α=0, ϵ=0 (b) α=1, ϵ=0 (c) α=5, ϵ=0

(d) α=10, ϵ=0 (e) α=50, ϵ=0 (f) α=100, ϵ=0

(g) α=1000, ϵ=0 (h) α=0, ϵ=1.0E−3 (i) α=0, ϵ=1.0E−2

(j) α=0, ϵ=0.1 (k) α=0, ϵ=0.5 (l) α=0, ϵ=1

(m) α=1, ϵ=1.0E−2 (n) α=5, ϵ=1.0E−2 (o) α=10, ϵ=1.0E−2

(p) α=20, ϵ=1.0E−2 (q) α=100, ϵ=1.0E−2 (r) α=1000, $\epsilon = 1.0E-2$

Figure 3.5: Results of the pendulum sensitivity analysis

3.4.2 Spatial double pendulum

In order to test stabilization method on a chain of constrained bodies, the double-pendulum example was analyzed for the variations of initial parameters for the stabilization method, see Fig. 3.6. Similarly with the pendulum example, the case of zero initial velocities was tested. It was discovered, that the non-zero initial velocities can be also stable, if they are not applied directly on the body, that is constrained with the frame (if yes, the violation is too high and non of the stabilization techniques works). The mechanical system consists of two identical bodies linked with the spherical joint (first body is linked to the frame), see Tab. 3.6.

$m_1 = m_2$	1	[kg]	Mass of the body
$a_1 = a_2$	0.6	[m]	Main principle axis
$b_1 = b_2$	0.4	[m]	Second principle axis
$c_1 = c_2$	0.2	[m]	Third principle axis

Table 3.6: Mechanical properties of the bodies

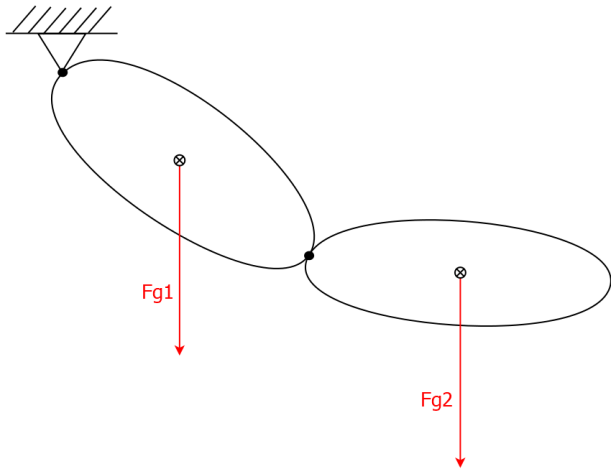

Figure 3.6: Spatial pendulum

Firstly, the Baumgarte stabilization method only is applied and results are as follows:

H]

d**R**	α	β	Direct violation	$\epsilon = d\epsilon$	Stable	Max. violation [m]	CPU [s]
0	1	1.41	YES	$1.0E{-}1$	YES	$1.0E{-}3$	0.331
0	5	7.07	YES	$1.0E{-}1$	YES	$6.0E{-}4$	0.337
0	10	14.14	YES	$1.0E{-}1$	YES	$1.2E{-}5$	0.401
0	50	70.71	YES	$1.0E{-}1$	YES	$6.0E{-}6$	0.743
0	100	141.42	YES	$1.0E{-}1$	YES	$3.0E{-}6$	1.091
0	1000	1414.21	YES	$1.0E{-}1$	YES	$1.2E{-}6$	5.124

Table 3.9: Sensitivity analysis of both methods for double pendulum

d**R**	α	β	Direct violation	Stable	Max. violation [m]	CPU [s]
0	0	0	NO	YES	$1.6E{-}3$	0.31
0	1	1.41	NO	YES	$7.0E{-}5$	0.319
0	5	7.07	NO	YES	$7.0E{-}5$	0.322
0	10	14.14	NO	YES	$2.4E{-}5$	0.317
0	50	70.71	NO	YES	$1.0E{-}5$	0.587
0	100	141.42	NO	YES	$9.0E{-}6$	0.956
0	1000	1414.21	NO	YES	$8.0E{-}6$	5.12

Table 3.7: Sensitivity analysis of α and β for double pendulum

Secondly, only direct violation method is considered:

d**R**	α	β	Direct violation	$\epsilon = d\epsilon$	Stable	Max. violation [m]	CPU [s]
0	0	0	YES	$1.0E{-}3$	YES	$4.0E{-}4$	0.481
0	0	0	YES	$1.0E{-}2$	YES	$2.0E{-}4$	0.419
0	0	0	YES	$1.0E{-}1$	YES	$4.0E{-}4$	0.361
0	0	0	YES	$5.0E{-}1$	YES	$1.6E{-}3$	0.342
0	0	0	YES	1.0	YES	$1.6E{-}3$	0.316

Table 3.8: Sensitivity analysis of ϵ and $d\epsilon$ for double pendulum

Thirdly, the combination of the methods, for the double pendulum example, with zero initial velocities. The value of error tolerance ϵ and $d\epsilon$ was chosen based on the best results of the previous analysis.

In following Figures 3.7, the violation of the constraint (relative motion of the frame joint) are plotted within the coordinates X, Y, and Z.

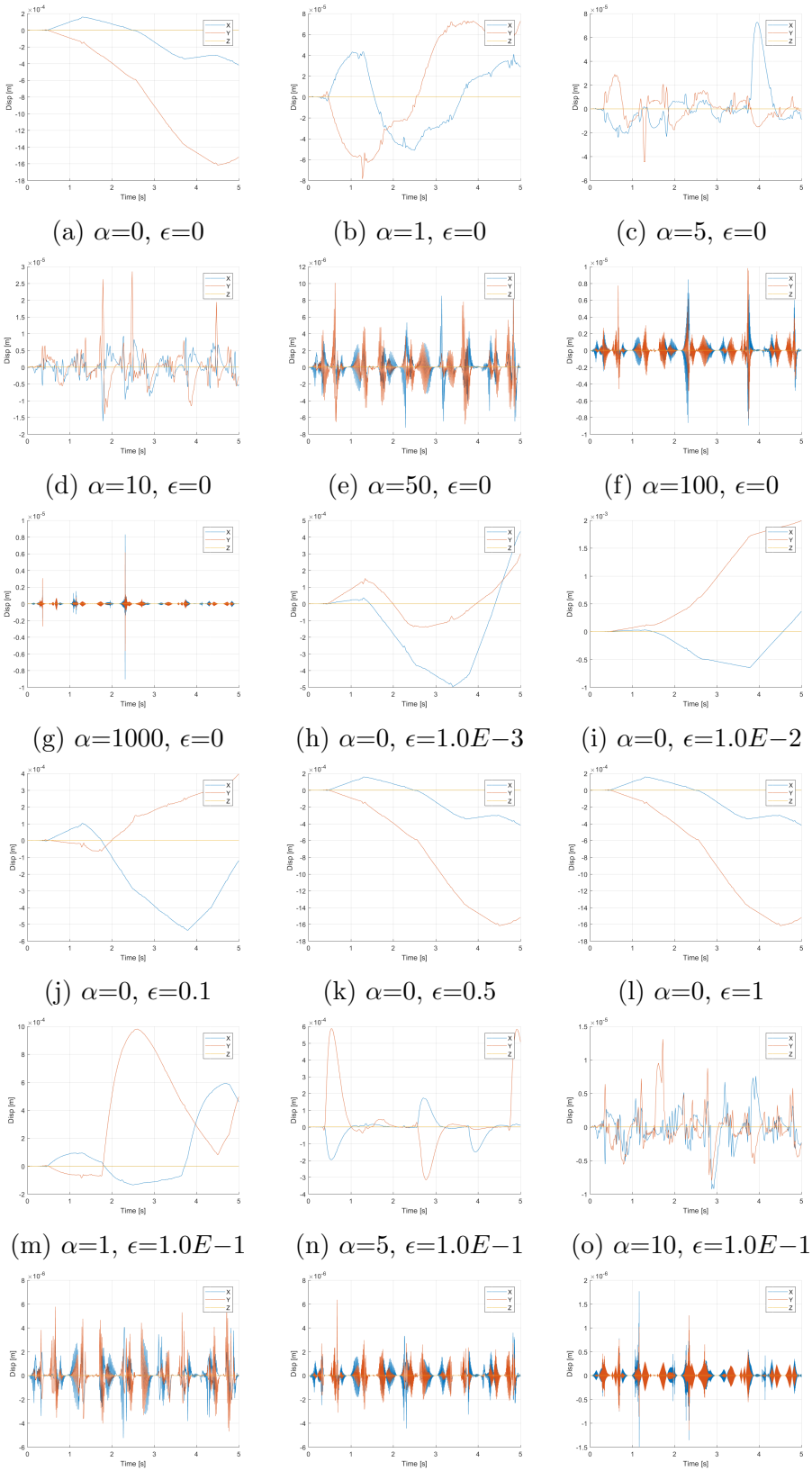

(a) α=0, ϵ=0 (b) α=1, ϵ=0 (c) α=5, ϵ=0

(d) α=10, ϵ=0 (e) α=50, ϵ=0 (f) α=100, ϵ=0

(g) α=1000, ϵ=0 (h) α=0, ϵ=1.0E−3 (i) α=0, ϵ=1.0E−2

(j) α=0, ϵ=0.1 (k) α=0, ϵ=0.5 (l) α=0, ϵ=1

(m) α=1, ϵ=1.0E−1 (n) α=5, ϵ=1.0E−1 (o) α=10, ϵ=1.0E−1

(p) α=20, ϵ=1.0E−1 (q) α=100, ϵ=1.0E−1 (r) α=1000, ϵ=1.0E−1

Figure 3.7: Results of the double pendulum sensitivity analysis

As was previously discussed, constrained dynamical system can behave stable, if the frame-linked body is not directly loaded with the initial velocities. In order to test this theorem and to show how the system behaves if the first or second body is loaded, the variation on the stabilization method together with the variation of the loading is presented. Initial translation velocity for each body is specified with the vector $d\mathbf{R} = [dx, dy, dz]$. Here in the analysis, all three velocities always equal and are defined as $d\mathbf{R}$ in the Table 3.10.

$d\mathbf{R}_1$	$d\mathbf{R}_2$	α	β	Direct violation	$\epsilon = d\epsilon$	Stable	Max. violation [m]	CPU [s]
0.1	0	0	0	NO	–	NO	–	–
0.1	0	1	1.41	NO	–	YES	$3.0E{-}2$	0.450
0.5	0	1	1.41	NO	–	YES	$1.6E{-}1$	0.41
1.0	0	1	1.41	NO	–	NO	–	–
0.1	0	0	0	YES	$1.0E{-}1$	NO	–	–
0.1	0	1	1.41	YES	$1.0E{-}1$	NO	–	–
0.5	0	1	1.41	YES	$1.0E{-}1$	NO	–	–
1.0	0	1	1.41	YES	$1.0E{-}1$	NO	–	–
0	0.1	0	0	NO	–	YES	$2.0E{-}3$	0.405
0	0.1	1	1.41	NO	–	YES	$7.0E{-}5$	0.379
0	0.5	1	1.41	NO	–	YES	$1.2E{-}4$	0.505
1	1.0	1	1.41	NO	–	YES	$1.4E{-}4$	0.526
0	0.1	0	0	YES	1.0e-1	YES	$1.4E{-}3$	0.606
0	0.1	1	1.41	YES	1.0e-1	YES	$3.0E{-}4$	0.391
0	0.5	1	1.41	YES	1.0e-1	YES	$4.5E{-}2$	0.806
1	1.0	1	1.41	YES	1.0e-1	YES	$2.0E{-}2$	0.774
0.1	0	5	7.07	NO	–	YES_A	$7.0E{-}3$	–
0.1	0	10	14.14	NO	–	YES_A	$3.2E{-}3$	–
0.1	0	50	70.71	NO	–	YES_A	$2.0E{-}3$	–
0	0.1	5	7.07	NO	–	YES_A	$2.0E{-}5$	–
0	0.1	10	14.14	NO	–	YES_A	$8.0E{-}6$	–
0	0.1	50	70.71	NO	–	YES_A	$4.0E{-}6$	–

NOTE A: The system behaves stable, until the numerical integration fails, due to length of the step size.

Table 3.10: Sensitivity analysis of ϵ and $d\epsilon$ for double pendulum with non-zero initial velocities

This dynamical system does not behave very stable for the non-zero initial velocities, or are stable until numerical failure, the plot of the constraint violation does not bring any additional information and thus, is not provided.

3.4.3 Discussion

The stabilization techniques analyzed here can be summarized in a few conclusion remarks.

- If the body, that is directly constrained to the frame, is loaded with non-zero initial velocity, the system is unstable and violation of the constraint still increases.
- Results of the analysis with the non-zero initial velocities proof this theory. The results in Table. 3.10 indicate that the system generally behaves more stable, if the second body is loaded (even is not fully stable during the entire simulation).
- If the Baumagarte method is used, increasing of the α and consequently β causes the decreasing of the violation but increasing of the CPU time.
- Increasing of the α added artificial damping element into the EOM and the constraint shows vibration (oscillation) effect.
- Direct violation method works less effective than Baumgarte, however, it can stabilize the pendulum and double pendulum for certain cases.
- The combination of both methods works less effective than Baumgarte itself for these particular configurations.
- In the further analysis, the Baumgarte method with the parameters α and β from 1 to 100 can be recommended as an initial value. If these does not work well, these values can be heightened and possibly the direct violation can be activated.

Chapter 4

Human body model - MBS

The aim of this work is to create MBS solver, to analyze its behavior, to test particular algorithms in an in-house software including 3D model of a human body for various loading scenarios. The human body model here is a system of rigid bodies linked with spherical joints and constrained in open kinematic tree structure, to approximate external shape of the human. This system, however cannot simulate behavior of human body for any kind of loading and thus, the suitable configurations must be specified and tuned up (validated) to get reasonable results. Consequently, the behavior of internal organs, fractures of bones or rupture of the muscles are not captured here. Purpose of this model is to describe global behavior of human body under different impact situations. The basic concept of this work is in the segmentation of the human body defined by Robbins [93, 62]. Human body is divided into the segments, whose motion are in agreement with the kinematic of human body under external loading, see Fig. 4.1.

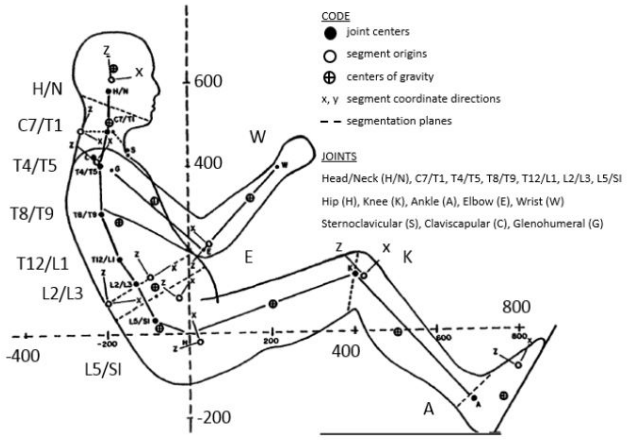

Figure 4.1: Segmentation of human body [93]

Hynčík [62] suggested the simply structure of the 2D model containing 11 rigid bodies,

see Figure 4.2, where all bodies are modelled as ellipses or circles, respectively.

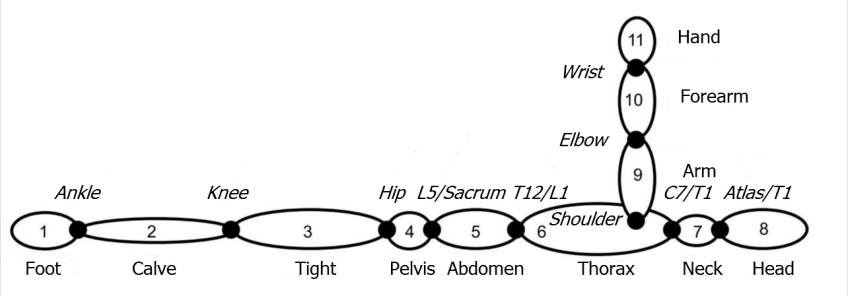

Figure 4.2: Segmentation of 2D human body model [62]

The spatial model segmentation is expanded within pair extremities, and thus the model has 17 rigid bodies, based on Fig. 4.2 and Fig. 4.1:

- Pelvis
- Abdomen
- Thorax
- Neck
- Head
- Left and Right Arms
- Left and Right Forearms
- Left and Right Hands
- Left and Right Tights
- Left and Right Calves
- Left and Right Feet

The connections between bodies are modelled within the 16 spherical joints, representing real human joints:

- Vertebrae L5/Sacrum, between abdomen and pelvis
- Vertebrae T12/L1, between thorax and abdomen
- Vertebrae C7/T1, between neck and thorax
- Vertebrae Atlas/T1 , between head and neck
- Left and Right Shoulder joints
- Left and Right Elbow joints
- Left and Right Wrist joints
- Left and Right Hip joints
- Left and Right Knee joints
- Left and Right Ankle joints

4.1 Mass distribution, geometry and inertia properties

This model is build to be a scalable, to capture the various size of the population [88]. The total weight and total height of the human are the inputs and the dimensions and mass of particular segments are calculated based on these defined values. The mass of the body segments can be calculated from the total mass and height of the human, generally with the two approaches [69, 106]. The first, and less accurate comes from mass distribution of the particular segments expressed in percentages. The second approach is method of Zaciorsky and Salujanov (1979) [106], who used radioisotope method for experimental measuring of 100 humans and defined coefficients for each body segments. The mass of the particular segment can be expressed with the simple equation

$$m_i = \beta_{0i} + \beta_{1i} m + \beta_{2i} v, \tag{4.1}$$

where m [kg] is the total mass of the body, v [cm] is weight of body and coefficients β are defined in Table 4.1

Segment	$\boldsymbol{\beta_0}$ **[kg]**	$\boldsymbol{\beta_1}$ **[-]**	$\boldsymbol{\beta_2}$ $[\boldsymbol{kg.cm^{-1}}]$
Pelvis	-7.498	0.0976	0.04896
Abdomen	7.181	0.2234	-0.0663
Thorax	8.2144	0.1862	-0.0584
Neck	0.096	0.0031	0.0022
Head	1.2	0.014	0.0123
Arm	0.25	0.03013	-0.0027
Forearm	0.3185	0.01445	-0.00114
Hand	-0.1165	0.0036	0.00175
Tight	-2.649	0.1463	0.0137
Calf	-1.592	0.03616	0.0121
Foot	-0.829	0.0077	0.0073

Table 4.1: Table of coefficients for calculation of body segment's masses [106]

Geometry of the segments was defined based on Robbins database, where dimensions of large, medium and small man and female, are published [98]. An average male of height equals to 180 cm was used as a reference one (measured in Czech Republic in 2011) [68], and all the dimensions from Robbins (medium male) are related to this value. Thus, the dimensions of each body segment are function of total height of body only and calculated based on the database. Such algorithm enable the user to model wide set of population (height and weight). However, it does not take into account different shape of the humans (thin, fat, large etc.). The model of a medium size male, with the height equals to 180 cm and weight equals to 80 kg; with the arms outspread and stretched out are shown in Figs. 4.3.

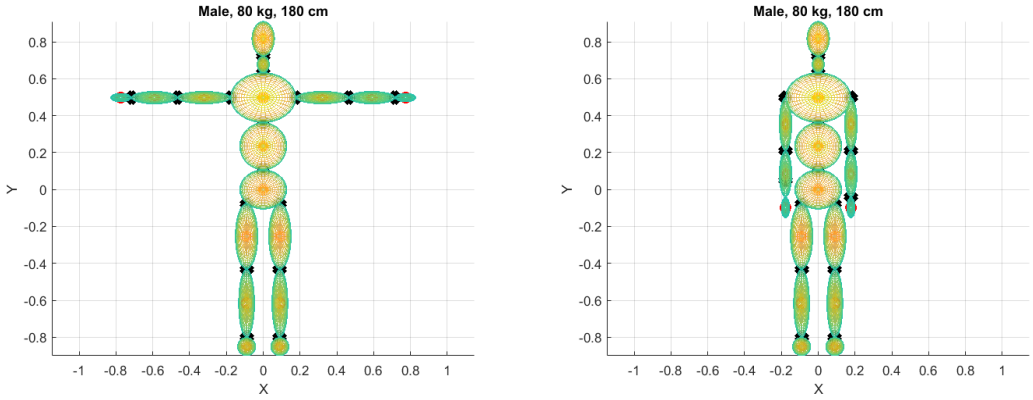

Figure 4.3: Male, 180 cm, 80 kg

Inertia properties of the body segments are calculated from mass and geometry of the particular body parts. Since the origin of the local coordinate system is assume to coincide with centre of mass of the body, the principal moments of inertia equal to zero and inertia tensor (ellipsoid) can be defined as:

$$\mathbf{I} = \begin{bmatrix} i_{xx} & i_{xy} & i_{xz} \\ i_{yx} & i_{yy} & i_{yz} \\ i_{zx} & i_{zy} & i_{zz} \end{bmatrix} = \begin{bmatrix} \frac{1}{5}m(b^2+c^2) & 0 & 0 \\ 0 & \frac{1}{5}m(a^2+c^2) & 0 \\ 0 & 0 & \frac{1}{5}m(a^2+b^2) \end{bmatrix}, \tag{4.2}$$

where a, b and c are lengths of semi-principal axes of the ellipsoid. The example of the scaled models are plotted in Fig. 4.4, where 5 models of different body size and weight are generated.

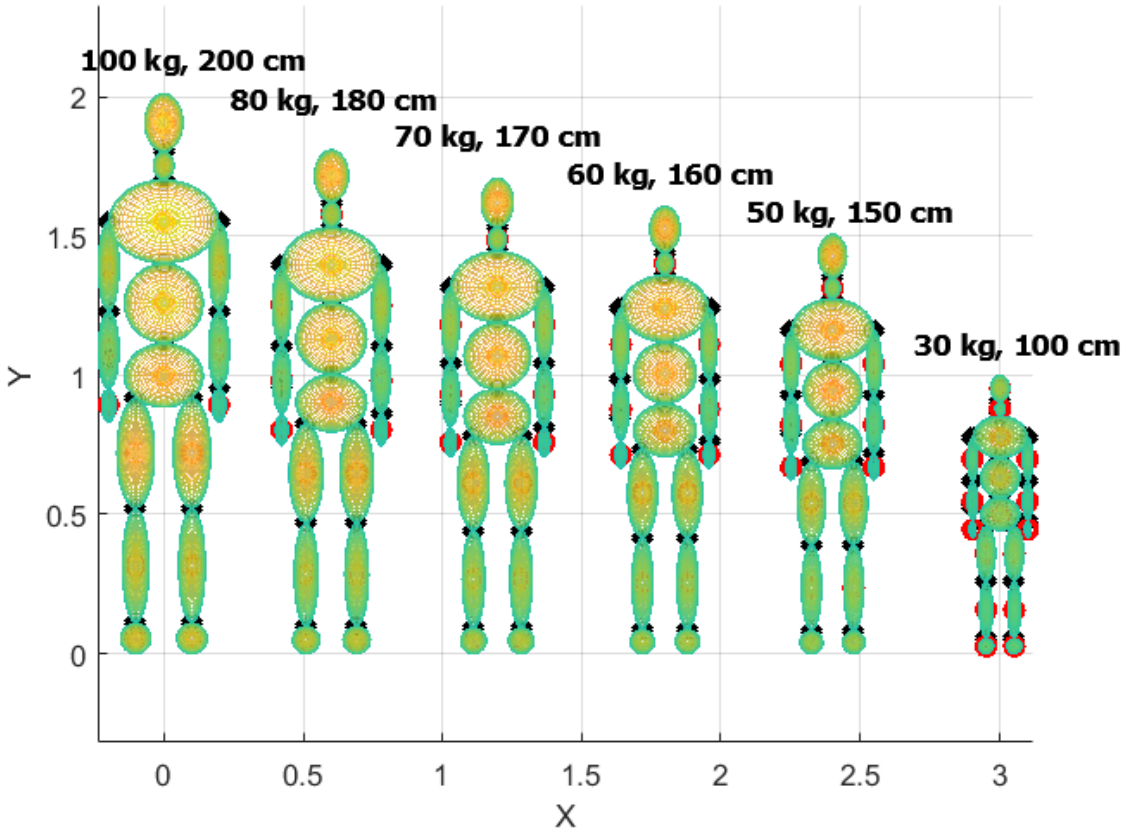

Figure 4.4: Scaled family of human body models (HBMs)

The masses of the scaled segments are presented in the Table 4.2, where average model (180 cm), 200 cm and 150 cm model are provided.

Model	80 kg, 180 cm	100 kg, 200 cm	100 kg, 200 cm
Segment	**Mass [kg]**	**Mass [kg]**	**Mass [kg]**
Pelvis	9.1	12.1	4.7
Abdomen	13.1	16.3	8.4
Thorax	12.6	15.2	8.8
Neck	0.7	0.8	0.6
Head	4.5	5.1	3.7
Arm	2.2	2.7	1.3
Forearm	1.3	1.5	0.8
Hand	0.5	0.6	0.3
Tight	11.5	14.7	6.7
Calf	3.5	4.4	2.1
Foot	1.1	1.4	0.7

Table 4.2: Masses of scaled body segments

4.2 Joint range of motion

The joints connecting the bodies in this mechanical system are modeled as spherical joints (unlimited spatial rotational motion). However, the real human joints have their physiological range of motion, and cannot withstand any possible sequence of rotations. Moreover, some joints allow only one main rotation about one axis (knee - flexion, Y axis), plus minor rotations around the rest two axes. The joints with only one degree of freedom (rotation) can be modelled with the revolute joint [91], or it can remain as a spherical joint with the additional internal stiffness to limit its range of motion (ROM). Internal stiffness can work as both, limits for range of motion and physiological stiffness of the joints. The stiffness can be defined by a curve, and then the model is loaded with the external torque, added on the RHS of the EOM Eq. 3.79. The physilogical range of motion was measured by Robbins and his team in 80's [93]. He measured anthropocentric dimensions, inertia properties, masses, joints range of motion for the mid-size male, small female and large male (the elementary concept of the dummy size). Based on the database [93, 105], the curves of internal stiffness for the particular joints were defined, and these can be used in this MBS human body model. The angles of rotations were measured from initial seating position, and were measured individually for X, Y, Z global axes. Thus, the transformation into the current set of rotation parameters (Euler parameters) is required, to correctly model the physiology of the human.

4.2.1 Quatermions

Using of the Euler parameters for the parametrisation of the spatial motion can show the advantage also here, in the measuring of the rotation of the body, with respect to the global coordinate system defined with axes: X,Y,Z. Euler parameters can be transformed into the set of the Euler angles (for example in standard sequence ZXZ). However, the angles calculated in such way cannot be used for the definition of the internal torque, since the stiffness curves and ROM are measured as an isolated rotation about the global axes X,Y,Z. respectively. Thus the transformation into any set of Euler angles does not bring any benefit. Moreover, the Euler angles would bring back the problem of singularities, that was eliminated with the Euler parameters.

Euler parameters are set of so called quatermions and this has, from the definition, some special features [27, 83, 99, 103, 118]. They were defined by William Rowan Hamilton in 1843 [52] as a 3D equivalent of the complex number and complex unit i. The main characterization of the quatermions is that they represent actual axis of rotation (global vector: 3 parameters) and the angle of rotation around this particular axis.

Let's have a generalized quatermion $\mathbf{\Lambda}$:

$$\mathbf{\Lambda} = [a, b, c, d]^T = [\cos\left(\frac{\upsilon}{2}\right), \sin\left(\frac{\upsilon}{2}\right)\mathbf{u}]^T \tag{4.3}$$

where a,b,c,d are four quatermion parameters, a stands for angle of rotation and b,c,d are connected with a vector of rotation, $\mathbf{u}$ is a global vector of actual rotation and υ a rotation angle.

In order to define the global rotation, the angles of rotation from the global axes separately must to be calculated. Here, the rotation of the body is defined with Euler parameters from which, the three angles can be calculated from Eq. 4.3.

$$\cos\left(\frac{\upsilon}{2}\right) = a, \tag{4.4}$$

$$\sin\left(\frac{\upsilon}{2}\right)\mathbf{u} = [b, c, d]^T. \tag{4.5}$$

Thus the angle and vector of actual rotation is

$$\upsilon = 2\arccos(a) \quad .... \quad [rad] \tag{4.6}$$

$$\mathbf{u} = \frac{[b, c, d]^T}{\sin\left(\frac{\upsilon}{2}\right)} \tag{4.7}$$

Finally, the angles of global rotations can be expressed directly from $\mathbf{u}$ and υ

$$\alpha = rot_x = u_x \upsilon \quad .... \quad [rad] \tag{4.8}$$

$$\beta = rot_y = u_y \upsilon \quad .... \quad [rad] \tag{4.9}$$

$$\gamma = rot_z = u_z \upsilon \quad .... \quad [rad] \tag{4.10}$$

where u_x, u_y and u_z are particular components of vector $\mathbf{u}$.

4.2.2 Physiological range of motion

The threshold of the physiological range of motion of the mid-size male are defined in the Tab. 4.3, where limits of positive and negative direction (with respect to the right-hand coordinate system of the model: X-left, Y-up, Z-front), the anatomical name of such motion and the reference are presented.

Table 4.3: Physiological range of motion for the human joints

Joint	**Rotation X** [°]			**Rotation Y**[°]			**Rotation Z** [°]			**Ref.**
	+	-	**Name**	+	-	**Name**	+	-	**Name**	
Sacrum/L5	70	30	flexion/extension	35	35	rotation	35	35	lat. flexion	[105]
L1/T12	15	20	flexion/extension	45	45	rotation	42	42	lat. flexion	[93]
T1/C7	15	20	flexion/extension	45	45	rotation	42	42	lat. flexion	[93]
C1/Head	55	49	ventral/dorsal flex.	67	67	rotation	35	35	lat. flexion	[93]
R shoulder	61	188	extension/flexion	50	120	rotation	5	120	abduction	[93]
R Elbow	5	142	flexion	100	10	pronation/supination	5	5	lat. flexion	[62]
R wrist	45	45		45	45		45	45		[93]
L shoulder	61	188	extension/flexion	120	50	rotation	120	5	abduction	[93]
L Elbow	142	5	flexion	10	100	pronation/supination	5	5		[62]
L wrist	45	45		45	45		45	45		[93]
R hip	45	102	flexion/extension	34	39	medial/lateral rot.	31	53	ad/ab-duction	[105]
R knee	5	125	flexion	35	43	medial rotation	5	5		[93]
R ankle	35	38	dorsi/plantar flexion	23	23	inversion/eversion	5	5		[93]
L hip	102	45	flexion/extension	39	34	medial/lateral rot.	53	31	ab/ad-duction	[105]
L knee	125	5	flexion	43	35		5	5		[93]
L ankle	38	35	dorzi/plantar flexion	23	23	inversion/eversion	5	5		[93]

For the purpose of modelling the internal stiffness and limits of the joint, an external torque (mathematically external) is calculated and added into Eq. 3.79 or Eq. 3.75 as an additional term into $\mathbf{n}^{\star}$.

The torque $\mathbf{N}_{joint}$ is calculated as

$$\mathbf{N}_{joint} = \begin{bmatrix} M_x \\ M_y \\ M_z \end{bmatrix} = \begin{bmatrix} -K_x\alpha \\ -K_y\beta \\ -K_z\gamma \end{bmatrix} \tag{4.11}$$

Where angles α, β and γ are calculated from Eq. 4.8, 4.9, 4.10 and K_i is the particular stiffness defined from database [62, 93]. The stiffness curves are defined in such way, that they generates small torque up to the limit of motion and significantly higher torque, if the angle exceeds the limit.

As an example of the internal stiffness, the curves for knee, elbow, wrist, hip, shoulder and ankle are shown in Figs 4.5.

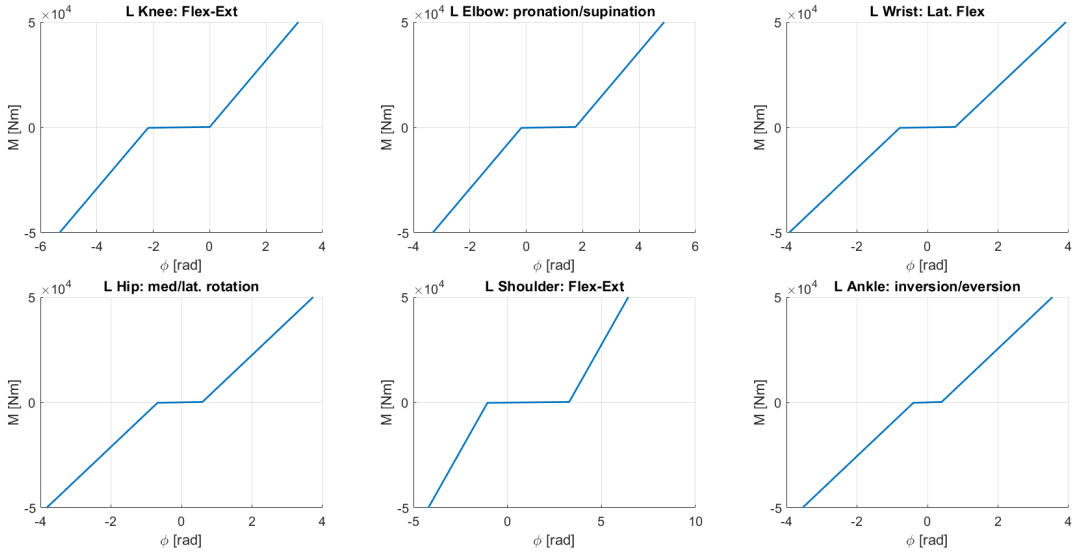

Figure 4.5: Internal stiffness curves [62, 93, 105]

The final torque $\mathbf{N}_{joint}$ is a vector of the size [3x1], and this must be transformed into the Euler parameters space [4x1]

$$\mathbf{N}^{EP}_{joint} = 2\mathbf{G}^{T}\mathbf{N}_{joint} \tag{4.12}$$

Chapter 5

Contact analysis

Purpose of this chapter is to include the impact/contact scenarios into the model. The calculation of the contact and contact force between the body and some external surface is a essential part of the crash modelling. Impact, or contact, is a complex phenomenon that occurs, when at least two bodies undergo a collision, see Fig. 5.3. Impact problem arises in many engineering applications, such as multi-body dynamics, robotics, aircraft, biomechanics and many others. Impact is defined as a collision of two bodies that occur over a significantly short time interval. The impact can be characterized with large reaction forces, large energy dissipation and very high change of accelerations.

5.1 Contact detection and minimum distance calculation

Calculation of the minimum distance between two objects of arbitrary shape is very important and it is deeply associated with impact applications. Ellipsoids are frequently used for representation of many natural organism, such as segments of the human body. There are many efficient algorithms for collision detection and related minimum distance calculation between objects [40, 100, 116]. First group of methods only provides information, whether the bodies are separated, contacting at one point or the bodies are in collision. Second group concerns algorithms, which computes distance between bodies, respectively between their surfaces.

5.1.1 Surface approximation

Sohn [100] presents an algorithm for computing distance between two free surfaces. The main idea is using a line geometry to approximate shape of bodies and to reformulate the distance calculation problem to intersection between surfaces, see Fig. 5.1.

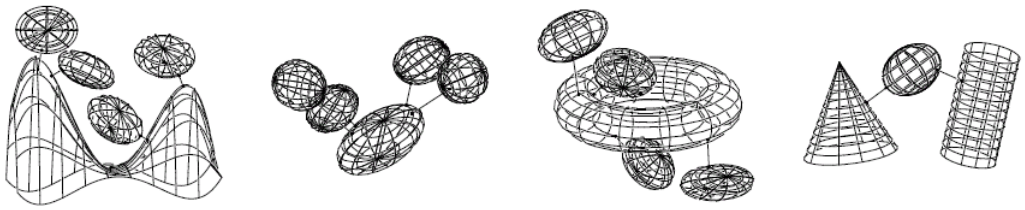

Figure 5.1: Line approximation of bodies [100]

5.1.2 Separating surface

Wang [116] presents efficient and accurate algorithm for detection of collision in case of two moving ellipsoids. This work contains two approaches, namely a simple algebraic test for disjunction of two ellipsoids and a method of construction of the separating surface. Compared with surface approximation algorithm by Sohn [100], this algorithm reduces calculation time and has a higher accuracy.

Collision detection

Interiors of two ellipsoids $\boldsymbol{A}$ and $\boldsymbol{B}$ are represented by matrix equations $\mathbf{X}^T\mathbf{A}\mathbf{X} < 0$ and $\mathbf{X}^T\mathbf{B}\mathbf{X} < 0$ respectively, where $\mathbf{A}$ and $\mathbf{B}$ are real symmetric matrices of dimension 4 and $X = [x, y, z, w]^T$ express a point in homogeneous coordinates.

A simple algebraic test for separating of two ellipsoids is established by defining two surfaces $\boldsymbol{A} : \mathbf{X}^T\mathbf{A}\mathbf{X} = 0$ and $\boldsymbol{B} : \mathbf{X}^T\mathbf{B}\mathbf{X} = 0$ and the quartic equation $f(\lambda) = det(\lambda\mathbf{A} - \mathbf{B})$. This quantity is called characteristic equation of $\boldsymbol{A}$ and $\boldsymbol{B}$.

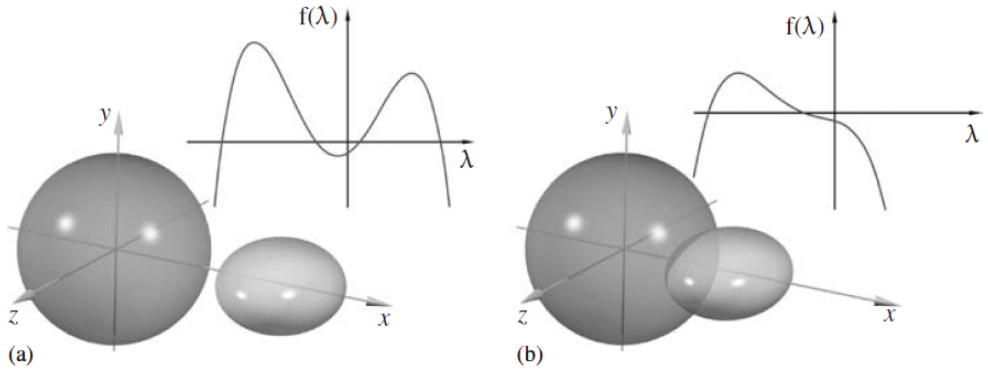

Figure 5.2: Two (a) disjoint and (b) overlapping ellipsoids and corresponding $f(\lambda)$ [116]

This two ellipsoids are disjoint if and only if equation $f(\lambda) = 0$ has two distinct positive roots. They touch each other in a single contact point if $f(\lambda) = 0$ has one positive double root. Note that ellipsoids are in contact, if the characteristic equation has no positive roots, see Fig. 5.2.

Separating plane

Wang in his work [116] described how to construct a plane, separating two ellipsoids. Since the plane is separating the bodies, there can be no collision between ellipsoids until one of them impacts the plane. Wang is applying affine transformation to plane and ellipsoid problem to reduce it to a problem of a sphere and a plane. Afterwards the problem of calculation between the sphere and the plane becomes a problem of distance between the centre of the sphere and the plane. However, affine transformation generally does not keep the distance magnitude, hence the truthfulness of this method can be discussed and should be proved.

5.1.3 Analytical method using transformation

The fully analytical algorithm for calculation of the contact between ellipsoid and plane in 3D space is described in [110, 112], where the analytic equation of the ellipsoid and plane is used to calculate the minimum distance between these two entities. The main idea is to create a new plane, perpendicular to the initial one and tangential to the body. Once the plane is defined, the tangential point (shared point for new plane and body) is also defined and the problem of the distance between body and plane is reduced to a problem of distance between point and plane, which is quite simple task.

5.1.4 Iteration process

Moser described a model of a human body for contact with vehicle application in his work [79]. Pedestrian model is coming into the contact with a rigid surface (shape of the car). Moser uses iteration process for testing distance between the surfaces of the bodies. The distance between any two points of bodies is checked and the minimum distance is calculated. This algorithm can be efficient for simple geometry, which does not require high number of points. However, for complicated structures, this method can significantly increases calculation time.

5.1.5 Quadratics equation of ellipsoid

Eberly [40] presented similar method as Wang [116] based on the solution of algebraic equations. However this method is only testing a collision and it is not interested in minimum distance calculation. Eberly introduced two algorithms for intersection calculation. First one is based on roots estimation and second one is using gradient approach.

Eberly defines an ellipsoid E_i by the quadratic equation

$$\boldsymbol{Q}_i(\boldsymbol{X}) = \boldsymbol{X}^T \boldsymbol{A}_i \boldsymbol{X} + \boldsymbol{X}^T \boldsymbol{B}_i + C_i \tag{5.1}$$

The $\boldsymbol{Q}_i(\boldsymbol{X}) < 0$ defines interior of the ellipsoid and $\boldsymbol{Q}_i(\boldsymbol{X}) > 0$ defines exterior. It is obvious that $\boldsymbol{Q}_i(\boldsymbol{X}) = 0$ defines point on the surface.

Roots calculation

Two polynomial equations $f(z) = \alpha_0 + \alpha_1 z + \alpha_2 z^2$ and $g(z) = \beta_0 + \beta_1 z + \beta_2 z^2$ have a common root if and only if the Bézout determinant is equal to zero

$$(\alpha_2\beta_1 - \alpha_1\beta_2)(\alpha_1\beta_0 - \alpha_0\beta_1) - (\alpha_2\beta_0 - \alpha_0\beta_2)^2 = 0. \tag{5.2}$$

When the Bézout determinant is equal to zero, common roots of $f(z)$ and $g(z)$ are

$$\tilde{z} = \frac{\alpha_2\beta_0 - \alpha_0\beta_2}{\alpha_1\beta_2 - \alpha_2\beta_1}. \tag{5.3}$$

Gradient approach

An alternative solution is to set up a system of differential equation, which walks along one ellipsoid and searches for the point of intersection with the second one. The method results in finding the particular point or evaluate that there is no such points.

The method starts with point $\boldsymbol{X}_0$ where $Q_0(\boldsymbol{X}_0) = 0$. It concerns any point placed on the surface. The first step is testing if $Q_1(\boldsymbol{X}_0) = 0$. If yes, contact point was directly found. This condition means that the particular point is on the surface of both ellipsoids. If $Q_1(\boldsymbol{X}_0) < 0$ the point $\boldsymbol{X}_0$ lies inside and if $Q_1(\boldsymbol{X}_0) > 0$, it lies outside the second ellipsoid, respectively. The main idea is to follow the direction of tangential vector of the first surface in such a way to reach value of $Q_1 = 0$. The best and fastest approach provides the direction of a gradient of Q_1. Once the point $\boldsymbol{X}_n$ where $Q_1(\boldsymbol{X}_n) = 0$ is found, the point distance method can be applied. For detailed description see [40].

5.2 Contact force models - overview

Purpose of this section is to provide an overview of impact and contact models. The contact modelling has main aspects and attached issues, such as energy absorption, behavior of a friction model, multi-contact problem, experimental testing and verification or overall methodology of contact problem. A brief review of results already presented in literature describing the existing models, their relationships and applications of these impact (contact) models are presented here. Contact is a scenario, when two bodies undergo a collision (touch each other in a specific time t_{cont}), while being separated before. The contact is always represented by the bodies (shape, mass, location of COG) and with the contact aspect (contact point, friction, stiffness, direction of impact and attached line of impact) and so on, see 5.3.

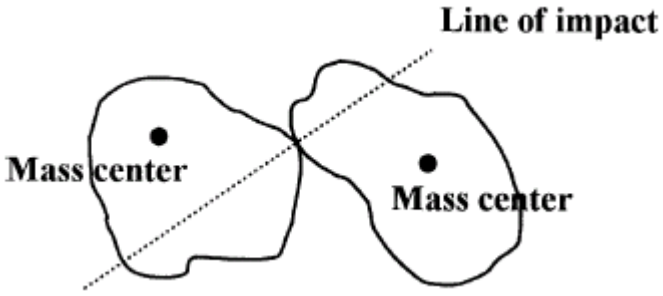

Figure 5.3: Impact of two bodies [48]

In general, two different approaches for contact analysis can be defined, discrete and continuous contact models. This text describes both, including unilateral constrain approach, that is generalization of discrete model for multi-contact problem.

5.2.1 Discrete contact model

The discrete contact model formulation is based on the assumption that the impact process is instantaneous, impact forces are impulsive kinetic variables having discontinuous changes, while no displacements occur during the impact and other forces are neglected. Such models are usually used for rigid or very hard bodies, whilst the effects of deformation at the contact point are taking into account through the particular coefficients. The impact problem is then solved by the linear and angular impulse-momentum characteristics between the variables before and after the impact using the coefficient of restitution.

Classical impact theory

Let's have a planar impact of two bodies with masses m_i, $i \in \{1, 2\}$ and initial velocities v_{i0}, $i \in \{1, 2\}$ and let us divide the impact process into 2 phases, see Fig. 5.4. Conse-

quently, loading in $t \in [t_1, t_2]$ is characterized by the linear impulse P_1 and unloading during $t \in (t_2, t_3]$ is characterized by the linear impulse P_2 as

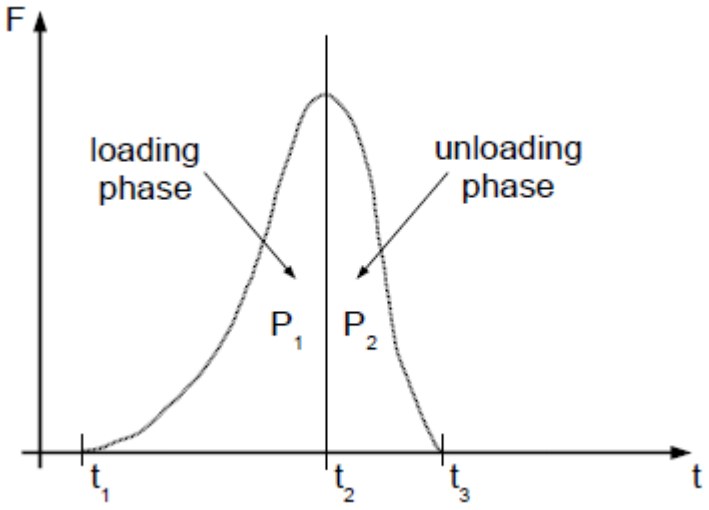

Figure 5.4: Loading and unloading phases of discrete contact model

$$P_2 = \epsilon P_1, \tag{5.4}$$

where the coefficient of restitution $\epsilon \langle 0, 1 \rangle$ describes the local changes and

$$P_1 = \int_{t_1}^{t_2} F dt, \tag{5.5}$$

is the impulse caused by the one dimensional impact, see Fig. 5.4. Here $t \in [t_1, t_3]$ is the impact interval. The $\epsilon = 1$ means completely plastic impact, $\epsilon = 0$ stands for completely elastic impact.

Linear and angular velocities of particular bodies can be defined [48]

$$\begin{aligned} v_1 &= v_{10} - (1+\epsilon)\tfrac{P_1}{m_1}, \\ v_2 &= v_{20} + (1+\epsilon)\tfrac{P_1}{m_2}, \\ \omega_1 &= \omega_{10} - (1+\epsilon) r_{S1} \tfrac{P_1}{I_{S1}}, \\ \omega_2 &= \omega_{20} + (1+\epsilon) r_{S2} \tfrac{P_1}{I_{S2}}. \end{aligned} \tag{5.6}$$

Equations (5.6) can be simply solved for impacts between 2 bodies. However, system with more bodies together is complicated to be handled because each impact state influences the remaining system kinematics.

Coefficient of restitution models

The triad vector (**n**, **t**, **b**) defines a coordinate system with origin at the contact point, where **n** is the normal vector to body at this point and vectors **t** and **b** define tangential planes. The total linear impulse can be written as

$$\boldsymbol{P} = P_n\boldsymbol{n} + P_t\boldsymbol{t} + P_b\boldsymbol{b}. \tag{5.7}$$

The relative linear velocity at the contact point has 3 components: compression velocity along normal direction and component velocity along vectors **t** and **b**, called sliding velocities. Some of existing restitution models are preseted here.

Poisson's model

The total normal impulse P_f is divided into two parts, P_c and P_r, corresponding to compression and restitution phases, respectively. Coefficient of restitution is than defined as

$$\epsilon = \frac{P_r}{P_c}, \quad P_f = P_c + P_r. \tag{5.8}$$

The condition for the end of compression phase is expressed by relative velocity along the normal direction equaling to zero.

Newton's model

The coefficient of restitution here is

$$\epsilon = \frac{\boldsymbol{C}(t_f)\ \mathbf{n}}{\boldsymbol{C}(t_0)\ \mathbf{n}} = -\frac{C_f}{C_0}. \tag{5.9}$$

This model is based on kinematic point of view and only the initial and final conditions for relative normal velocity are taken into account.

Stronge's model

This model is based on the internal energy dissipation hypothesis. The coefficient of restitution is defined as the square root of the ratio of energy released during restitution and the energy absorbed during compression phase. In the terms of work done by the normal force during compression and restitution phases, the coefficient or restitution can be calculated

$$\epsilon^2 = \frac{W_r}{-W_c}. \tag{5.10}$$

Unilateral constraints approach

The unilateral constraints approach is based on the discrete impact model, but it overcomes the problem by defining multiple impact. The multiple contact includes a problem of a large dimension. If one contact has changed, all other contacts are influenced and it makes a new set of contact configurations necessary to be analyzed [89]. Hence it makes sense to define the sets

$$\begin{array}{rcll} I_S & = & \{1,\ldots,m\}, & \text{with } m \text{ contact point,} \\ I_C(t) & = & \{j \in I_S(t) : \Phi_{N_j} = 0\}, & \text{with } m_C \text{ elements,} \\ I_N(t) & = & \{j \in I_C(t) : \dot{\Phi}_{N_j} = 0\}, & \text{with } m_N \text{elements,} \\ I_T(t) & = & \{j \in I_T(t) : |\dot{\Phi}_{T_j}| = 0\}, & \text{with } m_T \text{ elements} \end{array} \tag{5.11}$$

where I_S is the set of all contact points, I_C contains the constraints with vanishing distance with arbitrary relative velocity, I_N describes the constraints fulfilling the necessary conditions for continuous contact (vanishing distance at zero relative velocity in the normal direction) and I_T are the possibly sticking contacts. Φ_j and $\dot{\Phi}_j$ are the relative distances and velocities between the contacting bodies for the j-th contact. Since each contact event changes all other contact events in the multibody system, these sets depend also on the time. The transition between one state to another one are governed by complementary in normal and tangential directions defining the corresponding unilateral constraints [89].

Due to the complication of using the discrete contact modelling approach (timing in multiple contact using classical impact theory or computationally expensive quadratic programming using unilateral constraints approach), the approach assuming continuous contact force as the external force as a function of local indentation between the impacting bodies is usually assessed.

5.2.2 Continuous contact model

The continuous contact model is useful to overcome the problem with local deformation, non-smoothness in contact variables and energy absorption that is complicated to be described by the discrete contact models. The basement of the continuous model formulation for contact dynamics is in explicitly accounting of the deformation of the bodies during impact. Large class of continuous models is defined by applying the normal contact force F_n as an explicit function of a local indentation δ and indentation velocioty $\dot{\delta}$

$$F_n \equiv F_n(\dot{\delta}, \delta). \tag{5.12}$$

The dependence of force on the indentation is a crucial relation, which has to be known or otherwise unrealistic results might appear. In the following text, a summary of some existing contact force models are analyzed.

Elastic model

The elementary contact model is an elastic model known as a Hertz model [26, 48, 73]. It is non-linear and it does not include a damping. However, it is limited only to an impact of elastic deformation. Hertz model for contact problem can be constructed as interaction of two rigid bodies via a non-linear spring along the line of impact. The hypothesis is based on the assumption, that the deformation is concentrated only in the vicinity of the contact point (area). The elastic wave motion is not relevant and the total mass of each body is moving with the velocity of its center of gravity. The impact force is then defined

$$F_n = k\delta^n, \tag{5.13}$$

where k and n are constant parameters depending on material and geometric properties of bodies and can be calculated using elastostatic theory [81]. Parameter k represents stiffness of a virtual spring. For example, in case of two spheres impact, $n = \frac{3}{2}$ and k is function of Poisson ratios, Young modulus and radii of the spheres

$$k = \frac{4}{3(\sigma_i + \sigma_j)} \left[\frac{R_i R_j}{R_i + R_j} \right], \tag{5.14}$$

where material parameters σ_i and σ_j are defined by

$$\sigma_l = \frac{1 - \nu_l^2}{E_l}, \; l \in \{i, j\}, \tag{5.15}$$

in which quantities ν_l and E_l are Poisson ratio and Young modulus associated with particular sphere. Since the Hertz model does not take energy dissipation into account, the coefficient of restitution is equal to one. Gillardi [48] discussed this model as a suitable tool especially for low velocity impact within the hard materials. Elastic contact law of the Hertz model can be upgraded by adding plastic deformation. This can be accomplished by using hysteresis force law, which takes the form

$$F_n = F_{n,max}(\frac{\delta - \delta_p}{\delta_{max} - \delta_p})^n \tag{5.16}$$

where $F_{n,max}$ and δ_{max} are maximum normal force and maximum indentation during loading phases of impact, respectively, and δ_p is permanent indentation. Note that maximum values in the (5.16) is calculated in every instance of numerical solution, value δ is calculated in each time step, but δ_p is an additional parameter, and it has to be defined initially in particular contact model. This model is only a rarely used, since is being large, heavy or not effective.

Dissipative contact models

An alternative contact force model taking account energy loss during impact is a set of dissipative models, known as a spring-dashpot or Kelvin-Voigt model [48, 73]. The impact is schematically represented with a linear damper (dashpot) for dissipation of energy, parallel with non-linear spring for the elastic behavior, see Fig. 5.5. The normal contact force is defined as

$$F_n = k\delta + b\dot{\delta} \tag{5.17}$$

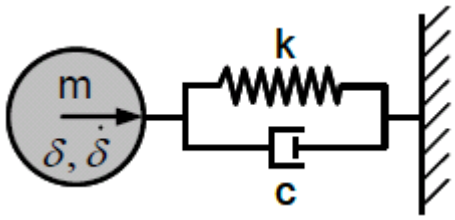

Figure 5.5: Spring-dashpot system [73]

Parameters k and b in Eg. 5.17 depend on material and shape of the contacting bodies. δ is indentation (or penetration) and $\dot{\delta}$ is relative normal contact velocity [48, 73]. Three weaknesses of this model are pointed out:

- At the beginning of impact, contact force is discontinuous, because of the damping term. During the real contact scenario, both elastic and damping forces should be initially equal to zero and are increasing over the time.
- When the objects are separating, the indention comes to zero and hence their relative velocity tends to be negative. The results is a negative normal force holding the objects together, is shown in Fig. 5.6.
- The coefficient of restitution for this model does not depend on the impact velocity and dependence of ϵ on the velocity has to be set up experimentally.

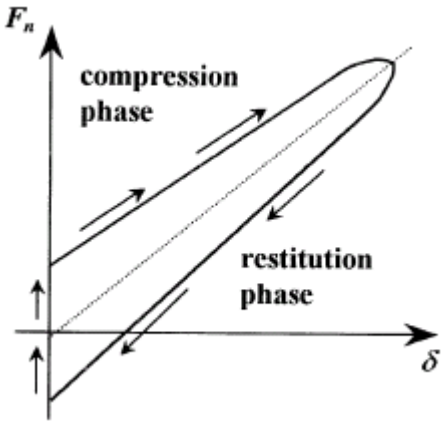

Figure 5.6: Contact force history for the spring-dashpot model [48]

Even the spring-dashpot model is not physically realistic, it is used very often because of its simplicity. It provides a reasonable method to capture energy dissipation effect without explicitly considering plastic deformation issues. Since it generally contains only two parameters (stiffness and damping ratio) it is a suitable tool for experimental validation and verification.

Non-linear damping As an extension of the spring dashpot model, the non-linear damping can be defined. Such model deals with problems of the spring-dashpot model and retains the advantages of the Hertz model [26, 48, 59, 73]. The non-linear damping term is considered and impact force comes to

$$F_n = k\delta^n + \chi\delta^p\dot{\delta}^q, \tag{5.18}$$

where p, q and n are constants and it is common to set them $p = n$ and $q = 1$. The damping parameter χ is related to the coefficient of restitution, because it is associated with energy dissipation phenomena, similarly with dashpot model. Based on the literature review and the physical effect, parameter χ is called the hysteresis damping factor. The basic and the most commonly used form of this parameters is

$$\chi = \frac{3k(1 - C_r)}{2\dot{\delta}^{(-)}}, \tag{5.19}$$

in which k represents the generalized stiffness parameter, C_r is the coefficient of restitution and $\dot{\delta}^{(-)}$ is the initial contact velocity. The main advantages of this model is realistic relationship between damping coefficient and indentation, and in the absence of discontinuities at initial and separating phases.

If the Eq. 5.19 is substitute into the Eq. 5.18, the final relationship for non-linear dissipative force can be defined. The hysteresis parameter χ can have several modifications defining the contact force model, named based on the authors:

- Hunt & Crosley model [59]

$$F_n = k\delta^n \left[1 + \frac{3(1-C_r)}{2}\frac{\dot{\delta}}{\dot{\delta}^{(-)}}\right], \tag{5.20}$$

- Lee & Wang model [71]

$$F_n = k\delta^n \left[1 + \frac{3(1-C_r)}{4}\frac{\dot{\delta}}{\dot{\delta}^{(-)}}\right], \tag{5.21}$$

- Herbert & Mc Whannell model [55]

$$F_n = k\delta^n \left[1 + \frac{6(1-C_r)}{[(2C_r-1)^2+3]}\frac{\dot{\delta}}{\dot{\delta}^{(-)}}\right], \tag{5.22}$$

- Lankarani & Nikravesh model [70]

$$F_n = k\delta^n \left[1 + \frac{3(1-C_r^2)}{4}\frac{\dot{\delta}}{\dot{\delta}^{(-)}}\right], \tag{5.23}$$

- Gonthier model [49]

$$F_n = k\delta^n \left[1 + \frac{(1-C_r^2)}{C_r}\frac{\dot{\delta}}{\dot{\delta}^{(-)}}\right], \tag{5.24}$$

- Zhiying & Qishao model [123]

$$F_n = k\delta^n \left[1 + \frac{3(1-C_r^2 e^{2(1-C_r)})}{4}\frac{\dot{\delta}}{\dot{\delta}^{(-)}}\right], \tag{5.25}$$

- Flores model [44]

$$F_n = k\delta^n \left[1 + \frac{8(1-C_r^2}{5C_r}\frac{\dot{\delta}}{\dot{\delta}^{(-)}}\right], \tag{5.26}$$

- Grahib & Hurmuzlu model [47]

$$F_n = k\delta^n \left[1 + \frac{(1}{C_r}\frac{\dot{\delta}}{\dot{\delta}^{(-)}}\right], \tag{5.27}$$

Friction model

Coulomb (discrete) contact law is frequently used to describe an effect of friction in the impact. Main disadvantage of the Coulomb law is the discontinuity of the friction force. To deal with this issue and to capture effect of friction, an alternative friction force law has been established [48, 73]. The first improvement of the law is obtained by using a non-local friction model, where value of friction at one point depends on value of its neighborhoods. Another improvement is in applying of the non-linear model to allow a continuous transition from sticking to sliding phases. The friction model is defined

$$\boldsymbol{F}_t = k_f \boldsymbol{s},\ \boldsymbol{s}(t) = \begin{cases} \boldsymbol{s}(t_0) + \int_{t_0}^{t} \boldsymbol{v}_t dt, & \text{if } |\boldsymbol{s}| < s_{max} \\ s_{max} \dfrac{\boldsymbol{v}_t}{|\boldsymbol{v}_t|}, & \text{otherwise, } s_{max} = |\mu| \dfrac{F_n}{k_f}\ , \end{cases} \tag{5.28}$$

where k_f is friction stiffness, $\mathbf{s}$ is the vector of friction displacement, t_0 is the starting time of the last sticking at the contact point, $\mathbf{v}_t$ is the relative tangential velocity and s_{max} is the parameter of maximum allowable deflection. An important aspect of this model is the effective calculation of friction force as a function of time.

Another model, but is is not common to present it as a friction model, is the Stronge model [48]. This model is using concept of tangential friction force, in the way of the Hertz model, thus the tangential force is defined as

$$F_t = k_t \delta_t \tag{5.29}$$

where δ_t is tangential component of indentation at the contact point and k_t is tangential stiffness.

5.3 Human body model - contact

The human body model described here is a system of the linked ellipsoids that can come into the contact with external infrastructure (ground or vehicle). It was found to be more effective to use modified iteration process to calculate distance of the bodies from the plane. Each ellipsoid is described with the set of points on its surface, and for each of this point, the distance from the plane is being checked. Since the distance between point and plane is simple analytic equation Eq. 5.30, the numerical process is still fast enough. Moreover, the selection of the body (the points on the surface) for the distance checking can by optimized only for some specific bodies (i.e. check the distance of the COG of each body and only if this distance is lower than some threshold/tolerance, the surface points are being checked). The equation of the distance between a body and plane in the 3D space is defined

$$d(X,r) = \frac{|ax_1 + bx_2 + cx_3 + d|}{\sqrt{a^2 + b^2 + c^2}} \tag{5.30}$$

where

$$X = [x_1, x_2, x_3]^T, \text{ is the point} \tag{5.31}$$

$$ax + by + cz + d = 0, \text{ is analytical equation of the plane} \tag{5.32}$$

If the distance between *i-th* point on the surface is bellow the zero (or some threshold - called contact thickness) the contact force is added to the system based on the specified contact force model. It acts at the *i-th* point on the body surface in the direction of normal vector of the plane. The system of the particular forces (at each point of the contact is replaced by the equivalent system of a total force F_{total} and a total moment M_{total} acting at the COG of the body, see Fig. 5.7.

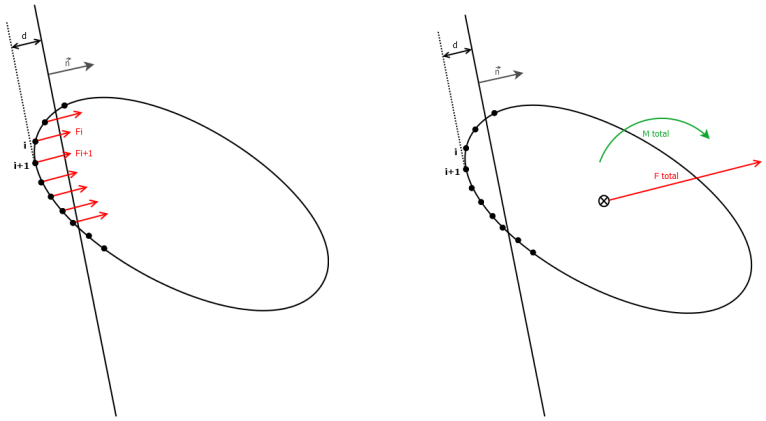

Figure 5.7: Incremental contact forces (left) and equivalent system of force and moment (right)

5.4 Human body model - total equation of motion

The total equation of motion of the human body Eq. 3.79 is expanded with the moment genereated by the internal thickness of the joint Eq. 4.12 and with the contact force Eq. 5.12 and Eq. 5.18. These external loading appear on the RHS of the equation of motion

$$\begin{bmatrix} \boldsymbol{M} & \boldsymbol{C_q}^T \\ [8n\times 8n] & [8n\times 3r] \\ \boldsymbol{C_q} & \boldsymbol{0} \\ [3r\times 8n] & [3r\times 3r] \end{bmatrix} \begin{bmatrix} \ddot{\boldsymbol{q}} \\ [8n\times 1] \\ \boldsymbol{\lambda} \\ [3r\times 1] \end{bmatrix} = \begin{bmatrix} \boldsymbol{F} + \boldsymbol{F}_{contact} + \boldsymbol{F}_{stiff} \\ [8n\times 1] \\ \boldsymbol{\gamma} \\ [3r\times 1] \end{bmatrix} \tag{5.33}$$

where

$$\boldsymbol{F}_{contact} = [F_n^x, F_n^y, F_n^z, 0, 0, 0, 0, 0]^T \tag{5.34}$$

and

$$\boldsymbol{F}_{stiff} = \left[0, 0, 0, N_{joint}^{EP_0}, N_{joint}^{EP_1}, N_{joint}^{EP_2}, N_{joint}^{EP_3}, 0\right]^T \tag{5.35}$$

Chapter 6

Application

Following section presents elementary problems and algorithms used in this model, to verify/validate their behavior on the simply benchmark examples. Firstly, the spatial motion of the free body (non-constrained) within the contact algorithm is tested on the simple bouncing ball falling on the flat rigid surface [26], where the various contact force models are applied. Next example is a contact of the ellipsoid falling on the inclined surface, to test the eccentricity of the contact. The principle of the spherical joint and joint stiffness is tested on the spherical pendulum with the pre-defined internal stiffness (defined with the curves in the same way as in the human joints). Finally, the contact problems of the full human body model are presented.

6.1 Numerical solution

The process of the numerical integration of the EOM uses the standard MATLAB function for solving differential equation of the first order, called ODE**, where symbols ** defines the method and order of the integration method. The application examples bellow are solved with the ODE45 method. The ODE45 is a numerical method with the variable time step, that decreases when the solver requires it, for instance in the contact. There exist more ODE solvers, pre-defined in MATLAB library. The solvers can be generally divided based on some criteria (fixed or variable time step; discrete or continuous; explicit or implicit; one step or multi step). The examples and main features of the solvers are presented here, where the solvers are distinguished based on their time step order.

6.1.1 Variable time step solvers

- **ODE23**: Solves *non-stiff* differential equations - low order method. Explicit one step Runge-Kutte formulation of a second order. Effective for *mild-stiff* problems or for examples, where the RHS of the differential equation $\mathbf{f}(t, \mathbf{y})$ is not continuous.

- **ODE23s**: Solves *stiff* differential equations - low order method. Implicit one step Rosenbrock formulation of a second order. Effective for *stiff* problems or for examples, where the RHS of the differential equation $\mathbf{f}(t, \mathbf{y})$ is not continuous.
- **ODE23t**: Solves *moderately stiff* ODEs and DAEs - trapezoidal rule. Implicit one step trapezoidal rule, effective for *medium stiff* problems and for set of differential-algebraic equations.
- **ODE23tb**: Solves *stiff* differential equations - trapezoidal rule + backward differentiation formula. Similar solver to the ODE23s and can be more effective for a lower accuracy.
- **ODE45**: Solves *non-stiff* differential equations - medium order method. Explicit one step Runge-Kutte formulation of a fourth order. Effective for *non-stiff* problems. Usually the first choice when solving a new problem.
- **ODE113**: Solves *non-stiff* differential equations - variable order method. Multi-step Adams-Bashforth-Moulton method with variable order (from 1 to 13). Effective for *non-stiff* problems, with non-continuous $\mathbf{f}(t, \mathbf{y})$.
- **ODE15s**: Solves *stiff* differential equations and DAEs - variable order method. Implicit multi-step method with variable order (from 1 to 5). Effective for *stiff* problems.
- **ODE15i**: Solves fully implicit differential equations - variable order method. Fully implicit method for a solution ODE and DAE equations.

6.1.2 Fixed time step solvers

The following solvers have fixed time step (user defined) and it cannot be changed during the integration. Generally, the fixed time step method is not recommended, but for some special cases, this can be a useful tool. These solvers are not included in the standard MATLAB library.

- **ODE1**: Euler formulation of a first order.
- **ODE2**: Euler formulation of a second order.
- **ODE3**: Bogacki-Shampine formulation of a third order of accuracy.
- **ODE4**: Standard Runge-Kutta formulation of a fourth order.
- **ODE5**: Dormand-Prince formulation of a fifth order.
- **ODE8**: Dormand-Prince formulation of a eight order.

Stiff problem:

In the previous lines, *stiff* and *non-stiff* problem were used. The general definition of the *stiff* problem can be the cases, where the time constants vary in order 2 and more. Or, it can be examples, where the time step (variable) approaches to zero. Or, linear systems with the negative real part of the eigenvalues. The *stiff* problem can be solved also with the *non-stiff* solvers, but with the higher computational time.

6.2 Bouncing ball

Equation of motion of a free body Eq. 3.72 is used to generate the system of one sphere and a rigid ground. The body is loaded only with gravity and freely fall, until it reaches the ground. The contact and contact force are calculated based on the equations described above. In order to capture a real behavior of this mechanical system, the stiffness and damping parameters must be optimized. The variation of these parameters changes the response of the numerical system until the results of the simulation and experiment would be similar enough. However, it is not purpose of this work to tune up parameters of the bouncing ball example. The goal of this chapter is to show, how the selection of the contact force model can affect the results and how the coefficient of restitution changes the results (within one force model).

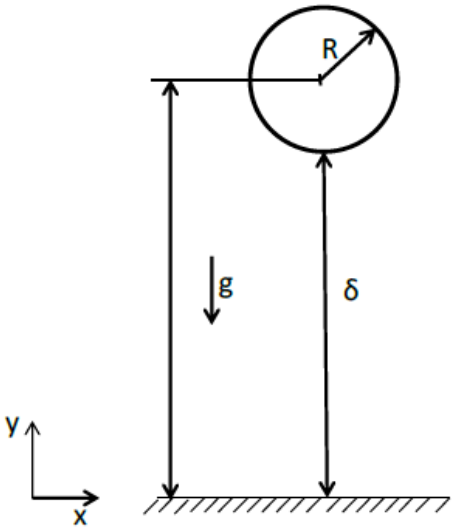

Figure 6.1: Bouncing Ball [26]

The body here is a sphere with the radius 0.2 m, mass of 1 kg falling from the initial height equaling to 0.5 m (position of COG). The stiffness parameter of the contact force model k is calculated based on the geometry and mass of the impacting bodies, see Eq. 5.14.

Coefficient of restitution:

First set of Figs. 6.2 are examples with the standard dissipative model (Hunt & Crosley, Eq. 5.20), where only the coefficient of restitution C_r have changed from 0 to 1 (0 = pure plastic, 1 = pure elastic contact). The behavior of the bouncing ball system shows the correctness of the force model with respect to the elastic-plastic behavior. In case of pure elastic contact ($C_r = 1$), the amplitude of the displacement does not change (only small variations due to numerical errror) and with the decreasing coefficient of restitution, the level of plasticity increases.

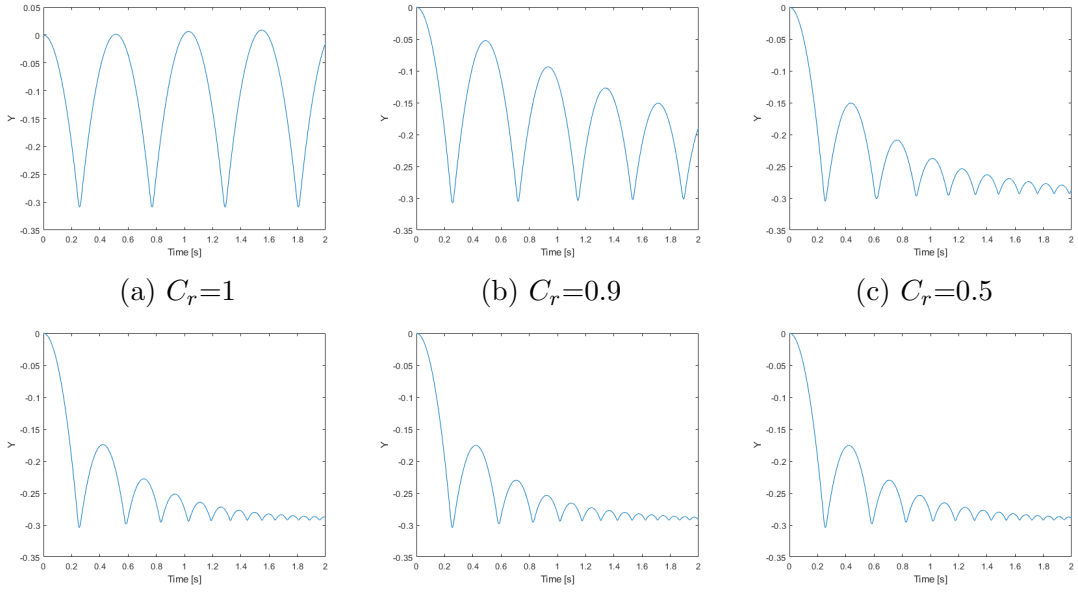

(a) C_r=1 (b) C_r=0.9 (c) C_r=0.5

(d) C_r=0.1 (e) C_r=0.0001 (f) C_r=0

Figure 6.2: Displacement of the COG

Force model:

This paragraph shows the difference between contact force models (Herzt elastic model Eq. 5.13 and dissipative models Eq. 5.20 - Eq. 5.27. The contact force Fig. 6.3a, maximum force Tab. 6.1 and a hysteresis curve (force vs. displacement) Fig. 6.3b are presented here to show the difference between the models. The selection of the contact force model affects also the CPU time. The simulation time was 0.5 s (identical in all simulations) to compare the models one to each other.

Force model	Max Force [N]	Max Disp [m]
Herzt	1320.6	0.2134
Hunt & Crosley	1697.7	0.0029
Lee & Wang	1500.1	0.0031
Herbert & McWhannel	1822.8	0.0027**
Lankarani & Nikravesh	1500.1	0.0031
Gontier	2075.2	0.0021
Zhying & Qishao	2035.1	0.0022 ***
Flores	2438.3	0.0018****
Grahib & Hurmuzlu	2075.1	0.0021***

Table 6.1: Maximum contact force and maximum displacement

NOTE *: The simulation exhibits 2 jumps (two contacts)

NOTE **: The simulation exhibits 3 jumps (three contacts)

NOTE ***: The simulation exhibits 6 jumps (six contacts)

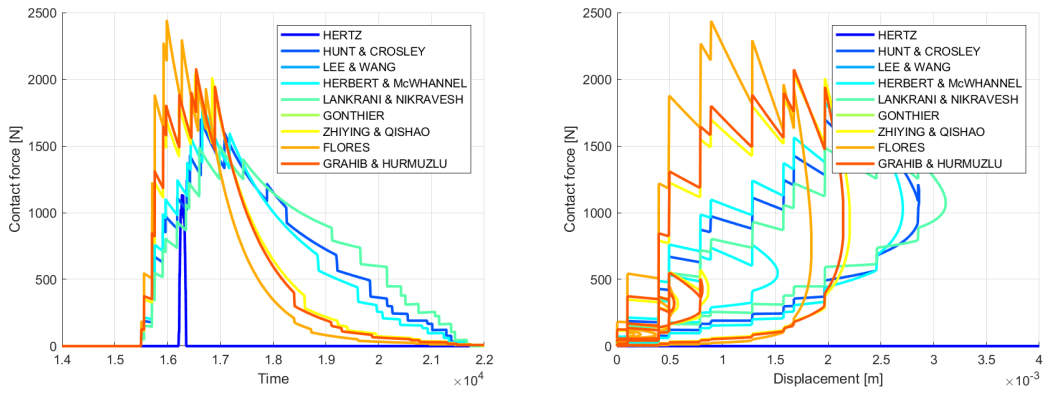

(a) Contact force (b) Histeresis curve

Figure 6.3: Variation of the force models in the bouncing ball example

There is a visible difference between the contact models (in the force as well as in the displacement). Moreover, for one model (Herbert & McWhannel) the ball performed two jumps, in two cases (Zhying & Qishao and Grahib & Hurmuzlu) three jumps and in case of Flores model, the ball jumped six times, for the same simulation time. The proper selection of the contact force model, as well as tuning of the contact parameters must be gauge individually for each particular case. There is no global recommendation for the model selection and no general definition of the parameters. This overview here is only going to show, how important is the selection of the correct force model and its parameters specification.

6.3 Ellipsoid on inclined surface

Equation of motion of a free body Eq. 3.72 is also used here, to evaluate behavior of the ellipsoid body, falling on the inclined rigid surface. The body here is an ellipsoid with the length of the main principle axis equals to 1.0 m, and two remaining principle axes equaling to 0.4 m, with the mass of 1 kg. The body falls under the gravity, until it reaches the surface, inclined with 45°, from the ground, see Fig. 6.4. The Hertz contact model is used (pure elastic contact). The kinematic of the body is shown in Fig. 6.5 to test and verify the contact algorithm (especially the torque, generated due to the eccentricity of the contact) (Eq. 3.70, Eq. 4.12 and Fig. 5.7).

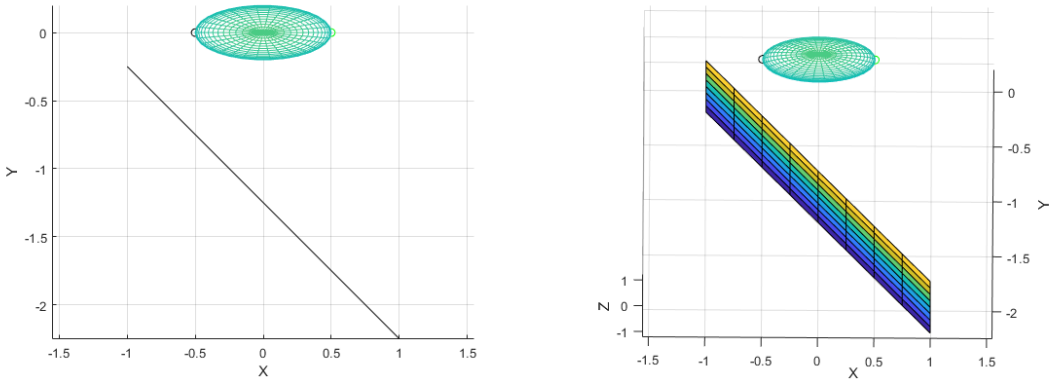

Figure 6.4: Initial configuration of the ellipsoid and inclined surface

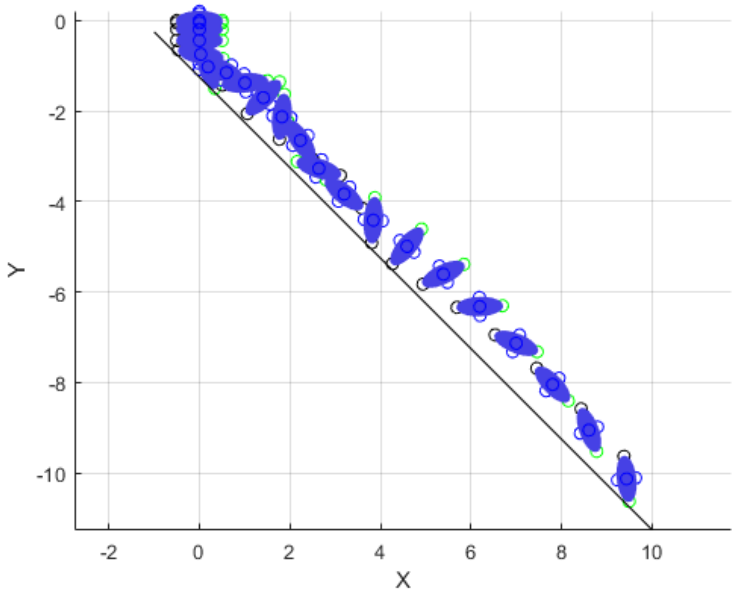

Figure 6.5: Falling ellipsoid

Since, there is a lack of testing/experimental data, only this basic example, where the results can be visually evaluated, was performed. The kinematics of the body implies the correctness of the contact algorithm. This example can approximate the rugby ball falling on the ground. However, to really validate this algorithm, the data from experimental tests would be required.

6.4 Spherical pendulum with internal stiffness

The spherical pendulum is an elementary problem of the constrained rigid body dynamics. Despite the fact it contains only one body, constrained to the frame with the spherical joint, it is a useful tool to test the constraint and also the internal stiffness algorithm. The validity of the derived constraints was already tested in the sensitivity analysis section 3.4. However, the internal joint stiffness algorithm need to be verified.

Firstly, the spherical pendulum is moving only in one plane (XY) - rotational motion around Z-axis and for each of this particular rotation, the several stiffness curves are applied. The goal here is to change the range of motion of the joint and to test how this affects the motion of the body. In the examples bellow, only γ angle is changing, so only limit for this particular curve was varied.

The sets of figures Fig. 6.6, Fig. 6.7 and Fig. 6.8 show the behavior of the spherical pendulum, with the variation of stiffness (limit angle respectively).

6.4.1 No stiffness

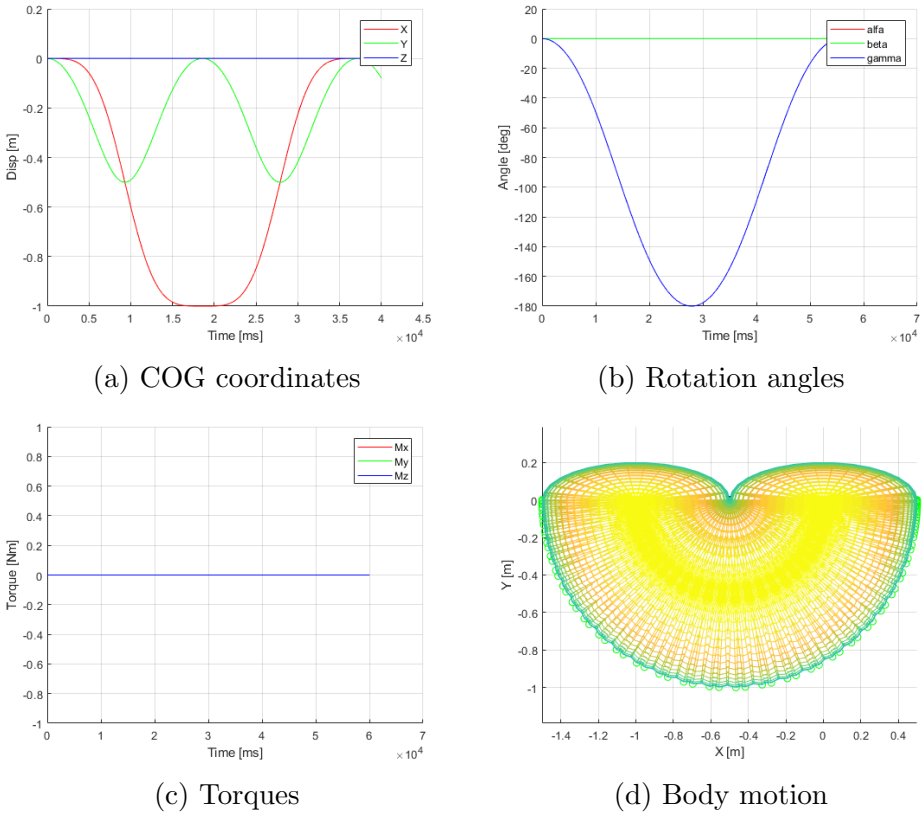

(a) COG coordinates

(b) Rotation angles

(c) Torques

(d) Body motion

Figure 6.6: Spherical pendulum with no internal stiffness. Coordinates of the COG (top left); angles of rotation (top right); internal torque (bottom left); motion of the body (bottom right)

The first set of Fig. 6.6 shows the motion with no stiffness, no damping. So, the body oscillates from the initial (horizontal) position, to its maximum (opposite horizontal position), with no decreasing. The coordinates of COG generates the *sin-like* curve (X and Y) and zero curve (Z), since the body rotates around Z axis. Consequently, the γ curve generates *sin* while α and β are constant and equal to zero curve. There is no torque generated by the motion.

6.4.2 Angle γ limit = 20° (rotation Z)

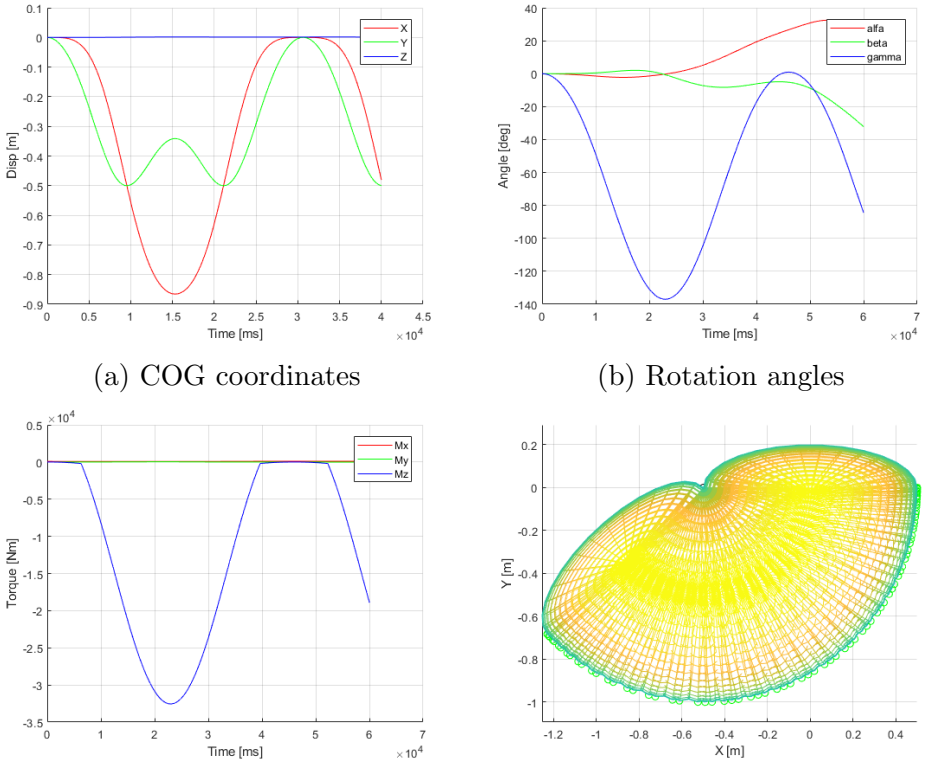

(a) COG coordinates

(b) Rotation angles

(c) Torques

(d) Body motion

Figure 6.7: Spherical pendulum with internal stiffness: $\gamma_{lim} = 20°$. Coordinates of the COG (top left); angles of rotation (top right); internal torque (bottom left); motion of the body (bottom right)

The second set of Fig. 6.7 shows the example, where the limit angle γ is set to be 20°. Note that the limit is not a maximum angle, that can be reached, it is the point, where stiffness curve changes its slopes, see Fig. 4.5. Thus, the body does not stop in this particular limit, but the internal torque rapidly increases after reaching this threshold. This phenomena can be seen in Fig. 6.7b and Fig. 6.7c, where the angles and torques are plotted. Due to the torque, acting on the body against its motion, the body does not reach the horizontal position (the maximum) and stops when the γ angle is approximately 135°, see Fig. 6.7b and Fig. 6.7d.

6.4.3 Angle γ limit = 70° (rotation Z)

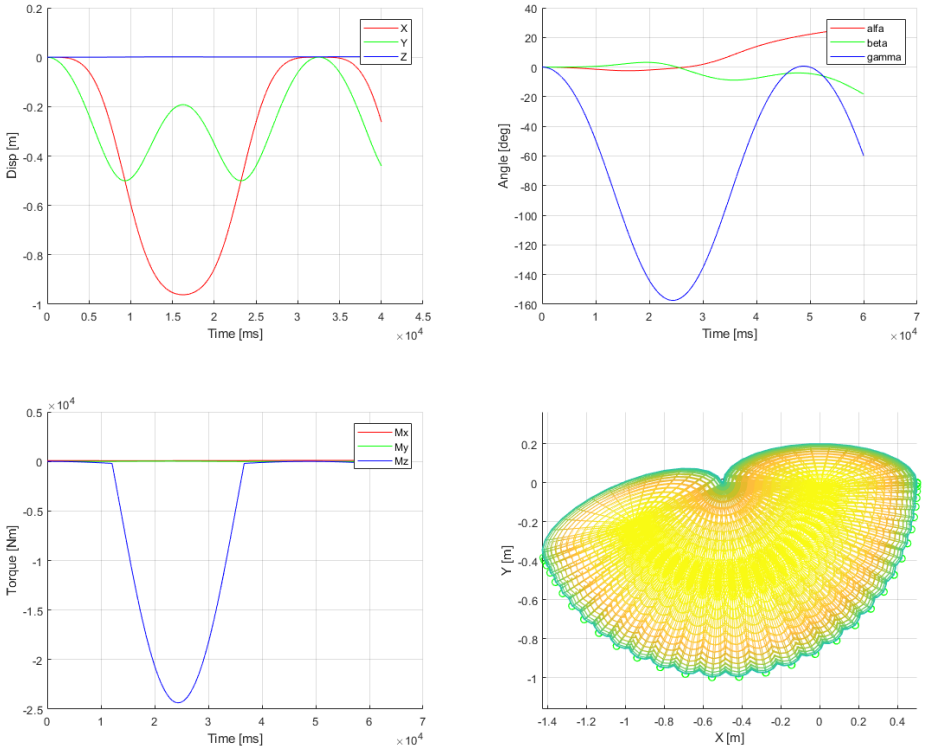

Figure 6.8: Spherical pendulum with internal stiffness: $\gamma_{lim} = 70°$. Coordinates of the COG (top left); angles of rotation (top right); internal torque (bottom left); motion of the body (bottom right)

The third set of Fig. 6.8 shows the same phenomena like in previous case, only the limit angle was changed to 70°. The body stops its movement when the angle γ is approximately 160°.

6.4.4 General motion

This section shows the motion of the spherical pendulum, releases from general position, under loading of gravity only, with the initial rotation in all three directions (the axis of rotation is a general axis and not coincides with any global coordinate axis). The initial position is defined via quatermion (Euler parameters), where the body is initially rotated with the angle $\pi/6$ [rad] around the vector $[1, 1, 1]^T$. The COG is placed at the origin of the global coordinate system, see Fig. 6.9.

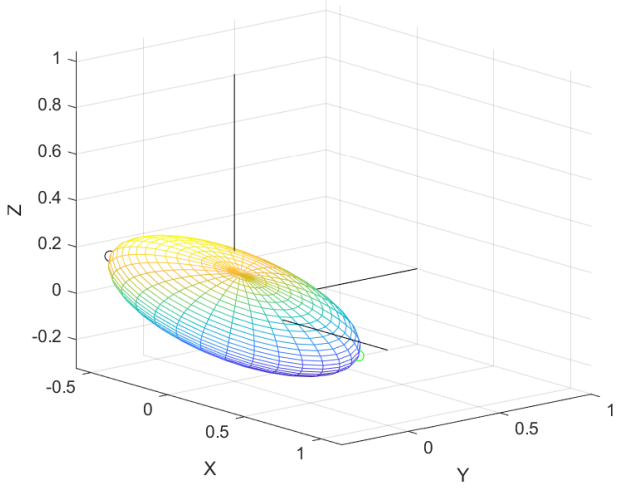

Figure 6.9: Initial position of the body

The motion of the body, as well as rotational parameters, torque are displayed in the set of the following Figs. 6.10.

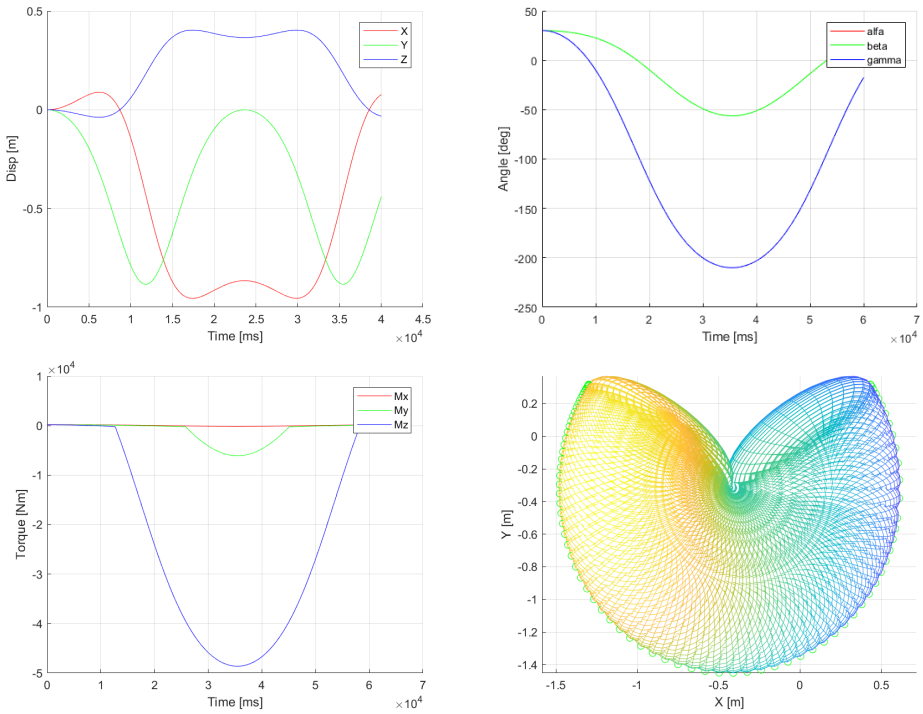

Figure 6.10: Spherical pendulum with internal stiffness, general initial position. Coordinates of the COG (top left); angles of rotation (top right); internal torque (bottom left); motion of the body (bottom right)

6.5 Human Body Model

The human body model (HBM) previously described is now tested in some basic case studies, to show its relevance and biofidelity for these particular cases. If the general biofidelity is required, the full validation and optimization of all parameters (especially contact stiffness and damping) must be done. However, such process is not easy task and it is not done here. The model here uses a global set of contact parameters, that were set-up in order to cover the relevance of the model.

The model, presented here can be named as a *"Validation-ready model"*. That means, the model is done, all parameters are defined to make the model working, the results are realistic and the model behaves human-like. However, for the specific application, such as dynamic crash scenario, the contact as well as numerical parameters must be optimized, to correctly set them up and to reach the biofidelity of the model.

The examples here are to show some cases, in which, this model can be used. The falling scenario is the main concern, since it is a common scenario in a real life, automotive safety or in forensic analysis [57, 56]. Moreover, the accident with the static obstacles (ground) is numerically more stable than with the dynamical one (pedestrian to car crash) and hence, is more suitable for testing of the model. The dynamical accident would require some numerical tuning of the model (contact parameters, numerical stabilization parameters, time step limit definition etc.). Moreover, the selection of the stabilization techniques (here Baumgarte and direct violation method) would require a sensitivity analysis for the full human body model, similarly as was done in case of pendulum and double pendulum, respectively). Since this work is more about preparation of the model, ready for validation and not the modelling of one specific example, optimization for the HBM case is not provided and only Baumgarte stabilization method, with standard ODE45 solver is used.

6.5.1 Human body falling on the rigid ground

This testing case shows the human body model falling from a minimum height (0.01 m) on the rigid surface (ground fall), see Fig. 6.11. This example provides the view on the model behavior in this contact scenario. The model is scaled to human with the weight of 80 kg and 180 cm of height. The ground is modelled as a rigid plane and the HBM is loaded only with gravity.

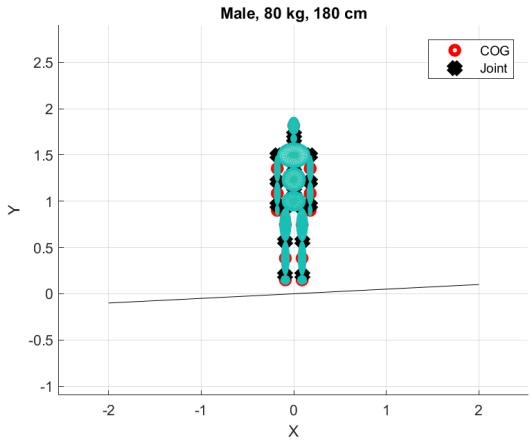

Figure 6.11: HBM falling on the ground from minium distance, inital conditions

Results: The Figures 6.12 show the motion of the body. When the body touches the ground (the distance is less then contact distance), the contact algorithm starts and with the change of the joint angle, the internal stiffness is introduced.

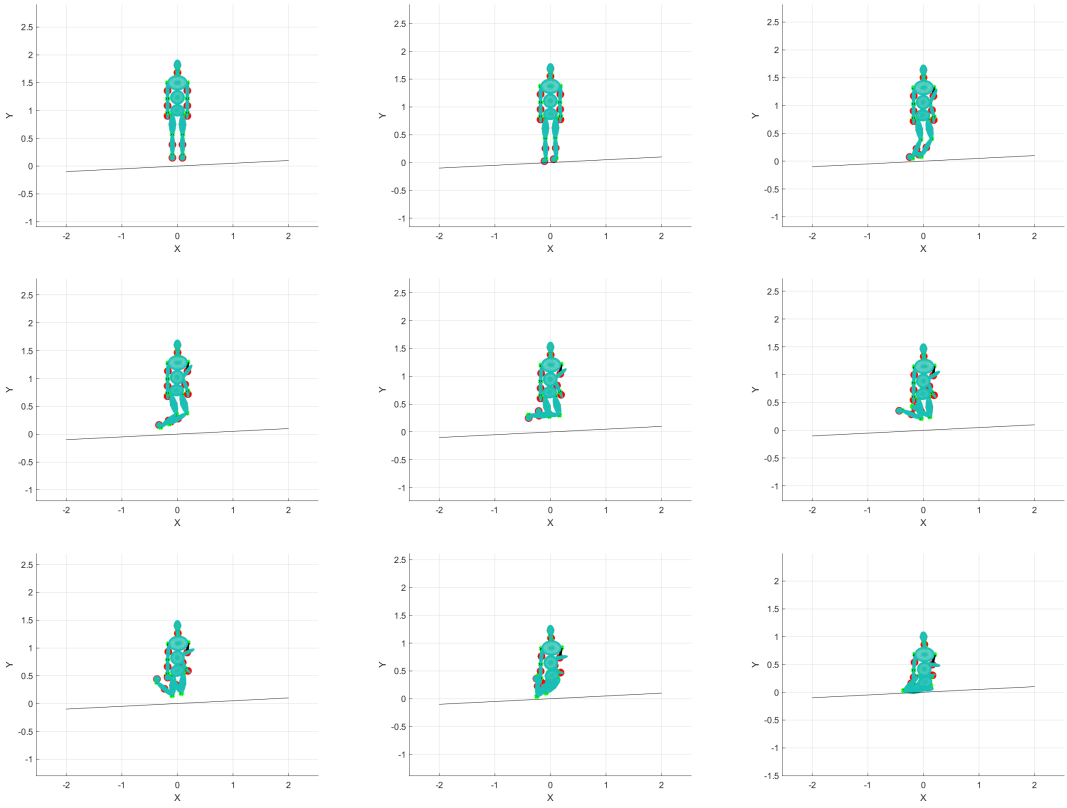

Figure 6.12: HBM falling on the rigid ground from 0.01 m height

Fall on the rigid ground from 4 m

This example is similar with previous one, but the initial height was defined to be 4 m above the ground (distance between the foot and the ground), see Fig. 6.13.

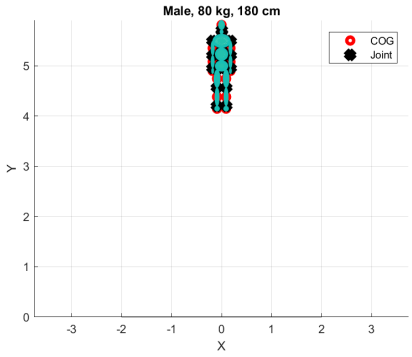

Figure 6.13: HBM falling on the ground from 4 m, inital condition

Results: The Figures 6.14 show the motion of the body.

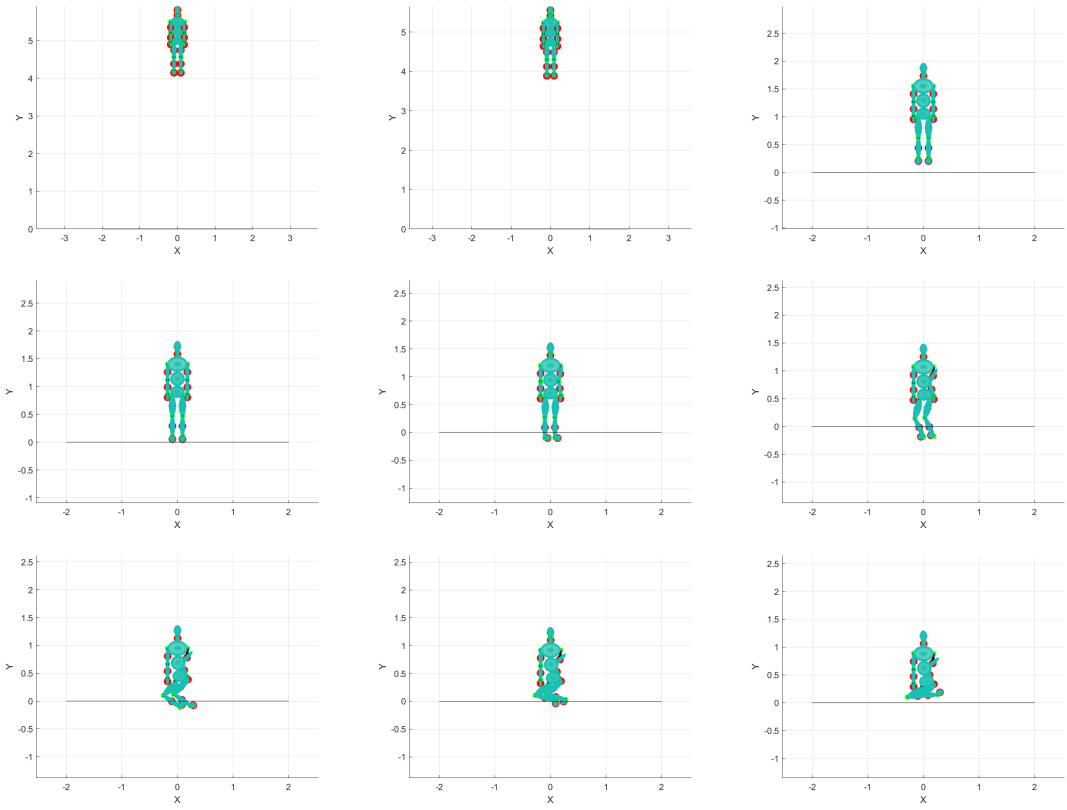

Figure 6.14: HBM falling on the rigid ground from 4 m height)

Fall on the rigid ground from 4 m with different contact parameters

This example is similar to the previous one, the initial height was defined to be 4 m above the ground but the contact is defined to be more elastic, see Fig. 6.15.

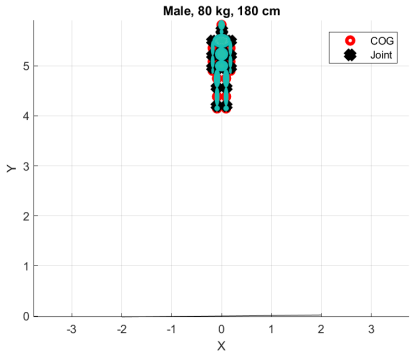

Figure 6.15: HBM falling on the "elastic" ground

Results: The Figures 6.16 show the motion of the body on the "elastic" ground. This example can be an approximation of the athlet jumping on the trampoline.

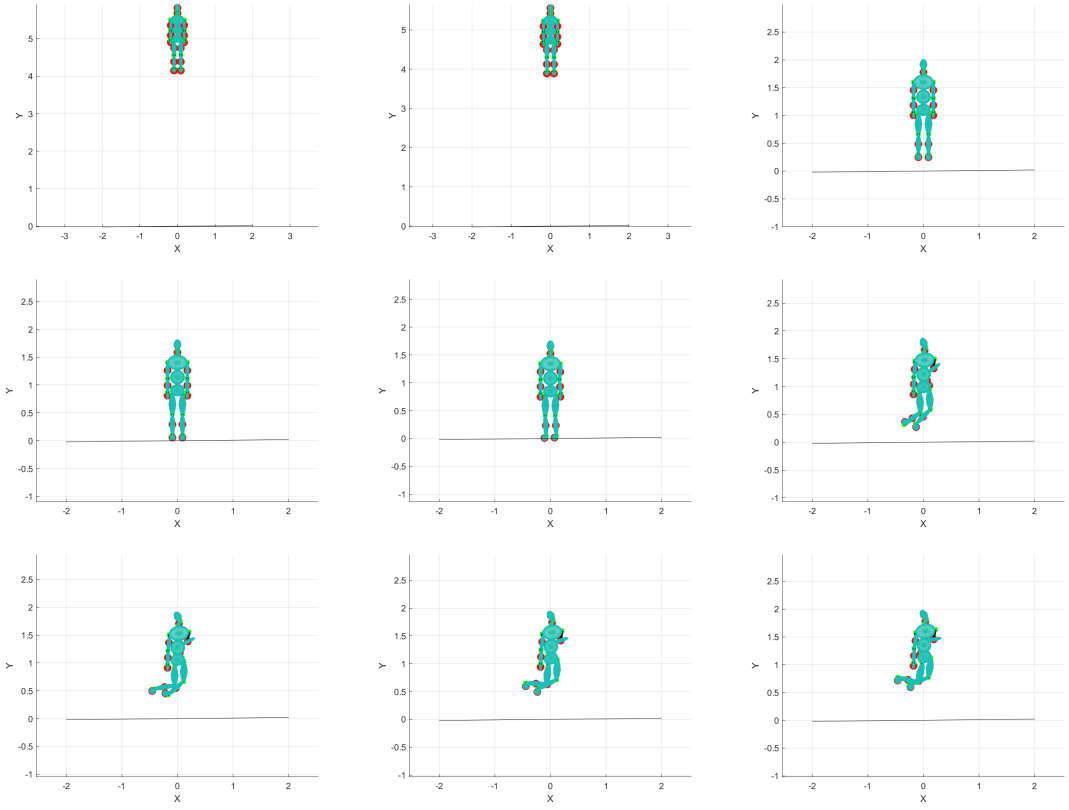

Figure 6.16: HBM falling on the rigid-elastic ground from 4 m height)

6.5.2 Human body falling on the inclined rigid ground

The example here is similar with the previous case (same HBM) but the ground is inclined from the horizontal plane. The contact in both cases is friction-less.

Inclined ground with 20°

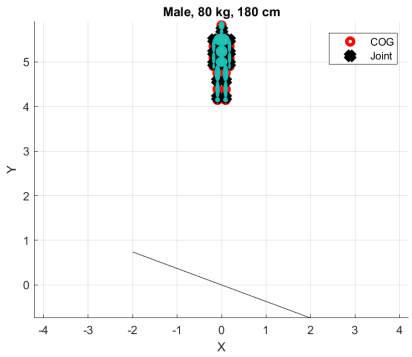

Figure 6.17: HBM falling on the ground inclined with 20°

Results: The Figures 6.18 show the motion of the HBM falling from 4 m on the 20° inclined rigid ground.

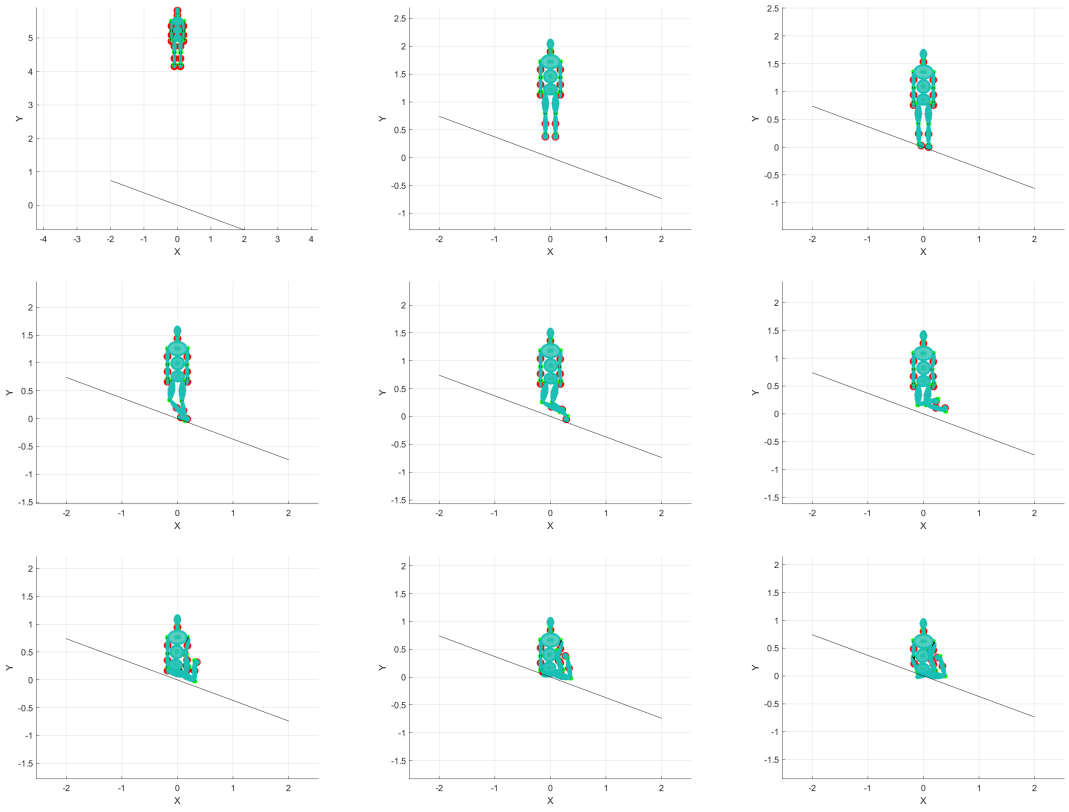

Figure 6.18: HBM falling on the 20° inclined ground

Inclined ground with 45°

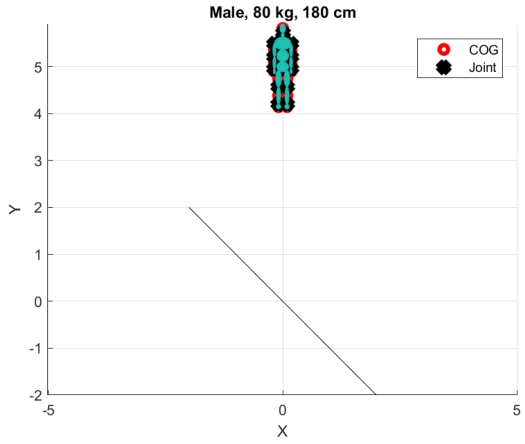

Figure 6.19: HBM falling on the ground inclined with 45°

Results:

The Figures 6.20 show the motion of the HBM falling from 4 m on the 45° inclined rigid ground.

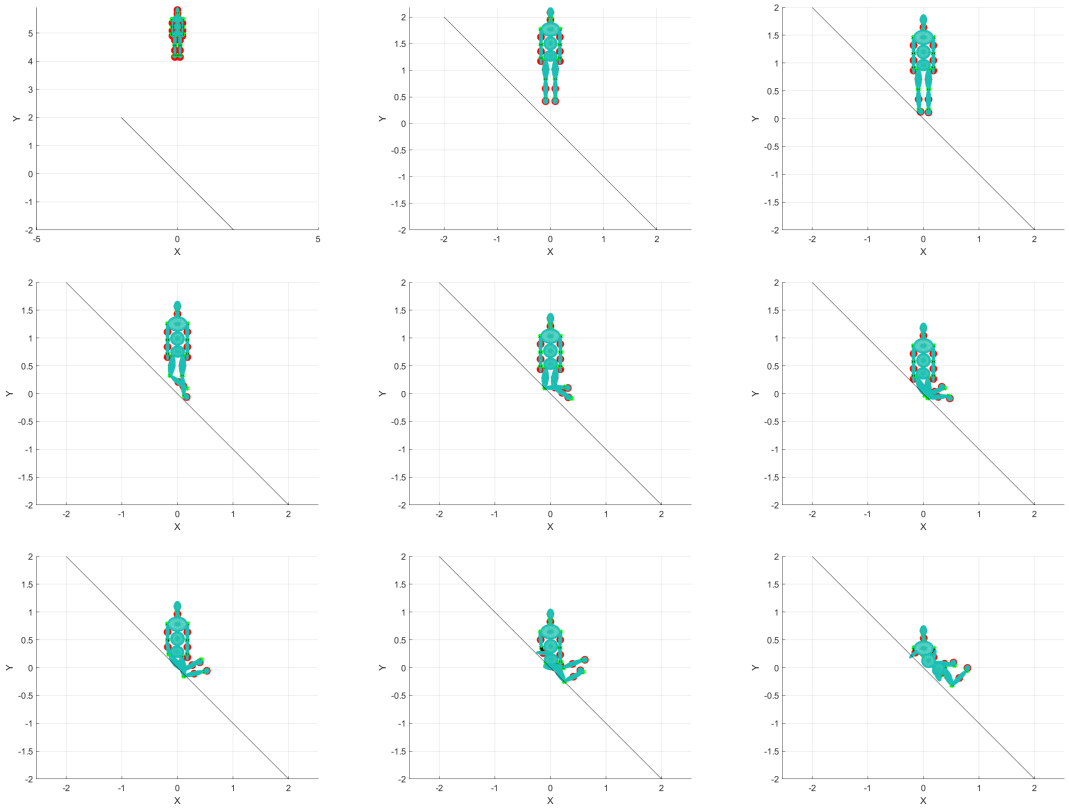

Figure 6.20: HBM falling on the 45° inclined ground

Inclined ground with 70°

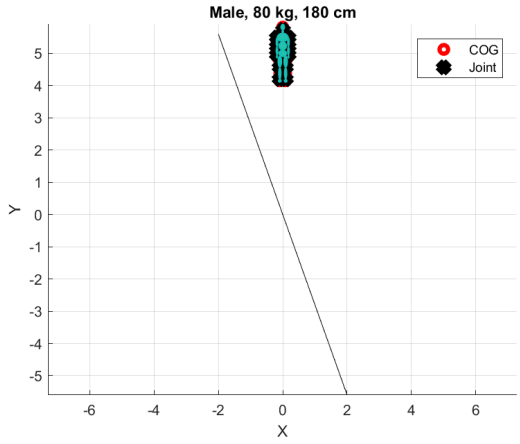

Figure 6.21: HBM falling on the ground inclined with 70°

Results:

The Figures 6.20 show the motion of the HBM falling from 4 m on the 70° inclined rigid ground.

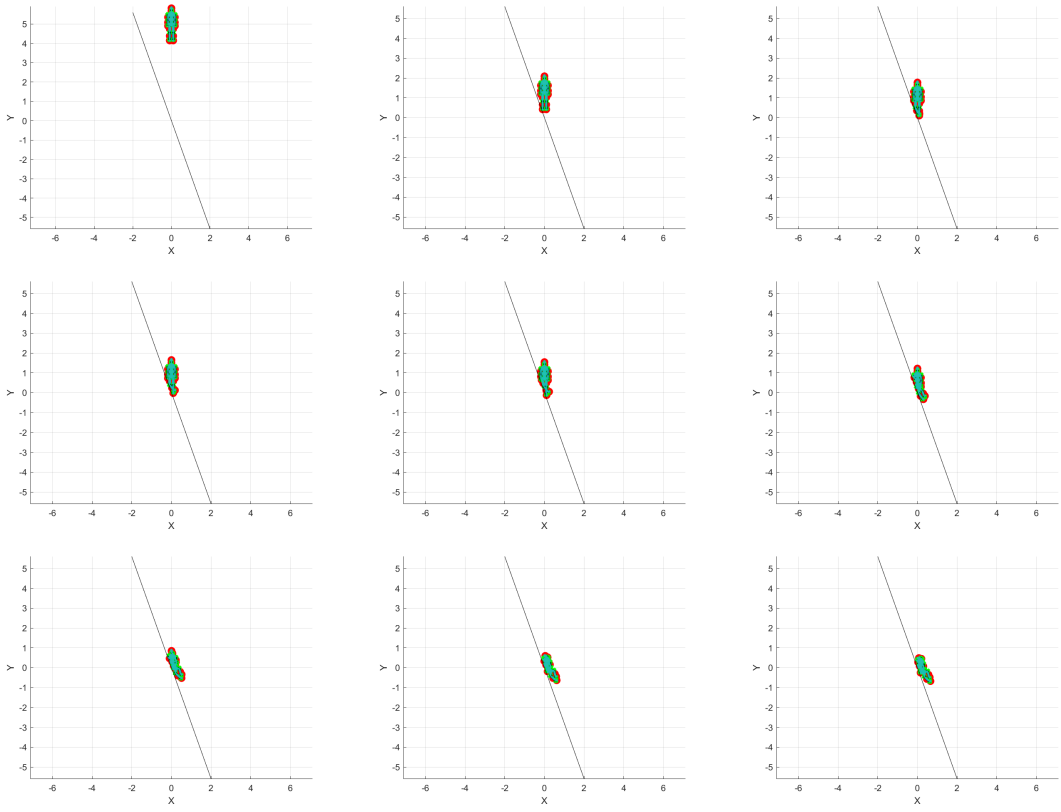

Figure 6.22: HBM falling on the 70° inclined ground

6.5.3 Inclined ground with 70° and non-zero initial velocity

The examples here shows the behavior of the model on the impact to the 70° rigid wall with the initial velocity in direction against the wall, see 6.23. This configuration can simulate collision with the car or other external infrastructure.

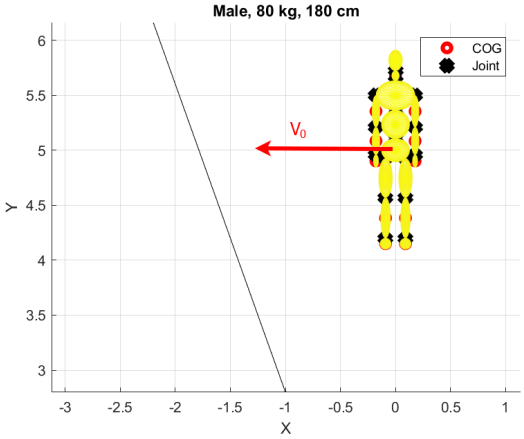

Figure 6.23: HBM falling on the ground inclined with 70° with the initial velocity v_0

.

Initial velocity 2 m/s

The following Figures 6.24 show the results of the impact scenario, where the initial velocity of the HBM is defined as a 2 m/s in the negative X direction (against the rigid wall).

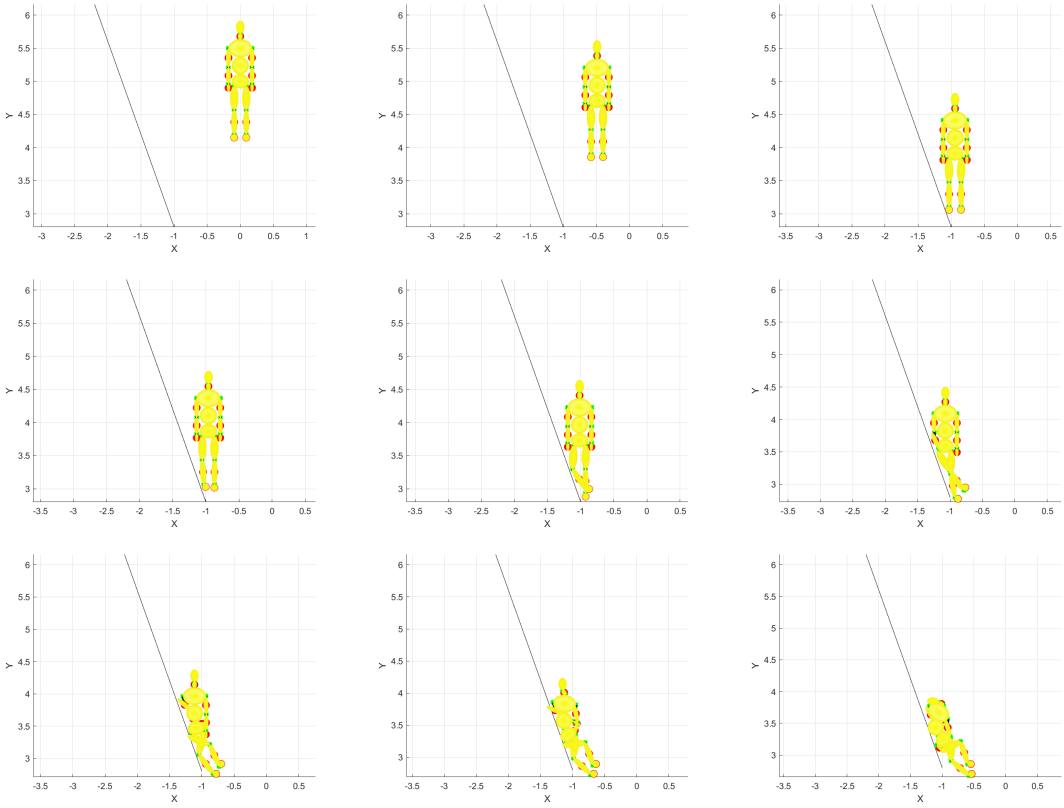

Figure 6.24: HBM falling on the 70° inclined ground with 2 m/s initial velocity

Initial velocity 5 m/s

The following Figures 6.25 show the results of the impact scenario, where the initial velocity of the HBM is defined as a 5 m/s in the negative X direction (against the rigid wall).

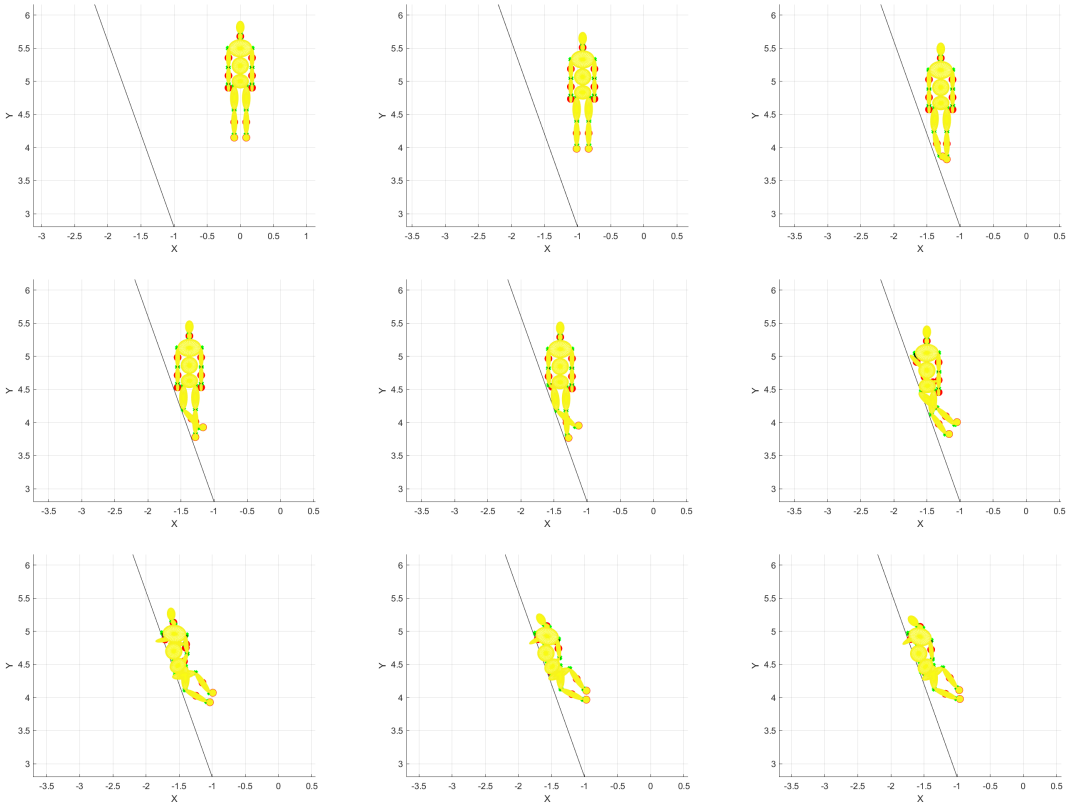

Figure 6.25: HBM falling on the 70° inclined ground with 5 m/s initial velocity

Initial velocity 10 m/s

The following Figures 6.26 show the results of the impact scenario, where the initial velocity of the HBM is defined as a 10 m/s in the negative X direction (against the rigid wall).

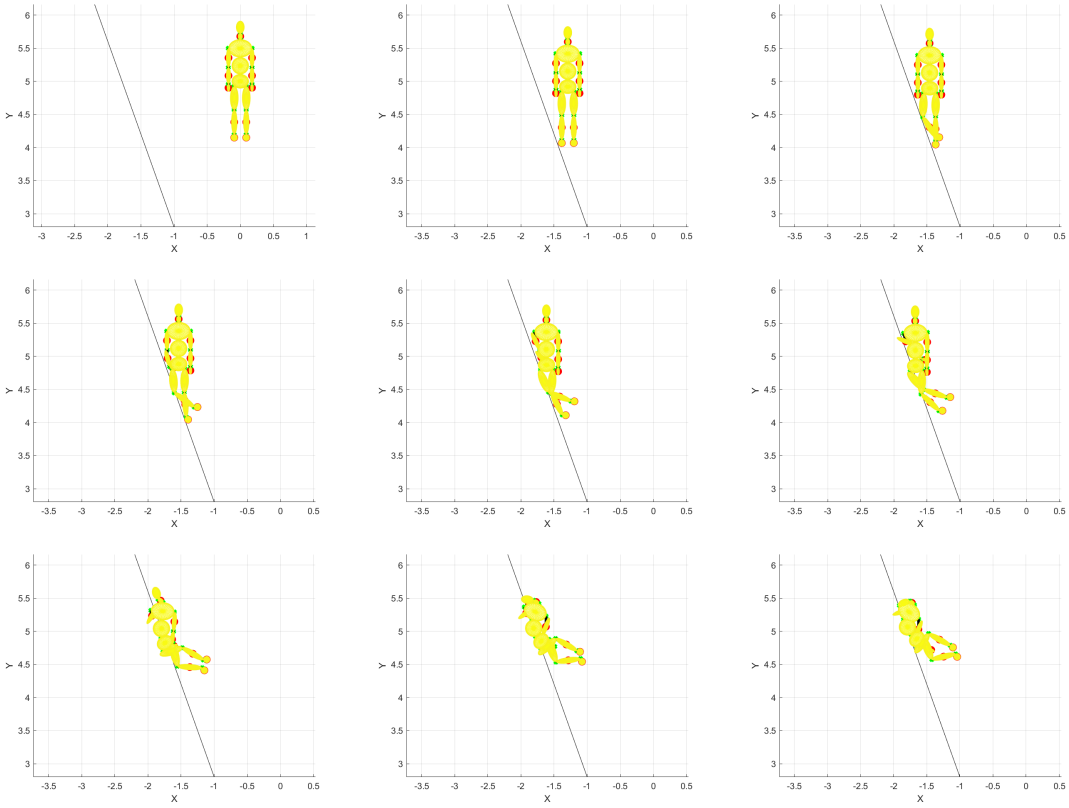

Figure 6.26: HBM falling on the 70° inclined ground with 10 m/s initial velocity

6.5.4 HBM falling on a rigid ground in the laying position

This configuration shows the behavior of the HBM in the falling configuration, when the body initially lays in horizontal position, and fall under loading of gravity.

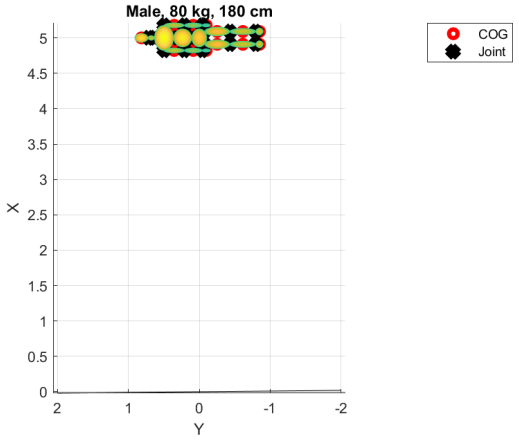

Figure 6.27: Laying HBM falling on the ground

The following Figures 6.28 show the results of the impact scenario, where the laying HBM falls on the ground from height of 5 m.

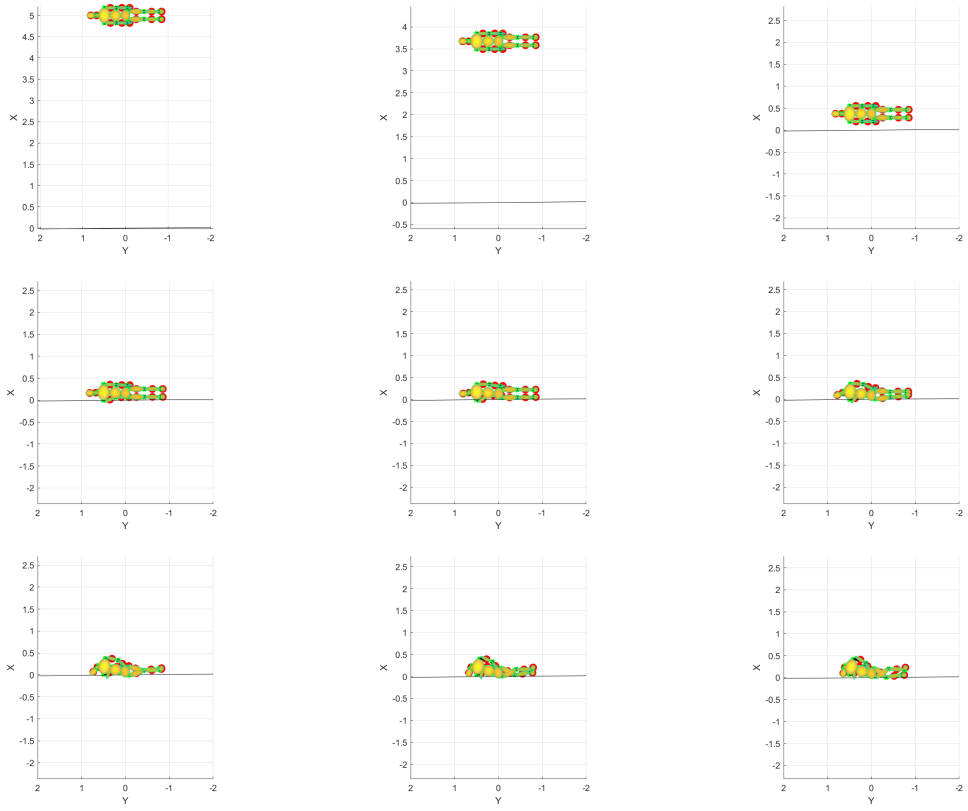

Figure 6.28: Laying HBM falling on the ground

6.5.5 Famous case of human body falling on the rigid ground from more then 14 meters

This section is going to show the behavior of the HBM in the famous and mysterious case in the history of Czechoslovakia. In the 1948, the body of death minister of foreign affair was found on the ground of the courtyard of the ministry at Černín palace. There are still a lot of uncertainties, myths and investigations around this event and the true is still not revealed and very probably it will remain such [54, 66, 101, 121]. The aim here is not to talk about this, but to utilize this model in such dynamic impact scenario. One can find more information for instance in [109], where some technical features as well as historical background are discussed. The author participated in the document, that led to the opening of the new (fifth) investigation on this event. Nevertheless, the collision scenario is a free fall of the male (180 cm, 100 kg, 62 year old) from the height of approximately 14-15 meters on a flat rigid surface. Based on the last knowledge, the body probably fell rearward with the initial velocity up and rear (oblique throw, rear jump). The main aim was only to test, if the model can withstand such scenario. The results are not really comparable with the Virthuman model used in [109] or with the real data, since the model is not validated (especially the contact parameters). The scenario here is a rear jump/fall with the initial velocities $dx = 0 - side, dy = 1m/s - up, dz = 1.5m/s - rear$ defined on the HBM.

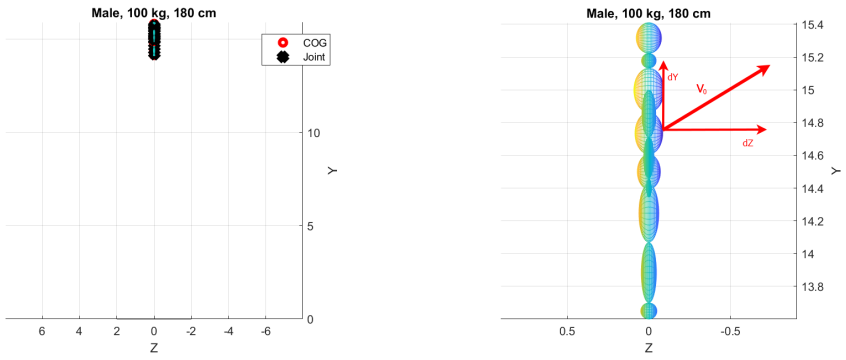

Figure 6.29: Human standing at the 14 m initial height [left], defined initial velocity [right]

Following Figures 6.30 show the initial phase of the rearward jump, with the initial velocities dy=1 ms and dz=-1.5 ms defined on the trunk of the body (chest, abdomen, pelvis). The values are based on the forensic study and experimental measurement on this case [109].

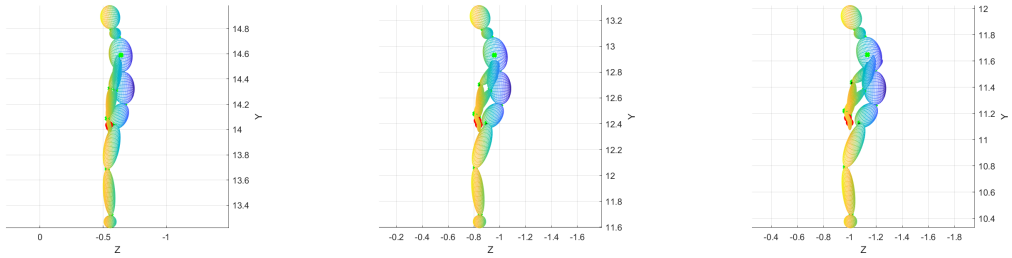

Figure 6.30: Initial phase of the rear jump

The sequence of the motion (initial phase, flight phase and landing/contact with the ground) is presented in the following set of Figures 6.31. The first contact of the body is through the feet, followed by the pelvis and chest. The head does not get into contact, which is in correspondence with the historical data (the head of the minister was not injured). Of course, the particular setting of the parameters (numerical stabilization, contact parameters and initial posture) can significantly affect the final stature of the body. The example here only shows the possibility of this human body model.

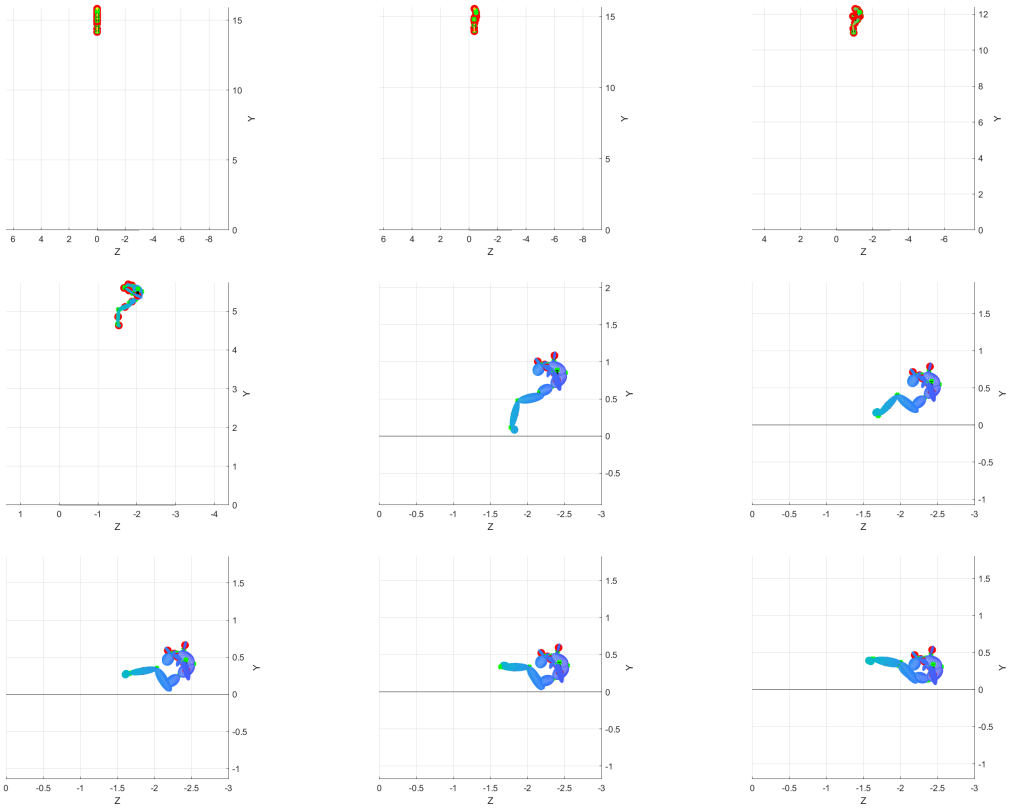

Figure 6.31: Phases of a rear jump

Note that the first three pictures show entire model, including initial location of the body

(feet 14 m above ground) and the ground, to see the full perspective, while the last 5 are focused on the landing area. As can be seen, the body significantly bends (flexion) in the torso area, which seems to be un-physiological. However, the body can flex up to 70° in Sacrum-L5 joint, see Tab. 4.3. Moreover, the model is not fully validated, it uses the joint limits and internal torques from the literature [93] and the proper setting would require a complex validation and verification. However, this model shows the good potential also in this crash scenario, where long time simulation (2000 ms) together with internal stiffness and contact algorithm.

6.6 Discussion

The full human body model (HBM) developed here was tested in some basic impact scenarios. The particular algorithms and sub-models were tested in a single body examples: bouncing ball, falling ellipsoid including various set of contact models and a spherical pendulum including internal stiffness of the joint. All these models show a good potential to be used in such applications. Despite the fact that the results are tested only with visual observation, the behavior of the bodies looks reasonable and realistic.

The full HBM contains 17 bodies, connected with the spherical joints. The model contains internal joint stiffness, contact algorithm for each body and also stabilization methods (Baumgarte and direct violation). The contact calculation and especially the joint stiffness brings a high non-linearity into the model. Moreover, the calculation in MATLAB with using the standard integration solvers for differential equations have some limitations and they might be slower for non-linear equations and they are not very useful for paralelization, that could make the calculation faster.

Based on the setting of the numerical parameters, the impact calculation with the full HBM can take relatively long calculation time (from a few minutes up to several hours), but all the particular algorithms work and the full model gives reasonable results. However, if the model will be used for some particular case, the proper setting of the contact, stiffness and numerical parameters must be tuned up, to validate model for this case. Moreover, for the further applications, all mathematical methods and algorithm described in this work could be written in programming language such as C++, or Java, where some features, such as paralelization can be done.

Generally, the model behaves good in the spatial motion, numerical stabilization, contact or internal stiffness implementation. However, if all scenarios meet in the same time, the calculation can make some troubles. For instance, contact algorithm works well (if the contact stiffness is properly set) for the first impact. Since secondary contact is already affected with the error from the first one, the results are not very clear. As was discussed before, several sets of parameters (contact, damping, internal stiffness, numerical setting and so on) need to be correctly set. The numerical optimization can help to do it, if the data (results) of the particular case are available, to be compare with the numerical results. The main aim of this work was to used the principle of MBS (with the main

focus on the spatial motion) to built a solver for the human body model, that can be used in the crash scenario. To properly model the human body in the crash scenarios, the contact algorithm (for contact), the internal stiffness (to limit joint range of motion) and numerical stabilization (to numerically stabilize the model) were included.

Chapter 7

Conclusion

Human body is a highly complicated and complex system, that is really hard to describe within some mathematical model. Since it is a live system, with non standardize geometry and material parameters. These all are changing with every single individual case, with the age, gender, history of the human body and also with the physical condition and body shape. Moreover, if some database is built (such as anthropometric database of ČSSR, [32]), it is limited for the special case (in this case population of the Czechoslovakia, Spartakiáda event - athletes, 80's, on so on). If the description of the body geometry is done (which is a doable task) the main limitation and concern would be the material description. Since the "human materials" are live, they are anisotropic, hyper or viscoelastic, temperature and chemical substance dependent, heterogeneous, active - muscle, it is not possible to precisely described all the human materials for all possible humans, for all possible scenarios. The material description of the human tissue is even more complicated, since there is a lack of experimental data, which is essential part of the material description. If there are some studies, they always have some limitations and uncertainties, such as how the test were performed, what was the history of subject and sample etc. The live tissues do not behave equally, if the sample is "fresh", frozen and de-frozen or if it remains couple of hours out of the body, so not alive anymore. The testing of the live tissue has also technical limitations (not all the required tests are feasible) and also ethical limitations.

However, there are number of high quality human body models (or its segments), but they are designed for a special field of applications, they have some limitations, where they can be successfully used, and these conditions must be always satisfied. For instance, the most complex human body model based on finite element methods GHBMC or THUMS can not be apply in muscle analysis, since they are not designed for such purposes. They can bring a very appropriate results in the dynamics analysis, deformations and stresses of the tissue of human body in crash configurations. On the other hand, musculoskeletal models (such as AnyBody) can analyze muscle activities and joint reaction forces in a real motion of the human, but do not provide any information about the tissue deformation, since they contain only rigid bodies and active muscle elements.

The word *model* can be connected with the physical models (in case of human body called *Dummy*) or virtual models (numerical models). This work presents some review of the current models stage (including dummies, numerical models of the dummies and numerical models of the human body) in the first chapter. To sum this up, each model of human body is always only an approximation of the human and it always has some limitations and rules, than must be always satisfied.

The main aim of this work is in the mathematical background of the multibody approach, that is used and described here. General theory of the mathematical equations, especially the 3D rotation is presented, where the well-known Euler angles and more robust Euler parameters are used to parametrise general 3D motion. The equation of motion for free and constrained body, as well as for a system of constrained bodies are derived here.

Since the multibody method generates differential-algebraic equations, that are numerically integrated in the standard MATLAB solvers, some methods of numerical stabilization must be used, to fulfill the constraints and to stabilize the model. Two methods of stabilization are presented here (Baumgarte and direct violation), including sensitivity analysis of such methods, on a simple constrained system (pendulum and double pendulum).

The crash examples (concern of this model) is connected with the contact and impact scenario. For this purpose, the review of contact detection algorithms and contact force models are presented (discrete or continuous models and variation of the normal contact force models). Finally, the contact detection method developed for this model is described and implemented as a right hand side to the total equation of motion. Each body of the system can potentially get into the contact with the rigid infrastructure, to include the crash applicability to the model.

Finally, all the methods, approaches and algorithms described here are tested via the full human body model. Such model contains of 17 rigid bodies, linked in a open tree structure within spherical joints. The joints include internal stiffness (to limit range of motion and to describe physiological rigidity of the joints) as an external torque, that is function of the relative rotation between the body segments.

The main purpose of this work is not to build a *brand-new* model of the human body. There are hundreds or thousand of the models, each of them long time developed for a very special usage. It would cost several years of development for a team of experts to create a new software, that could be comparable with the commercial software spread world-widely. The main concern was to study all the algorithms, that are used in MBS software, to test them in a very simple benchmark examples, to get an idea how they work, how they can be implemented and what are their pros and cons. The human body model described above is a results of all the particular examples and approaches trigger together in one complex model. The knowledge gained during the development will be used in the further modelling. The University of West Bohemia disposes with virtual human body Virthuman [62, 63, 64, 67, 76, 113, 114]. This model includes MBS fragments (the basic skeleton) and the algorithm developed here can extend this model

for a further applications. Especially the internal stiffness is a *fresh field* that is currently under concern of the researches to be included in the automotive industry. Consequently, the model shows a good potential also in the forensics analysis, which start to be also a perspective field for biomechanical models.

To sum this up, the model which is presented here is not a completed and fully validated model, ready to use. However, the model is in a status called *validation-ready*. This means, that the model successfully connected all the mathematical and numerical approaches to build a complex model. The model behaves good for a various crash examples. Of course it has same limitations, uncertainties and disadvantages, that were discussed above. If the description of some particular example (scenario) is required, the parameter variation and model validation would be the main task. The model was created from a *sketch* and all mathematical equations are provided and thus, for a further applications, a new software can be coded in some other programming languages, that can solve limitation of the MATLAB and its numerical solvers. Despite the limitations of the final human body model, the main task of this work was achieved. There are still a lot of the impact biomechanics tasks remaining, and this model can further help in their solution.

Bibliography

[1] Wayne state partners with toyota on safety research.

[2] The Evolution of the Crash Test Dummy, 2014.

[3] Pursuit for Vehicle Safety, toyota, 2015.

[4] Tassinternational MADYMO human models, 2015.

[5] World health organization, road traffic injuries, 2019.

[6] 3d slicer, 2020.

[7] Abaqus, dassualt systemes, 2020.

[8] Altair hyperworks, radioss, 2020.

[9] Amira, thermofisherscientific, 2020.

[10] Ansys, 2020.

[11] Ansys livermore software technology, total human model for safety, 2020.

[12] Biological tissue mathematical constitutive models in human body models for enhanced human safety, 2020.

[13] Dynamore, total human model for safety, 2020.

[14] Esi group, virtual performance solution, 2020.

[15] Federal aviation administration, 2020.

[16] Global human body model consorcium, 2020.

[17] Mimic, materialise mimicss, 2020.

[18] National highway traffic safety administration, united states department of transportation, 2020.

[19] Osccar, future occupant safety for crashes in car, 2020.

[20] Society of automotive engineers, sae international, 2020.

[21] Society of automotive engineers, standards j944 196512, 2020.

[22] Tass international, madymo human models, 2020.

[23] University of viginia, engineering, 2020.

[24] University of waterloo, engineering, 2020.

[25] DC Alpini, A Cesarani, and A Hahn. Whiplash associated somatic tinnitus (wast). In *Whiplash Injuries*, pages 139–149. Springer, 2014.

[26] Janete Alves, Paulo Flores, and Nuno Peixinho. Contact analysis for different viscoelastic contact force models. ECCOMAS, 2013.

[27] Farid Amirouche. *Fundamentals of multibody dynamics: theory and applications*. Springer Science & Business Media, 2007.

[28] Bezopasnyy avtomobil. Safety car. *Internet-zhurnal 'Bezopasnyy avtomobil'Bezopasnyy avtomobil'*, 1999-2015.

[29] Nicholas Ayache. *Computational Models for the Human Body: Special Volume*, volume 12. Gulf Professional Publishing, 2004.

[30] Pascal Baudrit, Jean Hamon, Eric Song, Jean-Yves Le Coz, et al. Comparative studies of dummy and human body models behavior in frontal and lateral impact conditions. Technical report, SAE Technical Paper, 1999.

[31] S. Bikowski. Multibody-system model of bus with man. *COPERNICUS Project, volume=Deliverable D51/1, Part A, number= No. 94-0520, year=1997, publisher= Institute of Mechatronics, Chemnitz*.

[32] Pavel Bláha. *Antropometrie československé populace od 6 do 55 let*. Ústř. štáb Čs. spartakiády 1985, 1987.

[33] Vladimír Brát. *Maticové metody v analýze a syntéze prostrových vázaných mechanických systémů*. Academia, 1981.

[34] Jaromír Brousil, Jaromír Slavík, and Vladimír Zeman. *Dynamika*. SNTL, 1989.

[35] Philippe G. Ciarlet and Nicholas Ayache. *Computational Models for the Human Body*, volume XII. Special volume. Elsevier, North Holland, 2004.

[36] JC Combest. Current status and future plans of the ghbmc. In *6th Symposium Human Modeling and Simulation in Automotive Engineering*, 2016.

[37] John J. Combest. Status of the Global Human Model Consortium. *4th International Symposium on Human Modelling and Simulation in Automotive Engineering, May 13th and 14th*, 2013.

[38] J Garcıa de Jalón and Eduardo Bayo. Kinematic and dynamic simulation of multibody systems. *Mechanical Engineering Series, Springer, New York*, 1994.

[39] Vincent G Duffy. *Handbook of digital human modeling: research for applied ergonomics and human factors engineering*. CRC press, 2016.

[40] David Eberly. Intersection of ellipsoids. Technical report, Technical report, Geometric Tools, LLC, 2008.

[41] EuroNCAP. Pedestrian CAE Models & Codes. *EURONCAP Technical Bulletin*, 2019.

[42] SVS FEM. Ls-dyna, 2020.

[43] Stephen Fliggins. Biomechanics and the Cyberhuman. *Computer Graphics and Applications, IEEE*, 2002.

[44] Paulo Flores, Margarida Machado, Miguel T Silva, and Jorge M Martins. On the continuous contact force models for soft materials in multibody dynamics. *Multibody system dynamics*, 25(3):357–375, 2011.

[45] Paulo Flores, Rui Pereira, Margarida Machado, and Eurico Seabra. Investigation on the baumgarte stabilization method for dynamic analysis of constrained multibody systems. In *Proceedings of EUCOMES 08*, pages 305–312. Springer, 2009.

[46] Francis Scott Gayzik, Daniel P. Moreno, Nicholas A. Vavalle, Ashley C. Rhyne, and Joel D. Stitzel. Development of the global human body models consortium mid-sized male full body model.

[47] Mohamed Gharib and Yildirim Hurmuzlu. A new contact force model for low coefficient of restitution impact. *Journal of applied mechanics*, 79(6), 2012.

[48] G. Gilardi and I. Sharf. Literature survey of contact dynamics modelling. *Mechanism and machine theory*, 37(10):1213–1239, 2002.

[49] Yves Gonthier, John McPhee, Christian Lange, and Jean-Claude Piedboeuf. A regularized contact model with asymmetric damping and dwell-time dependent friction. *Multibody System Dynamics*, 11(3):209–233, 2004.

[50] ESI group. Pacific Engineering System International, 2014.

[51] Michal Hajžman and Pavel Polach. Application of stabilization techniques in the dynamic analysis of multibody systems. 2007.

[52] William Rowan Hamilton. Xi. on quaternions; or on a new system of imaginaries in algebra. *The London, Edinburgh, and Dublin Philosophical Magazine and Journal of Science*, 33(219):58–60, 1848.

[53] Eberhard Haug, Hyung-Yun Choi, Stéphane Robin, and Muriel Beaugonin. Human models for crash and impact simulation. *Handbook of numerical analysis*, 12:231–452, 2004.

[54] Jan Havel. Smrt jana masaryka očima kriminalisty. *Ve stínu úvah a ve*, 1998.

[55] RG Herbert and DC McWhannell. Shape and frequency composition of pulses from an impact pair. 1977.

[56] Miroslav Hirt, Michal Beran, Miroslav Ďatko, Petr Hejna, Jan Chrastina, Martin Janík, Ivana Komáreková, Jan Krajsa, Zdeněk Novák, Ivo Říha, et al. *Tupá poranění v soudním lékařství*. Grada Publishing, 2011.

[57] Miroslav Hirt, Andrea Brzobohatá, Miroslav Ďatko, Jan Krajsa, Tomáš Vojtíšek, Michal Zelenỳ, Miloš Sokol, Kateřina Hirtová, Aleš Vémola, et al. *Dopravní nehody v soudním lékařství a soudním inženỳrství*. Grada, 2012.

[58] Humanetics. Inovative Solutions, 2020.

[59] Kenneth H Hunt and Frank R Erskine Crossley. Coefficient of restitution interpreted as damping in vibroimpact. 1975.

[60] Luděk Hynčík. Počítačový model figuríny člověka pro potřeby nárazových zkoušek, Diplomová práce, 1998.

[61] Luděk Hynčík. Rigid body based human model for crash test purposes. In *Proceedings of the Engineering MECHANICS*, volume 8, pages 1–6, 2001.

[62] Luděk Hynčík. *Škálování hybridního modelu člověka*. PhD thesis, Západočeská univerzita v Plzn, January 2014. Habilitation thesis.

[63] Luděk Hynčík, Hana Čechová, Luděk Kovář, and Pavel Bláha. On scaling virtual human models. Technical report, SAE Technical Paper, 2013.

[64] Luděk Hynčík, Jaroslav Špička, Janand Maňas, and Jan Vychytil. Stature Based Approach towards Vehicle Safety. *SAE Technical Paper 2015-26-0209*, 2015.

[65] Kambiz Kayvantash, Samuel Bidal, and Franck Delcriox. HUMOS - An FE Model for Advanced Safety and Comfort. 2009.

[66] Pavel Kosatík and Michal Kolář. *Jan Masaryk-pravdivỳ příběh*. Albatros Media as, 2016.

[67] Luděk Kovář and Jana Hluchá. Esi virthuman models for impact. In *DHM and Posturography*, pages 169–185. Elsevier, 2019.

[68] Martin Kovařík. *Antropometrickỳ výzkum dospělé populace a jeho aplikace v oblasti interiéru a architektury*. PhD thesis, Vysoké učení technické v Brně. Fakulta architektury, 2011.

[69] Jiří Křen, Přemysl Janíček, and Josef Rosenberg. *Biomechanika*. Západočeská univerzita, Fakulta aplikovaných věd, 2001.

[70] H. M Lankarani and P.E. Nikravesh. A contact force model with hysteresis damping for impact analysis of multibody systems. *Journal of Mechanical Design*, 112:369–376, 1990.

[71] Ting W Lee and AC Wang. On the dynamics of intermittent-motion mechanisms. part 1: dynamic model and response. 1983.

[72] Torholm S. Lund, M. E. and M. Jung. Anybodymodelling system, eprint = Web page, publisher = The AnyBody Managed 193 Model Repository (AMMR), year = 2018,.

[73] M. F. Machado and P. Flores. A novel continuous contact force model for multibody dynamics. In *Proceedings ofthe ASME 2011 International Design Engineering Technical Conferences & Computers and Information in Engineering Conference IDETC/CIE 2011*, 2011.

[74] Suresh Mahi, Zhu Feng, et al. Finite element evaluation of human body response to vertical impulse loading. *Blucher Mechanical Engineering Proceedings*, 1(1):1809–1818, 2014.

[75] P Maißer, CD Wolf, A Keil, K Hendel, U Jungnickel, H Hermsdorf, PA Tuan, G Kielau, O Enge, U Parsche, et al. Alaska, user manual, version 2.3. *Institute of Mechatronics, Chemnitz*, 1998.

[76] Jaroslav Maňas, Luděk Kovář, Jan Petřík, Hana Čechová, and Stanislav Špirk. Validation of human body model virthuman and its implementation in crash scenarios. In *Advances in Mechanisms Design*, pages 351–356. Springer, 2012.

[77] R MATLAB. Version 8.1. 0.604 (r2018b). *Natrick, Massachusetts: The MathWorks Inc*, 2019.

[78] Pradeep Mohan, Dhafer Marzougui, Roel Van De Velde, and Cing-Dao Steve Kan. Development of detailed finite element dummy models. In *6th LS-DYNA Forum, Frankenthal, Germany*, 2007.

[79] Andreas Moser, Hermann Steffan, and G Kasanickỳ. The pedestrian model in pc-crash–the introduction of a multi body system and its validation. *SAE transactions*, pages 794–802, 1999.

[80] Krystoffer Mroz, Ola Boström, Bengt Pipkorn, Jac Wismans, and Karin Brolin. Comparison of hybrid iii and human body models in evaluating thoracic response for various seat belt and airbag loading conditions. In *IRCOBI Conference*, 2010.

[81] S. Muthukumar and R. DesRoches. A hertz contact model with non-linear damping for pounding simulation. *Earthquake engineering and structural dynamics*, 35:811–828, 2006.

[82] Ralph Nader. Unsafe at any speed. *The Designed-in danger of the American Automobile*, 1999.

[83] Parviz E Nikravesh. *Computer-aided analysis of mechanical systems*. Prentice-Hall, Inc., 1988.

[84] PE Nikravesh, OK Kwon, and RA Wehage. Euler parameters in computational kinematics and dynamics. part 2. *Journal of Mechanisms, Transmissions, and Automation in Design*, 107(3):366–369, 1985.

[85] PE Nikravesh, RA Wehage, and OK Kwon. Euler parameters in computational kinematics and dynamics. part 1. *Journal of Mechanisms, Transmissions, and Automation in Design*, 107(3):358–365, 1985.

[86] Chinmoy Pal, Okabe Tomosaburo, Muthanandam Muthukumar, and Satheesh Narayanan. Human fe model to estimate head contact time for pedestrian protection.

[87] Gwansik Park, Taewung Kim, Jeff R Crandall, Carlos Arregui Dalmases, Benito Javier Luzón Narro, et al. Comparison of kinematics of ghbmc to pmhs on the side impact condition. 2013.

[88] Daniel Perez-Rapela, Jason L Forman, Samuel H Huddleston, and Jeff R Crandall. Methodology for vehicle safety development and assessment accounting for occupant response variability to human and non-human factors. *Computer Methods in Biomechanics and Biomedical Engineering*, pages 1–16, 2020.

[89] F. Pfeiffer and C. Glocker. *Multibody dynamics with unilateral contacts*. Wilet-VCH GmbH & Co. KGaA, 2004.

[90] Pavel Polach. A simple parametric multibody model of human (jednoduchý parametrický multibody model člověka). Technical report.

[91] RF Portal, JP Dias, and CA Mota Soares. Multibody models for vehicle accident reconstruction. In *ECCM 2006-III European Conference on Computational Mechanics-Solids, Structures and Coupled Problems in Engineering*, 2006.

[92] Daniel E Rivera, Manfred Morari, and Sigurd Skogestad. Internal model control: Pid controller design. *Industrial & engineering chemistry process design and development*, 25(1):252–265, 1986.

[93] DH Robbins. Anthropometric specifications for mid-sized male dummy. *University of Michigan Transportation Research Institute (UMTRI) report number UMTRI-83-53-2*, 1983.

[94] Stéphane Robin. Humos: Human model for safety˜ a joint effort towards the development of refined human-like car occupant models. Technical report, SAE Technical Paper, 2001.

[95] SAE. SIMon, Simulated Injury Monitor, The next generation of the SIMon Head Finite Element Model, 2015.

[96] Sofia Scataglini and Gunther Paul. *DHM and Posturography*. Academic Press, 2019.

[97] Kai-Uwe Schmitt, Peter F. Niederer, and Felix Walz. *Trauma biomechanics*. Springer, 2010.

[98] L.W. Schneider, D.H. Robbins, M.A. Pflüg, and R.G. Snyder. Development of anthropometrically based design specifications for an advanced adult anthropomorphic dummy family, volume 1. final report. 1983.

[99] Ahmed A. Shabana. *Computational dynamics*. John Wiley & Sons, 2009.

[100] K.A. Sohn, B. Jüttler, M.S. Kim, and W. Wang. Computing distance between surfaces using line geometry. *IEEE Computer society*, 2002.

[101] Claire Sterling. *Případ Masaryk*. LepreZ, 1991.

[102] Tomij Sugimoto and Kunio Yamazaki. First results from the JAMA human body model project. *Europe (HUMOS: Human Model for Safety)*, 3:4, 2005.

[103] Svejda, M. Uvod do robotiky a mechatroniky (urm), reprezentace obecneho pohybu v robotice, 2017.

[104] Erik G Takhounts, Rolf H Eppinger, J Quinn Campbell, Rabih E Tannous, Erik D Power, and Lauren S Shook. On the development of the simon finite element head model. Technical report, SAE Technical Paper, 2003.

[105] Pedro Talaia, Luděk Hynčík, and Michal Hajžman. A multipurpose multi-body human model for accident reconstruction with emphasis to ptw and injury assessment. 2011.

[106] Eva Tlapáková. Geometrie hmotností lidského těla [online], 2011.

[107] Linda Valdmanová. Kosterně svalová rovnováha horní končetiny, Diplomová práce.

[108] Linda Valdmanová. Model horní končcetiny ve 2D jako vázaný mechanický systém, Bakalářská práce, 2009.

[109] Martin Čermák, Jan Špička, Tomasz Bonkowski, Roman Kroft, and Jan Vychytil. Support of the numerical mechanics in the clarification of the mysterious death of jan masaryk. In *Proceedings of the Computational Mechanics*, 2020.

[110] Jan Špička. Double pendulum contact problem, Master thesis, 2013.

[111] Jan Špička, Michal Hajžman, and Luděk Hynčík. Double pendulum contact problem. *Applied and Computational Mechanics*, 8:115–128, 2014.

[112] Jan Špička, Michal Hajžman, and A Bouncing Ball Benchmark Problem Polach, Pavel. Solution of an ellipsoid-to plane contact. In *Proceedings of The 3rd Joint Conference on Multibody System Dynamics, The 7th Asian Conference on Multibody Dynamics*, pages 29–30.

[113] Jan Vychytil, Luděk Hynčík, Jaroslav Maňas, and Luděk Kovář. Accident reconstruction with scalable virtual human model VIRTHUMAN. 2014.

[114] Jan Vychytil, Luděk Hynčík, Jaroslav Maňas, Petr Pavlata, Radim Striegler, Tomas Moser, and Radek Valášek. Prediction of injury risk in pedestrian accidents using virtual human model virthuman: real case and parametric study. Technical report, SAE Technical Paper, 2016.

[115] Jan Vychytil, Jaroslav Maňas, Hana Čechová, Stanislav Špirk, Luděk Hynčík, and Luděk Kovář. Scalable multi-purpose virtual human model for future safety assessment. Technical report, SAE Technical Paper, 2014.

[116] W. Wang, Y.K. Choi, B. Chan, M. S. Kim, and J. Wang. Efficient collision detection for moving ellipsoids using separating planes. *Computing*, 72:235–246, 2004.

[117] Wikipedia. Crashtest- Dummy, 2020.

[118] Wikipedia contributors. Quaternion — Wikipedia, the free encyclopedia. `https://en.wikipedia.org/w/index.php?title=Quaternion&oldid=967118529`, 2020. [Online; accessed 21-July-2020].

[119] Emrah Yigit, Jens Weber, Philipp Huber, Adrian Prüggler, Stefan Kirschbichler, and Matthias Kröger. Influence of soft tissue material modelling on occupant kinematics in low g scenarios using FE human body models. 2014.

[120] Q Yu and I-M Chen. A direct violation correction method in numerical simulation of constrained multibody systems. *Computational Mechanics*, 26(1):52–57, 2000.

[121] Pavel Žáček et al. Dává se na vědomí... jan masaryk ve svodkách čs. zahraničního zpravodajství. *Paměť a dějiny*, 7(01):56–69, 2013.

[122] Pan Zhenkuan et al. An automatic correction method for position and velocity constraint equations violations in multibody systems. *Dynamics of Multibody Systems and Control*, pages 31–35, 1996.

[123] Qin Zhiying and Lu Qishao. Analysis of impact process based on restitution coefficient. *J. Dyn. Control*, 4:294–298, 2006.